COMBINED LIGAND AND STRUCTURE-BASED STUDIES TO MODULATE L-TYPE AMINO ACID TRANSPORTER-1 (LAT1) IN CANCER

By

RABIA GULZAR

(NUST 00000318908-MSBI-Fall19)

(MS Bioinformatics)

Supervised by:

Prof. Dr. Ishrat Jabeen

SCHOOL OF INTERDISCPLINARY ENGINEERING

AND SCIENCES (SINES).

National University of Science and Technology (NUST)

Islamabad, Pakistan.

Date: July 2022

Dedication

I dedicate this work to my beloved Parents for their prayers, love, support, and most of all their huge believe in me and my dreams. Thanks For enlightening me and making me who I am.

Certificate of Originality

I hereby certified that this thesis is based on my own research and struggle. Furthermore, none of its contents have been plagiarized or submitted for a higher degree. Other people's contributions to this project are acknowledged and referenced.

_____

Rabia Gulzar
(NUST00000318908-MSBI-Fall21)

ACKNOWLEDGMENT

[Glory be to You; we have no knowledge except what you have taught us. Verily, it is You, the All-Knower, the All-Wise. (Surah Baqarah-2:32)]

Allah-there is no deity except Him, the Ever-Living, the Sustainer of [all] existence. We pay our all gratitude to Allah, the Almighty, from whom we seek help, and, in whose premises, there are all lives and matters. We are obligated to Him for all knowledge He has provided us in the completion of this project. I would like to pay my gratitude towards Allah Almighty as it was my faith and believe that reminded me that for every sickness there is cure which help in inclination towards this research.

This research journey would not have been possible without constant guidance and support of my Supervisor Dr. Ishrat Jabeen, who taught me about hard work and dedication research work necessitate. I am deeply indebted for her precious advice, time, efficient contribution, and supervision during my work. I could not have imagined having a better advisor and mentor for my study. I would also like to thank my guidance committee members: Dr. Zamir Hussain and Dr. Muhammad Tariq Saeed from SINES, NUST for their encouragement and insightful comments. I would like to thank all the faculty members and lab assistants at SINES, NUST for their guidance and support.

I would like to acknowledge my parents Gulzar Hussain and Naseera Bano (Late), who believe in me, when I was failing to do the same. I would also like to thank my husband M.Zia ul Haq, for his constant support. He not only provided me with the financial aid to acquire this degree but also remain a constant emotional support during the overwhelming research phase. I would like to express thanks to my Father in law Dr. Basheer Ahmad Samim who taught me how to ask questions and search for answers not matter how hard to find.

I am grateful towards my fellow research group fellows Mah e Hareem, Fatima Ali Khan, Laiba Fatima, Marvah Mehmood Rana, Talha Sarfraz, Awais Attique and Umar Amjad. They not only supported me during my research but also helped in get back on my feet during research setbacks. I would also like to pay my thanks to my seniors Dr.Yusra Sajid Kiyani and Humaira

Ismatullah as they share their knowledge and research experience which help me during my research.

Last but not the least, I would like to acknowledge National Institute of Information Technology and SINES and especially IT staff for providing the infrastructure that made this research possible.

Contents

List of Tables:

List of Figures:

Figure 2.4: The compounds KYT-0353 (2), (Z)-4-chloro-N-(4-(trifluoromethoxy) phenyl) -5H-1,2,3-dithiazol-5-imine (3), and (Z)-2-Amino-2-norbornanecarboxylic acid (BCH) (1) are inhibitors of the large neutral amino acid transporter 1 (LAT1)..

Figure 3.1: The Overall workflow diagram of methodology (Molecular Modeling). First, the data collection was done. LAT1 structural and chemical data was collected and preprocessed. The screening set of LAT1 ligands was generated using molecular docking. Molecular modeling steps were performed on LAT1 dataset. Docking results were evaluated using molecular dynamics (MD) simulations. The binding pattern was identified which helped in the selection of template. Further, the predictive modeling was executed using template and rest of dataset to generate conformations. Template was used for the selection of features. The final model was evaluated.

Figure 3.2: Binding pocket of LAT1 along with the binding residues important in Ligand-Protein interaction.

Figure 3.2.1: Protocol of Molecular Docking. The biological data was retrieved from Protein Databank under the PDB id 6IRT. However, the chemical data of 58 ligands were collected from Chembl, and Literature. Then molecular docking was performed by GOLD software where binding pocket was identified. By taking the coordinates 3.7800 (X), 3.4725 (Y), and -0.9642 (Z) docking was performed. After that, the pose analysis and selection were made for correlation analysis and binding hypothesis formation.

Figure 3.3: Overall workflow of Molecular Dynamics Simulations of selected ligand complex. This process was done by moving LAT1 Complexes from the docked complex and processed towards system building. After energy minimization MD production for 100nsec was made and the results were analyzed by means of trajectory analysis.

Figure 3.4: Overall workflow of structure-based Pharmacophore Model Generation using stable complex from MD simulation studies. The step was done by extracting the feature from the template and generation of confirmation from rest of the ligand data. Based on features, model was generated and screened against the packed confirmation for internal set validation.

Figure 4.2: Protein RMSD plot of LAT1 protein after MD. RMSD stabilized after 250ns at 2.0-2.4Å.

9

Figure.4.2.1: Protein RMSF plot of stabilized LAT1 complex Two regions (221-243 & 421-424) showed fluctuations due to the presence of loops.

Figure 4.2.2: The 3D structure of LAT1. The pink region shows the loop area in both diagram which corresponds to amino acid residues (Lys221-Asp223) and (Arg421-Glu424) respectively.

Figure 4.3: Correlation plots between biological activity values (pIC_{50}) and Molecular weight. The R in the plots denotes the correlation coefficient which shows direct positive correlation.

Figure 4.4: Correlation plots between biological activity values (pIC_{50}) and Gold Fitness Score. The R2 in the plots denotes the correlation coefficient

Figure 4.5: The docking results of Top poses of LAT1 Representation of Gold Score on X-axis and biological activity (pIC_{50}) on Y-axis. The red data points are ligand 1,2,8,13,54 and 58.

Figure 4.6: Correlation plots between biological activity values and logP(o/w). The R2 in the plots denotes the correlation coefficient.

Figure 4.7: Protein-ligand interactions of selected ligands docked on LAT1 complex. (A.) Ligand_1 showed interactions with P336, G197, T259, L333 (B.) Ligand_2 does not show any interaction before MD simulation (C.) Liagnd_3 showed unique interactions with P142, P338, G341 (D.) Ligand_4 showed interactions with I140, A141, P336 and (E.) Ligand_5 interacted with I140, A141. (F.) Ligand_6 interacted with S144.

Figure 4.8: RMSD plots of protein-ligand complex_1 of active ligand 1, the complex showed less deviation after 40ns. X-axis represents the time duration of MD Simulation in nano seconds while Y-axis shows the RMSD deviation from the backbone structure.

Figure 4.9: RMSD plots of protein-ligand complex_2 with active ligand 2, ligand_2 stabilized after 40ns with less deviations. X-axis represents the time duration of MD Simulation in nano seconds while Y-axis shows the RMSD deviation from the backbone structure.

Figure 4.10: RMSD plots of protein-ligand complex_3 of active ligand 8, ligand_8 stabilized after 50ns with less deviations. X-axis represents the time duration of MD Simulation in nano seconds while Y-axis shows the RMSD deviation from the backbone structure.

Figure 4.11: RMSD plots of protein-ligand complexes of inactive ligand_54. X-axis represents the time duration of MD Simulation in nano seconds while Y-axis shows the RMSD deviation from the backbone structure.

Figure 4.12: RMSD plots of protein-ligand complexes of active ligand_13. X-axis represents the time duration of MD Simulation in nano seconds while Y-axis shows the RMSD deviation from the backbone structure.

Figure 4.13: RMSD plots of protein-ligand complex_6 of inactive ligand_58 which does not show stability throughout 100ns simulation time. X-axis represents the time duration of MD Simulation in nano seconds while Y-axis shows the RMSD deviation from the backbone structure.

Figure 4.14: H-bond plot analysis of protein complex with ligand_1. The protein residues, S66, L204, T259, A141, G136, P252, S338 had a stable interaction with ligand.

Figure 4.15: H-bond plot of ligand_2 protein complex. T259, Arg141, Gly256, Phe252, Phe400 had a stable interaction in the simulation time of 100ns.

Figure 4.16: Some protein residues Arg141, Lys204, Tyr259, Phe252, Ser338, Gly197, Ser66 showed highly stable interaction pattern throughout simulation time in protein complex with ligand_3.

Figure 4.17: H-bond plot of ligand_4. The residues Arg141, Ser144, Ser342, Tyr259, Ile140, Ser338 showed stable interactions throughout the simulation time.

Figure 4.18: H-bond plot of ligand_5. Asp116, Lys132, Asn258, Gly136, Tyr259, Ser342, Tyr103 had stable interactions throughout the simulation time.

Figure 4.19: H-bond plot of ligand_6 protein complex. Ligand showed a stable interaction with protein residues, Ser144, Phe252, Tyr259.

Figure 4.20: Interaction pattern of active ligand-protein complexes after MD. (A.) ligand_1 (B.) ligand_2 (C.) ligand_3 (D.) ligand_4 (E.) ligand_5 and (F.) Ligand_6

List of Abbreviations

LAT1	L-Type amino acid transporter 1
CD98	cell-surface glycoprotein
GLUT1	Glucose transporter 1
SLC7A5	solute-carrier-family-7 member 5
SLC3A2	solute-carrier-family-3 member 2
BBB	Blood Brain Barrier
BCH	2-Aminobicyclo-(2,2,1)-heptane-2-carboxylic acid
mTORC1	Mechanistic Target of Rapamycin kinase complex 1
HATs	heterodimeric Amino Acid Transporters
TMs	Trans membranes
ECD	Extra cellular Domain
GBM	Glioblastoma
ASCT2	Alanine, Serine, Cysteine Transporter 2
MYC	Proto-oncogenes
EZH2	Enhancer of zeste homolog 2
S6K1	Ribosomal protein S6-kinase-1
4E-BP1	Eukaryotic-translation initiation factor-4E (eIF4E)binding protein
GSH	Glutathione
αKG	Alpha keto glutarate
NADPH	Nicotinamide Adenine Dinucleotide Phosphate
FADH2	Flavin adenine dinucleotide.

BRM	Biological Regulatory Mechanistic
cAMP	Cyclic AMP
Cryo-EM	Cryo-Electron Microscopy
IC$_{50}$	Half-maximal inhibitory concentration
pIC$_{50}$	Negative log of Half-maximal inhibitory concentration
PKA	Protein Kinase A
MMFF94X	Merck Molecular Force field
MOE	Molecular Operating Environment
QSAR	Quantitative Structural Activity Relationship
GRIND	GRID independent Descriptor
CLACC	Consistently large and auto cross-correlation
HBA	Hydrogen bond acceptor
HBD	Hydrogen bond donor
PLS	Partial least square analysis
MDS	Molecular Dynamics Simulation
RMSD	Root Mean Square Deviation RMSF Residue
SMILE	Simplified Molecular-Input Line-Entry System
ChEMBL	Chemical database of European Molecular Biology Laboratory
PDB	Protein data bank
GOLD	Genetic algorithm of ligand docking
MD	Molecular dynamics
RMSD	Root mean square deviations
RMSF	Root mean square fluctuations

MCC	Matthews correlation coefficient
Nsec	Nano seconds
nM	Nano Molar
µM	Micro Molar

Abstract:

The hallmark of cancerous cells is chronic proliferation for which they rely heavily on nutrients like essential amino acids. Membrane transporters strictly control the uptake of essential amino acids across the cell membrane. Among many membrane transporters, LAT1 (SLC7A5), an L-type amino acid transporter, has been frequently reported overexpressed in a wide range of malignancies. Many studies confirm that LAT1 modulation inhibits protein synthesis in cancer cells by downregulation of the mTORC1 signaling pathway and by the activation of General Amino Acid Control (GAAC) pathway. LAT1 is thus a potential molecular target for cancer diagnostics and treatment.

This study aims to explore LAT1 as a potential drug target against variety of cancers and helps in the identification of most important features of LAT1 inhibitors. For this purpose, approaches like MD simulation has been used for the structural modeling of LAT1. Inhibitors data against LAT1 is collected from through literature study and chembl database, which leads to database of 72 inhibitors against LAT1. Most stable 3D binding conformation of the target protein after MD simulation was used for 3D Molecular modeling and predictive modeling. The docking experiments have been used to probe the best binding conformation of the ligands with the target protein and to formulate a binding hypothesis. To further investigate our binding hypothesis, pose analysis was performed which leads to the discovery of some important protein-ligand interactions. To validate this hypothesis, MD simulation of some ligand complexes was performed to evaluate the ligand-protein interaction profiles and to evaluate protein residues responsible for binding highly active compounds towards target protein such as Ser66, Lys204, Tyr259 and Phe252. The most stable complex after the MD simulations was selected as a template for the pharmacophore query building. The model was developed with the accuracy of 95% having one hydrogen bond donor (Ser66), and three hydrophobic features (Tyr259, Lys204, and Phe252), which might have the ability to inhibit LAT1 in variety of cancers. The LAT1 inhibitors dataset was used for screening the pharmacophore model. The resultant hits proposed that our model can differentiate between active and inactive compounds with up to 95% accuracy. In this research work, we outline recent breakthroughs in our understanding of LAT1's role in cancer, as well as preclinical studies. Because of LAT1 inhibitors' unique mode of action, it could help treat several cancers that are

resistant to conventional treatments, whether alone or in combination with other anti-tumor medications.

CHAPTER 1

INTRODUCTION

INTRODUCTION

1.1 Importance of amino acid transporter in cancer

Transporters are membrane proteins that allow selected organic and inorganic solutes to pass through the plasma membrane and the membrane of intracellular organelles. System-L refers to a group of amino acid transporters that are sodium and pH independent and transport large neutral amino acids across the plasma membrane [4]. Amino acids are required for cellular development, protein synthesis, and metabolism to occur. LAT1, LAT2, LAT3, and LAT4 are the four transporters that make up this system. Only LAT1 and LAT2 are heterodimers with a disulfide bond connecting one catalytic light chain (SLC7A5) and a heavy chain (CD98). In this order, LAT1 mediates the transport of aromatic branched chain or bulky neutral amino acids: Phe > Trp > Leu > Ile > Met > His > Tyr > Val [15]. Despite the fact that it is unable to transport anionic or cationic amino acids, it has a tissue distribution that is distinct from that of other system L transporters. It is always highly expressed in cells that require a steady supply of energy, such as placental cells, blood-brain-barrier endothelial cells, neural glial cells, and activated T-cells [41]. Furthermore, LAT1 is invariably overexpressed in metastases and malignancies among all the system L transporters. LAT has many different types and there is huge similarity between LAT1 and LAT2 and many inhibitors are unable to differentiate between these two such as BCH. This highly similarity of these two transporters can lead to the off-target toxicity which can be controlled by increasing the specificity of drug towards the LAT1 such as JPH203. It is designed using the structure-activity (SAR) relationship of LAT1 ligands. In preclinical tests, it reduces tumor growth in vivo without causing severe harm at dosages sufficient to suppress tumor growth. Overexpression of LAT1 has been linked to a poor prognosis and patient survival in a variety of malignancies, including breast, lungs, prostate, head and neck, colorectal, and gliomas. As a result, LAT1 has sparked a lot of interest as a diagnostic medicine, but more crucially as a therapeutic drug target that can stop cancer cells from multiplying [37].
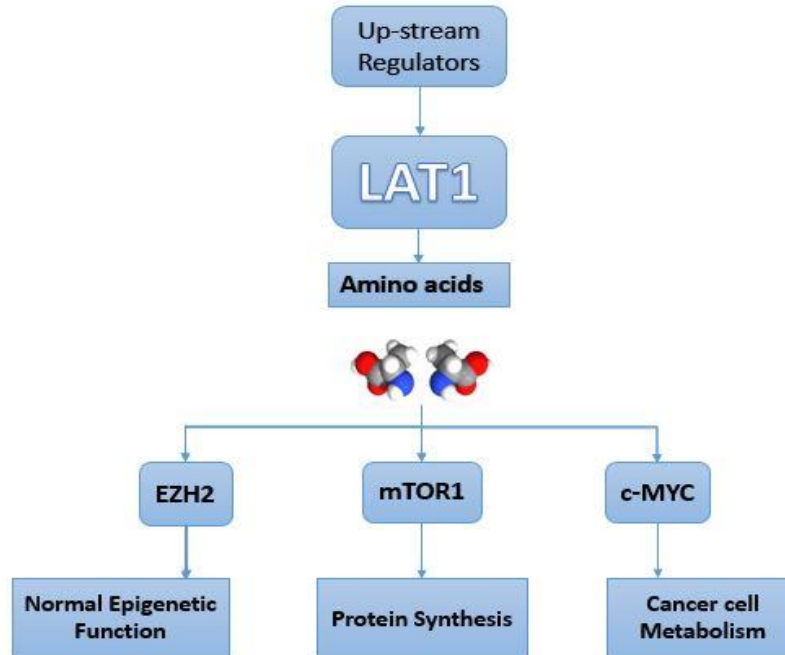
Figure 1.1: Downstream regulation of LAT1 and how it enhances cancer progression.

Many chemotherapeutic drugs such as BCH, Quinolones are developed to prevent nucleic acid biosynthesis in rapidly proliferating cells. As a result, systematic chemotherapies are thought to be highly cytotoxic to the physiologically fast development of some normal cells, resulting in a variety of negative side effects [61]. As a result, many established targeted medications in recent decades have been engineered to target specific molecular cancer cells, sparing non-target organs while maintaining therapeutic impact [12]. Despite the availability of the most advanced targeted drug therapies, as monotherapy or in combination to combat the heterogeneous character of tumors, they are insufficient to prevent drug resistance from developing. As a result, novel molecular targets are urgently needed to overcome these difficult anti-cancer hurdles [10].

Cancer cells regulate their metabolic needs on their own, and they almost always find a method to fuel their uncontrolled reproduction and growth. Glucose hyper metabolism (GLUT1 overexpression) has been used as a cancer biomarker; however, it is not unique to cancer [8]. On the other hand, because no normal organ hyper metabolizes amino acids physiologically, hyper metabolism of amino acids is regarded a potential cancer biomarker in relation to tumor selectivity and has fewer negative effects for normal cells [5].

INTRODUCTION

The major transporter of large neutral and branched chain amino acids, L-type amino acid transporter 1 (LAT1), provides critical amino acids and is overexpressed in many cancers [11]. LAT1 contributes to the increased need for bulk protein synthesis, which in turn promotes cell survival and proliferation. Various studies have shown that inhibiting LAT1 causes a delay in tumor growth by inhibiting the uptake of essential amino acids, proving that LAT1 is a promising molecular target for targeted cancer treatment [3].

1.2 L-Type Amino Acid Transporter 1

LAT1 (SLC7A5) belongs to the L type system transporter subfamily, which also contains LAT2, LAT3, and LAT4 of the SLC7 amino acid transporter family. It aids in the movement of large and neutral branched-chain amino acids. As a LAT1/CD98 complex, LAT1 forms a heterodimeric complex with CD98, also known as 4F2hc (SLC3A2). Although CD98 is not directly engaged in the transportation mechanism, it serves as a molecular chaperone, providing stability to the complex at the plasma membrane, allowing it to carry out its function appropriately [13].

LAT1 is primarily responsible for transporting necessary amino acids through the BBB and placenta. Many medicines that are related to amino acids, such as melphalan, L-DOPA, BCH, baclofen, thyroxine (T4), triiodothyronine (T3), and gabapentin, are transported through LAT1 [17]. Breast cancer, glioma, pancreatic cancer, stomach cancer, cancer of the oesophagus, tongue, larynx, hypopharynx, hepatic cancer, renal cell carcinoma, and ovarian cancer are among the malignancies in which LAT1 is invariably elevated. LAT1 expression is very low in normal cells. BBB epithelial cells, monocytes, macrophages, the placenta, pancreatic beta cells, and the testis are all known to express it. As a result, LAT1 is an excellent molecular target for cancer treatment. When compared to external substrates, LAT1 has a high affinity for intracellular substrates, indicating that intracellular substrate concentration influences the rate of substrate transport [25]. As a result, rational drug design for LAT1-targeting medicines requires the following: 1) LAT1-specific inhibitors, 2) non-transportable inhibitors, and 3) viable with high affinity LAT1 substrates are critical not just for protein synthesis, but also for the replenishment of tricarboxylic acid cycle intermediates, which are used to create other macromolecules such as nucleotides, which are required for malignant cells' survival and uncontrolled growth [31]. Sestrin2 recognizes one of LAT1's substrates, Leucine, which activates mTORC1 (Mechanistic

target of rapamycin kinase complex 1), which promotes cell survival and proliferation while inhibiting autophagy and apoptosis [22]. In **Figure 1.2** 3D molecular structure of LAT1 is shown which is downloaded from PDB in inward open conformation (ID: 6IRT) [28]. LAT1 has two subunits, one is heavy chain subunit (4F2hc), and the other is light chain subunit (LAT1). Blue represents the CD98 while the Turquoise color represents the transporter unit LAT1. These two subunits form a heterodimeric amino acid transporter complex together. LAT1 interacts with 4F2 cell surface antigen heavy chain which is also known as the type II Glycoprotein, essential for the stabilization of LAT1 on plasma membrane.
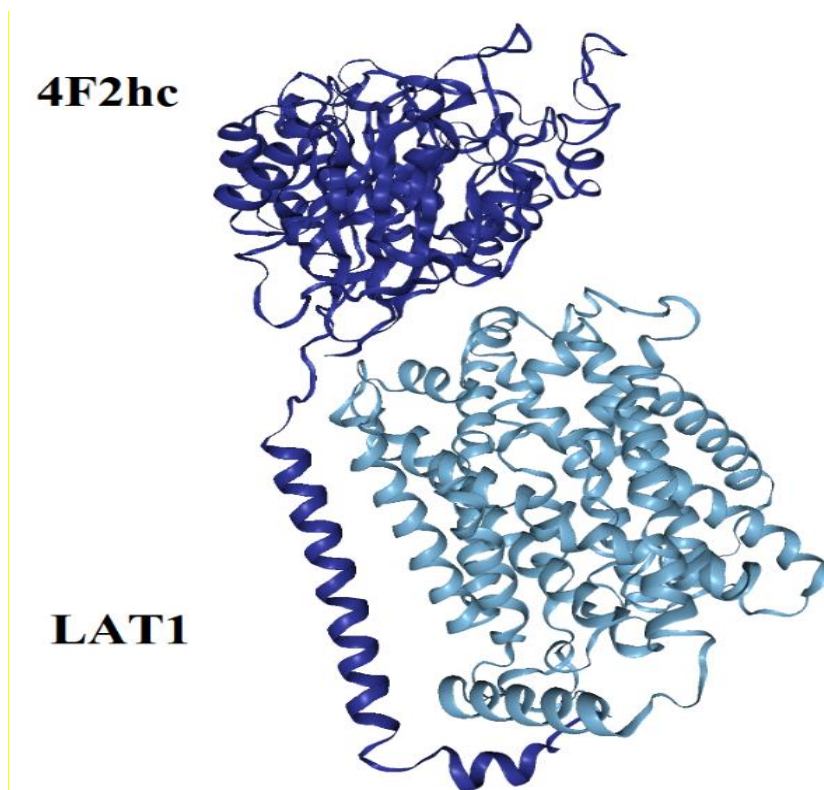

Figure 1.2: MD Molecular structure of LAT1 retrieved from Protein Data Bank under the PDB ID 6IRT. Upper part shows the CD98/SLC3A2 subunit which act as a molecular chaperone and help in the stabilization of LAT1 during transportation, while the lower part is LAT1/SLC7A5 which has the main transporter role.

1.3 Structural features of LAT1-CD98 complex

Lat1 being a significant member of heterodimeric amino acid transporter family (HATs), which are made up of two subunits: the light chain subunit (SLC7), which facilitates amino acid transport, and the heavy chain subunit (SLC3), which acts as a molecular chaperone and aids in the localization and stabilization of the transporter unit (light chain unit) at the cell membrane. LAT1 is made up of 12 hypothetical trans membrane segments (TMs) organized in two layers. TMs (1, 3, 6, 8, and 10) make up the inward layer, which is encircled by TMs on the outside (2, 4, 5, 7, 9, 11, and 12) [23].

LAT1's N and C terminals are found intracellularly, while CD98's N and C terminals are found both intracellularly and extracellularly [17]. The 4F2hc heavy chain subunit is a TYPE II membrane N-glycoprotein with four potential N-glycosylation sites: N264, 280, 323, and 405. It has one big extracellular domain and one trans membrane domain (ECD) [18]. Through a conserved disulfide bond, LAT1 and CD98 are covalently connected. This link exists between the light chain's putative extracellular loop and the heavy chain's cysteine (C164, C109), which are placed significantly apart from the TMs of 4F2hc. Extracellularly, LAT1 is believed to be covered by CD98's extracellular domain, and both subunits are involved in suspected non-covalent interactions [22]. In **figure 1.3**, Cryo-EM map of LAT1-4F2fc co plex is shown, Blue color represents CD98 subunit while the turquoise color represents LAT1 subunit, respectively. The trans membrane segments are shown and numbered from 1 to 12, LAT1's 12 trans membrane segments are folded into the conventional LeuT fold. A short loop disrupts LAT1's TM1 and TM6, resulting in the half helices TM1a/1b and TM6a/6b. The cryo-EM map did not show the N-terminal residues 1–162 for 4F2hc and 1–50 for LAT1. LAT1's extracellular loop 5–6 (EL5–6) joins the TM5 and TM6 trans membrane regions. Because of its flexibility and the side chains in this, it was poorly resolved. There were no loops assigned. The sequences, except for these locations, Both LAT1 and 4F2hc were resolved clearly [13].
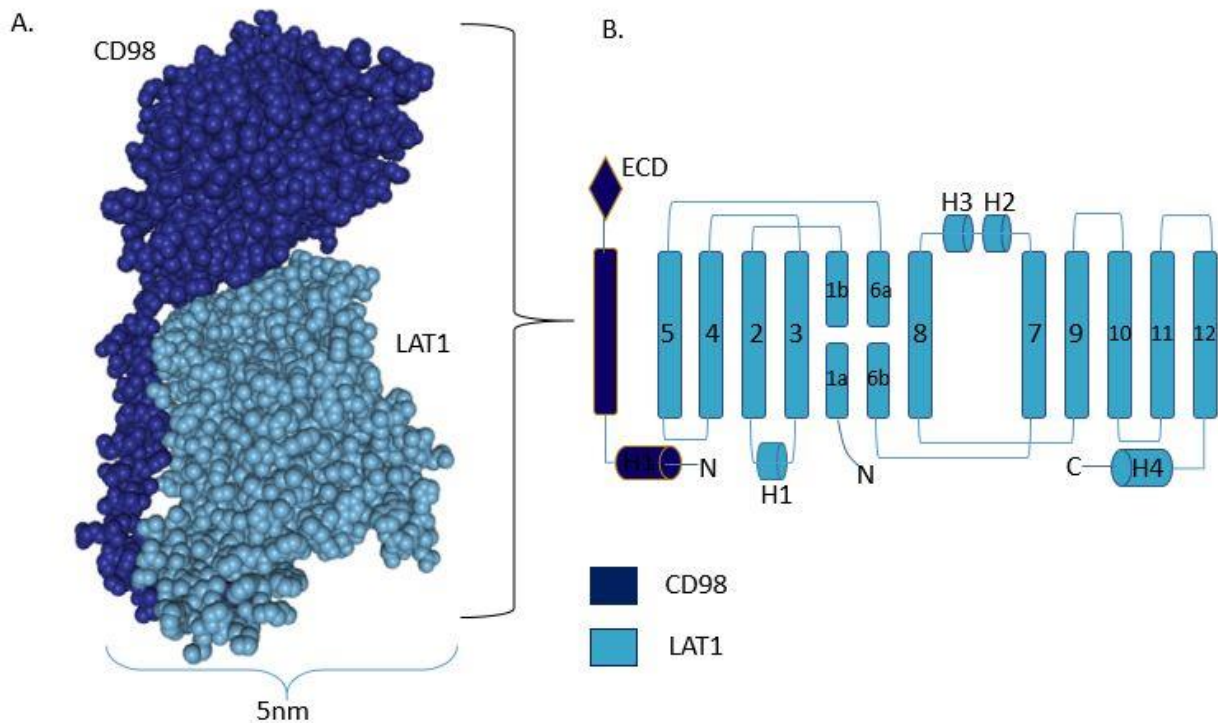
Figure 1.3: LAT1–4F2hc topology model. LAT1 has 12 putative trans membrane segments (TMs) and connects to 4F2hc via a conserved disulfide bridge between C164 and C109. 4F2hc is a type II membrane N-glycoprotein having an internal N-terminus and an extracellular C-terminus (one TM; four glycosylation sites in the extracellular domain: N264, N280, N323, and N405).

1.4 Mechanism of Substrate Translocation

The so-called "Rocking Bundle Alternating Access Method" is the most probable mechanism for the translocation of substrate through the plasma-membrane of LAT1 and other proteins with a "LeuT-like fold" [12]. The coupling of intracellular and extracellular gates at a centrally positioned substrate binding site is promoted in this classic paradigm by the binding of substrate between two structurally dissimilar domains. The scaffold domain is represented by TM3, TM4, TM8, and TM9 in the LeuT-fold mechanism, while the core domain is represented by TM2, TM1, TM6, and TM7 [11].

Between the two domains, the TM5 and TM10 serve as a linker **(Figure 1.4)**. The substrate binding is enabled when the outward facing gate opens. The substrate is subsequently released

into the cytosol once the intracellular gate is opened. To transport substrate across the plasma membrane, LAT1 undergoes several conformational changes [32]. Based on the structural findings, a workable model for HATs was presented in **figure 1.4**, in which the core domain rotated towards the hash domain to close the inward gate as an inner facing conformation transited to an outward facing conformation, which might be evoked by substrate interaction. Meanwhile, the unwinding regions of TM1 and TM6 undergo a conformational shift to allow substrate to be accommodated in the LAT1's outward facing conformations [38]. Following that, TM1b and TM6a undergo further rotations to start the transition to the outward facing open conformation and push the gating residue Phe252 out of the occluded state, causing substrate release. TM1a and TM6b essentially remain in the same position throughout the operation, but TM2 and TM7 rotate somewhat. The extracellular domain of the heavy chain CD98 rotates as well, assisting in the stability of LAT1 during the transport cycle [37].
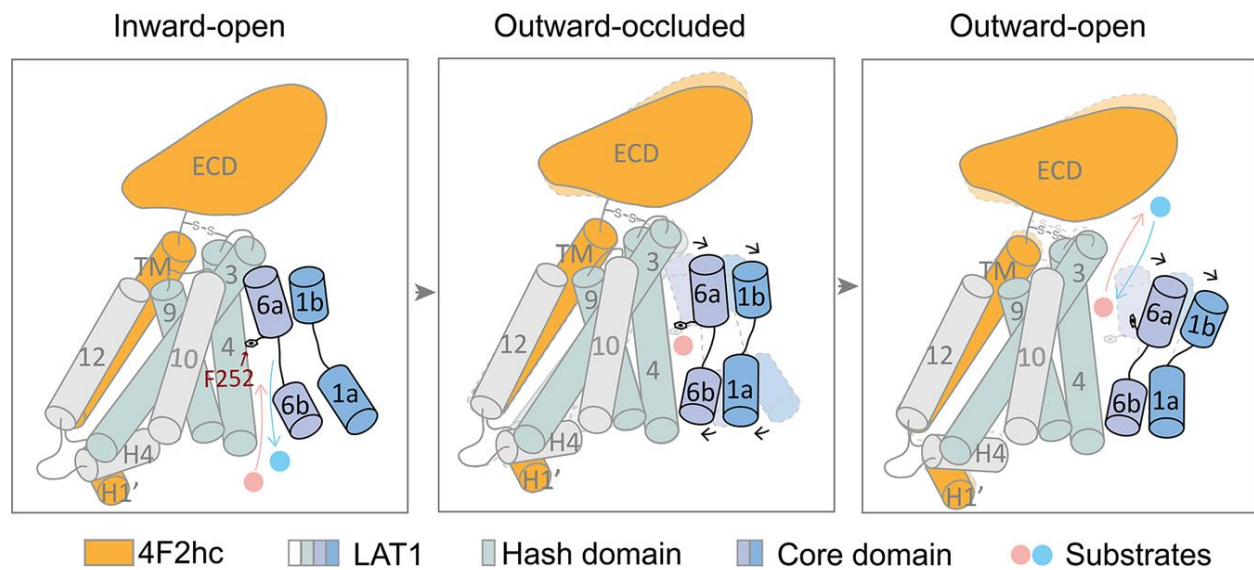
Figure 1.4: A Functional working model for the LAT1-4F2hc complex substrate translocation.

The model depicts (**figure 1.4**) the LAT1 transport mechanism. TM1a and TM6b spin to the hash domain to close the inward gate when LAT1 loads substrates in the cytoplasm. TM1a and TM6b continue to spin throughout the switch from the inward-facing conformation to the outward-facing conformation, whereas TM1b and TM6a begin to rotate away from the hash domain. The gating residue Phe252 is then pushed away from the occluded conformation by TM1b and TM6a, enabling substrate release. The core domain's TM2 and TM7, as well as the

hash domain's TM8, are not presented here for clarity. ECD stands for extracellular domain. The letter H stands for helix. TM stands for transmembrane helix [29].

1.5 Risk factors

Molecular heterogeneity associated with cancers are responsible for the least understood molecular pathogenesis mechanisms. Among the most influential risk factors of cancer some of the most important ones are lifestyle/demographic factors, genetic and epigenetic alterations and uncontrolled signaling pathways that collectively adds toward inception and proliferation of cancers. In addition to all these factors, some other germline mutations play key roles in the process of tumor initiation and progression. Moreover, the hyper activation of gene products in the integrated signaling networks is primarily responsible for the uncontrolled growth of signals, leading towards cell proliferation, cell differentiation and cell motility.

1.6 Proposed Strategy

Increased uptake of amino acids by L-type amino acid transporter 1 may induces cell growth and proliferation in different types of cancers causing uncontrolled cellular growth and proliferation. To overcome this problem, we proposed the modulation of LAT-1 by drug like compounds which may add in the regulation of cell growth/apoptosis in cancerous cells.

1.7 Objectives

These are some of the objectives of my research:

- To probe the binding hypothesis of new chemical agents for the chemotherapeutic treatment of cancer
- Validation of Binding Hypothesis and to evaluate the stability of extracted 3D feature.
- Predictive Pharmacophore model building and validation strategies

CHAPTER 2

LITERATURE REVIEW

2.1 Structural Topology of LAT1

LAT1's structure is made up of 12 transmembrane helices (TMs) structured in a 5+5 two-fold inverted repeat pattern. The other component is CD98hc (4F2hc, SLC3A2), a glycoprotein that is covalently linked to LAT1 via a conserved disulfide bond. According to reports, LAT1 is the lone transporter unit, whereas 4F2hc serves as a molecular chaperone that aids in the localization and stability of LAT1 at the plasma membrane [25]. LAT1 is a light chain protein, whereas CD98hc is a heavy chain protein, and the two are linked by a conserved disulfide bond to create a heterodimeric complex that belongs to the HATs family of heterodimeric amino acid transporters. LAT1 has 12 transmembrane helices (TMs) **figure 2.2**, which are architecturally similar to other bacterial members of the amino acid polyamine organocation family, commonly known as the APC family. A "LeuT-like fold" is embraced by this family [34]. The 12 TMs are made up of 10 core TMs as well as TM11 and TM12. The ten core TMs, like the rest of the APC family, are separated into three functional domains: hash (TMs 3, 4, 8, and 9), bundle (TMs 1, 2, 6, and 7) and arms (TMs 1, 2, 6, and 7). (TMs 5 and 10). The fragmented structure of the TM1 and TM6 helices is disentangled in the center to create 1a-1b; 6a-6b, which houses the ligand binding site **figure 2.2**.

Trans membrane unit 1a and 1b are connected by residues Ile64-Ser66, whereas TM6a and 6b are joined by residues Y254-N258 [41]. The cryo-EM map resolves the majority of the loops. On the extracellular side, there are six extracellular loops (EL1-6) and five intracellular loops (IL1-5) while on the intrinsic side, there are five intracellular loops (IL1-5) The longest extended loop in this model is EL3, which is 26 residues long and connects TM5 and TM6 with V217-N242 [11]. Because modelling such large loops is difficult, the predicted loop structure must be regarded as speculative, and it may or may not have a major impact on the outcomes of docking experiments. TM1a and 6b fluctuate towards the lipid bilayer, forming a solvent-exposed region on the cytoplasmic side, according to structural studies [15]. Many hydrophilic residues border this region, forming a possible substrate route. This cavity creates a cytoplasmic gate in other APC members, hence LAT1's cytoplasmic gate is open in the current circumstance. There is a conserved substrate binding site at the end of this cavity that is seen in all APC transporters. Sitemap was used to investigate if LAT1 has a well-defined binding pocket. TMs 1, 3, 6, 8, and 10 surround the binding site [31]. The amphiphilic helices that surround the binding site are generally made up of both hydrophilic and hydrophobic residues. Tyr62, Ile63, Ile64, Ser66,

Gly67, Phe252, Asn253, Tyr259, and Glu255 are the anticipated binding site residues, which are consistent with earlier findings. The binding pocket's site score is 1.18, with a value of >1 being regarded promising [30]. The pocket has a total surface area of 5382, with hydrophobic and hydrophilic areas of 1682 and 2852, respectively. Unlike LAT1, the AdiC pocket has a surface area of 324.582, with hydrophobic and hydrophilic areas of 75.12 and 216.32, respectively. The existence of a big non-polar region in LAT-1 might clarify why hydrophobic and neutral amino acids are preferentially transported with a high affinity (Km = 1550 M), whereas AdiC largely transfers charged arginine and agmatine [29].
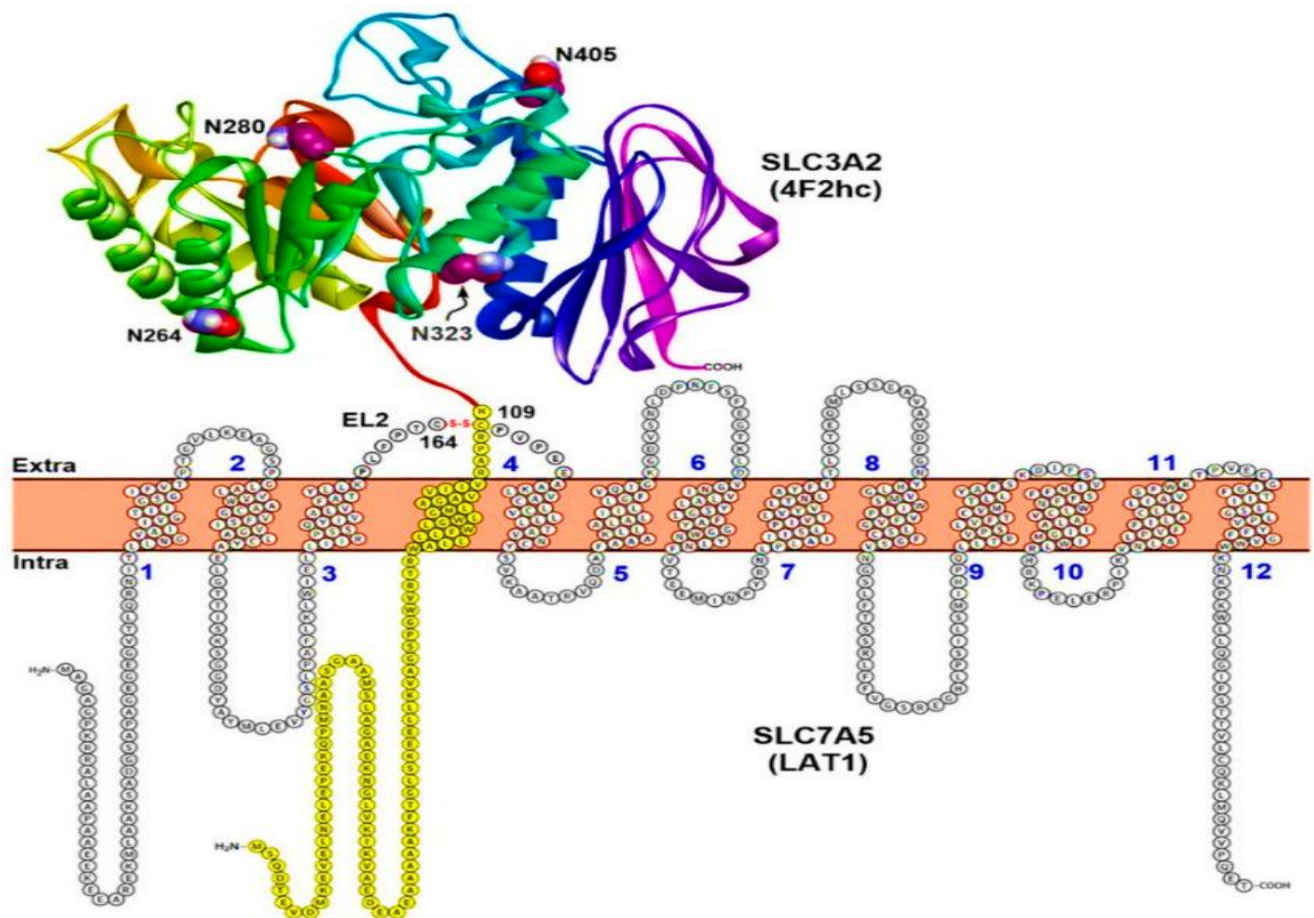
Figure 2.2: Model of LAT1-topology. 4F2hc's The conserved disulfide bridge between C164 and C109 connects LAT1, which has 12 putative transmembrane segments (TMs), to 4F2hc. The protein 4F2hc is a type II membrane N-glycoprotein with an internal N-terminus and an extracellular C-terminus (one TM, in yellow; four glycosylation sites in the extracellular domain: N264, N280, N323, and N405 are depicted in space-filling style with carbon atoms coloured

maroon). LAT1, in contrast, lacks glycosylation and possesses an intracellular N- and C-terminus. The extracellular domain (ED) of human 4F2hc's crystal structure is depicted in ribbon form (PDB ID: 2DH2) [38].

F394, the hypothesized upper front gating residue of LAT1, whereas Ser66 and Phe252 are the proximal gating residues, and Ser342 is the intermediate layer. LAT1 distal residues, like AdiC, engage in a hydrogen bond network, indicating that the transport mechanism is conserved. Many hydrophobic residues in LAT1, such as aliphatic Ile139, Ile140, Val148, and aromatic Phe252, Phe402, and Trp405, appear to promote binding of substrate via hydrophobic interactions and Vander Waals forces (e.g., π−π and alkyl) [11]. The proximal pocket, distal pocket, positive and negative poles make up LAT1's substrate binding site. Primary side chains are accommodated in the proximal pocket, whereas hydrophobic secondary substitutions are bound in the distal pocket. The carboxyl and amino groups of the substrate are recognized by the positive and negative poles, respectively [43]. The aromatic and heavy branched chain amino acids, notably leucine, tryptophan, and phenylalanine, have a high affinity for LAT1. It has a lesser affinity for glutamine, threonine, and proline, and it does not recognize alanine or charged amino acids. LAT1 is implicated in "Glutamine addiction," a basic characteristic of cancer, due to its propensity to swap glutamine with other amino acids. LAT1 and its companion ASCT2 are involved in the glutamine and leucine transport cycle **figure 2.3**, which is important for cancer development and progression. It is, in fact, regarded as a prognostic indicator of malignancy [23].

2.2 Ongoing Treatments and Research Involving LAT1

Because LAT1 is highly expressed in tumors, it is thought that blocking its activity might diminish tumor cell growth, indicating that it could be a promising target for new anticancer medicines [13]. As a result, a cancer therapy that targets LAT1 might be an inhibitor that denies vital nutrients to malignant cells or a cytotoxic LAT1 substrate with an inherent target. LAT1 inhibitors are commonly used in conjunction with chemotherapy to improve anti-tumor efficacy. Despite widespread pharmacological interest, there are currently just a few strong LAT1 inhibitors on the market, necessitating the discovery of new inhibitors in the field [32].

BCH, or 2-amino-2-norbornane carboxylic acid, is a low affinity, non-selective inhibitor of the L-type amino acid transporter family that is reported to reduce tumor cell proliferation and death.

The antiproliferative actions of BCH need a very high concentration (>10mM). With an IC_{50} of 0.14 in S2 cells and 0.06 in human colon cancer cells, the new tyrosine analogue JPH-203 is a very potent and specific inhibitor of LAT1 [25]. Other amino acid-based LAT1 inhibitors, such as substrate tyrosine derivatives like Diiodo-Tyr, various meta-substituted phenylalanine derivatives, and KMH-233, have been described in addition to JPH203 and JPH203-related structures. Other modified amino acids, such as conformationally limited phenylalanine derivatives, have been found to be enhanced LAT-1 substrates in addition to amino acid-based inhibitors [31]. When compared to the clinically approved drug melphalan, the alkylating agent DL-2-amino-7-bis[(2-chloroethyl) amino]-l,2,3,4-tetrahydro-2-naphthoic acid has been shown to be a potent competitive inhibitor of BCH transport in murine L1210 leukemic cells, with enhanced in vitro antitumor activity and reduced myeloid-suppressive activity 36[]. Furthermore, a recent study found that irreversible inhibitors based on 1,2,3-dithiazole had a high effect inhibition potential against LAT1 in proteoliposomes [31].

In several tests, upregulation of LAT1 has been shown in human cancers such as cholangiocarcinoma, malignant glioma, multiple myeloma, and lung, bladder, bone, pancreatic, thyroid, prostate, uterine cervix, breast cancer, and other malignancies compared to benign tissue as a control [8]. The importance of LAT1 as a prognostic biomarker for the prediction of outcomes of many forms of cancer has been highlighted by a relationship between LAT1 overexpression and considerably shorter survival in several types of malignancies. Amino acids are essential nutrients that drive translation, transcription, and cell development via the mammalian target of rapamycin (mTORC1) pathway [9]. It also serve as substrates for protein synthesis and cellular ATP production. In vitro, the biological importance of overexpressed LAT1 was linked to its contribution to cellular proliferation via mTORC1 pathway control. LAT1 dysregulation affects a variety of functions, ranging from intracellular-energy metabolism to neurotransmission, and pointers to metabolic reprogramming, triggering carcinogenic progression by maintaining an amino acid puddle in the cytosol and being implicated in the progression of various cancers [10].

2.3 Signaling pathway of LAT1

The most efficient strategy for LAT1 to stimulate the activity of Mechanistic Target of Rapamycin Kinase Complex 1 is to increase leucine absorption into cells (mTORC1). In cancer

cells, LAT1 not only promotes mTORC1 activity, but it also promotes MYC and EZH2 signaling. A huge supporting cast of proteins, including a chaperone protein, glutamine transporters, and upstream regulators of LAT1 expression, is required for the maintenance of high LAT1 expression and activity in cancer. By enhancing cancer cell metabolism, epigenetic regulation, and protein production, all of these variables contribute to the fast development of cancer. Upregulation of LAT1 in tumor cells affects caspase activity, causing apoptosis to be altered. Down regulation of LAT1 by BCH has shown to decrease cellular growth by inducing apoptosis via caspase-3 and caspase-7 [12, 13]. Because it transports an amino acid into the cytosol, such as (leu) and one amino acid to extracellular environment such as Glutamine, in this way it acts as an Antiporter. Leu is essential for mTORC1 activation, which phosphorylates the downstream regulator S6K1, a ribosomal protein, and 4E-BP1 which is an eukaryotic translation initiation factor [11]. All these proteins have a vital role in protein synthesis and mRNA regulation, as well as cellular growth.

Proto-oncogenes and tumour suppressor genes, such as c-Myc and E2F, has been shown to bind to promoter regions of the ASCT2 gene in the nucleus, causing altered metabolism of glutamine via SLC1A5 dysregulation **Figure 2.3**. ASCT2 is responsible for the transport of glutamine (Gln) to the extracellular environment, as well as the transport of a neutral amino acid (AA). Gln is utilised to make glutathione (GSH), an antioxidant that protects against oxidative stress. Oxidative stress suppresses apoptosis in a cascade that includes ASCT2-related caspases-2 and -9 downregulation and LAT1-related caspases-3 and -7 downregulation. Instead, Gln can be utilised to biosynthesize other components crucial for cell development, or it can be transferred in the mitochondria and entered in the glutaminolysis proocess, which produces metabolites including -KG, pyruvate, and lactate, as well as FADH2 and NADPH, which are required for the ATP synthesis **figure 2.3**. All of these variables have a role in cancer growth and proliferation, making LAT1 a promising target for anticancer treatment [15].
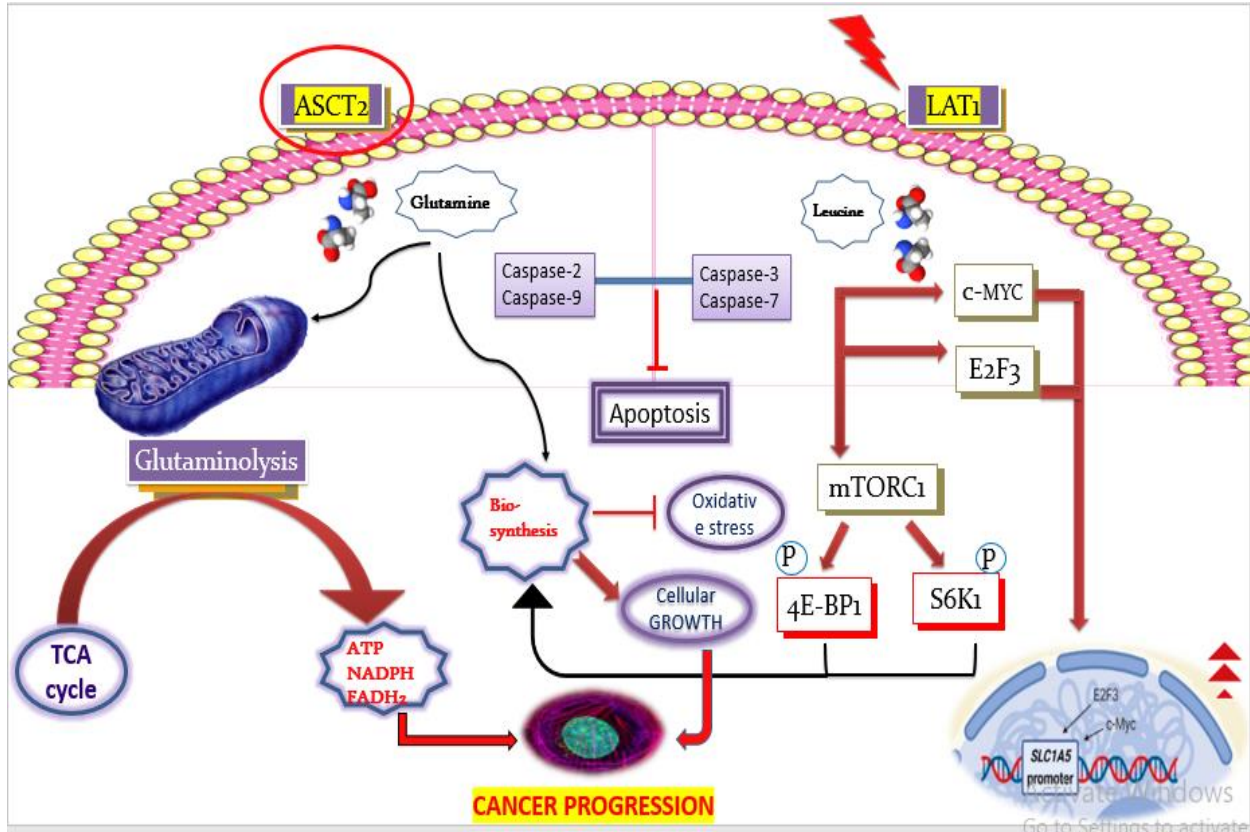
Figure 2.3: A) ASCT2 expression via Glutamine transportation into the cell. B) LAT1 expression via exchange of leucine and Glutamine.

2.4 Downregulation of LAT1 and Tumor Cell Growth

LAT1 expression was lowered through gene downregulation in numerous investigations to investigate the association between LAT1 and tumour development. Breast [14], endometrial [36], gastric [83], oral [84], ovarian [90], pancreatic [92], and prostate [17,93,94] cancer cell lines have all been shown to be inhibited by LAT1 downregulation via RNA interference. The research done in breast [14] and endometrial [36] cancer cell lines is particularly useful because it also shows that LAT1 is upregulated in patient-derived tumour tissues, implying that LAT1 has a functional role in these cancers. Zinc finger nuclease-mediated deletion of LAT1 in lung and colorectal cancer cell lines resulted in considerable reductions in cell proliferation [78].

Furthermore, downregulation of LAT1 inhibited migration and invasion of gastric and prostate cancer cell lines [17,83], indicating that the higher LAT1 expression found in metastatic lesions relative to the originating location [104] may play a role in metastasis development.

2.5 Drug-Mediated Inhibition of LAT1

Finding new chemotherapeutic medicines to use in conjunction with current anticancer medications for the treatment of various tumors was the primary motivation behind the early discovery of LAT1-targeting ligands [8, 9]. Despite the intense pharmacological interest, there are now just a few strong LAT1 inhibitors, which make the discovery of new drugs in this field necessary. Based on several studies showing that LAT1 is overexpressed in a variety of malignancies and the effectiveness of down regulating LAT1 to reduce tumor cell development, attempts were made to synthesize and identify strong inhibitors of LAT1-mediated amino-acid transport (summarized in Table 2). Among these, BCH (2-aminobicyclo [2.2.1] heptane-2-carboxylic acid) has been demonstrated to inhibit the proliferation of a range of cancer cell lines, including breast [14,73], prostate [93,95], and lung [30]. (see Table 2). BCH, on the other hand, is an L-type amino acid transporter inhibitor that inhibits LAT1–4 [9,105–107]. As a result, it's uncertain if inhibiting LAT1 alone is enough to alter cell proliferation in these experiments. Oda et al. published a drug (KYT-0353 or JPH203) in 2010 that selectively inhibited LAT1 in HT-29 colon cancer cells with an IC50 value of 0.06 M but did not block LAT2 at this dose [79]. JPH203 effectively reduced tumor growth in a xenograft model and inhibited HT-29 colon cancer cell proliferation with an IC50 of 4.1 M [79]. JPH203 is a tyrosine analogue inspired by the structure of the thyroid hormone triiodothyronine (T3), which is a LAT1 and LAT2 substrate [108,109].

JPH203 was next investigated in different cancer types and found to inhibit the growth of cell lines from the brain [71], stomach [80], head and neck [86], leukemia [50], lung [78], kidney [78], prostate [95], thymic carcinoma [96], and thyroid cancer [59]. Importantly, JPH203 inhibition of LAT1 has been found to reduce tumor growth in xenograft models of human leukemia cells [50] and colon cancer cells [79]. Furthermore, we recently demonstrated that JPH203 caused cytostatic growth halt in a genetically engineered mouse model (GEMM) of anaplastic thyroid cancer [59], despite the mice's immune systems being intact. Interestingly, we found that LAT1 expression levels may not always predict JPH203 sensitivity in thyroid cancer

cells [59], suggesting that they may not be the main determining factor of a therapeutic response to JPH203.

Another group recently found similar results in gastric cancer cells independently [80]. In addition, the action of JPH203 in vitro is strongly reliant on the concentration of LAT1 substrates in the culture media, implying that JPH203 functions as a competitive inhibitor of LAT1 [59]. Most conventional culture media include EAA concentrations that are significantly higher than those observed in plasma. As a result, research examining the effect of JPH203 in vitro should be conducted in a tailored medium that closely resembles clinical settings. It's important to note that cancer patients' plasma levels of LAT1 substrate amino acids differ significantly: plasma LAT1 substrates were discovered to be higher in lung [110,111], prostate [112], and breast cancer patients [113,114]. Furthermore, EAA were considerably higher in the most aggressive tumor subtype of breast cancer than in the least aggressive subtype [113]. LAT1 substrates, on the other hand, were reported to be lower in gastrointestinal [115,116], myeloma [117], and pancreatic cancer patients [118]. Because the control of plasma amino acid concentrations in cancer patients is exceedingly complex, the reason(s) for cancer-specific variations of plasma EAA remains largely unclear.

Multiple factors influence plasma EAA levels, including food, whole-body protein metabolism, and tumor amino acid intake. Late-stage cancer patients, for example, are frequently malnourished due to a lack of appetite, which can lead to lower plasma levels of LAT1 substrates [119,120]. It's still unclear whether changes in plasma LAT1 substrates are constant in the tumor microenvironment and whether plasma EAA can predict LAT1 inhibition response. Because JPH203 is a competitive inhibitor, it's possible that high intra-tumoral LAT1 substrate amino acids will lessen or eliminate the drug's action. In order to determine if the intra-tumoral concentration of LAT1 substrates effects the efficacy of competitive LAT1 inhibitors like JPH203 in vivo, more research is needed. Furthermore, the influence of plasma EAA on the outcome of patients who are not malnourished has not been studied to our knowledge. Future research should focus on the impact of plasma EAA levels on patient outcomes and whether plasma EAA can be used to predict LAT1 inhibitor response, particularly in the case of the competitive LAT1 inhibitor JPH203.

LITERATURE REVIEW

Among the most notable instances is 2-Amino-2-norbornanecarboxylic acid (BCH) (Figure 2.4-1), which is regarded as a common inhibitor of all large amino acid transporters (LAT14, or System L), and which is said to cause the suppression of cancer growth and apoptosis. To achieve anti-proliferative effects, however, a very high concentration (>10 mM) of BCH is needed because it is a low-affinity and non-selective substrate of LAT1. An effective and selective LAT1 inhibitor, KYT-0353 (JPH-203) (Figure 2.4-2) has an IC50 of 0.14 M in S2 cells and 0.06 M in human colon cancer (HT-29) cells. Additionally, it prevented tumours from xenografts and cancer cells from growing. Additionally, 1,2,3-dithiazole-based irreversible covalent inhibitors were identified in a recent paper (Figure 2.4-3) **(Figure 2.4-3)** that showed potent inhibition of human LAT1 reconstituted in proteoliposomes.
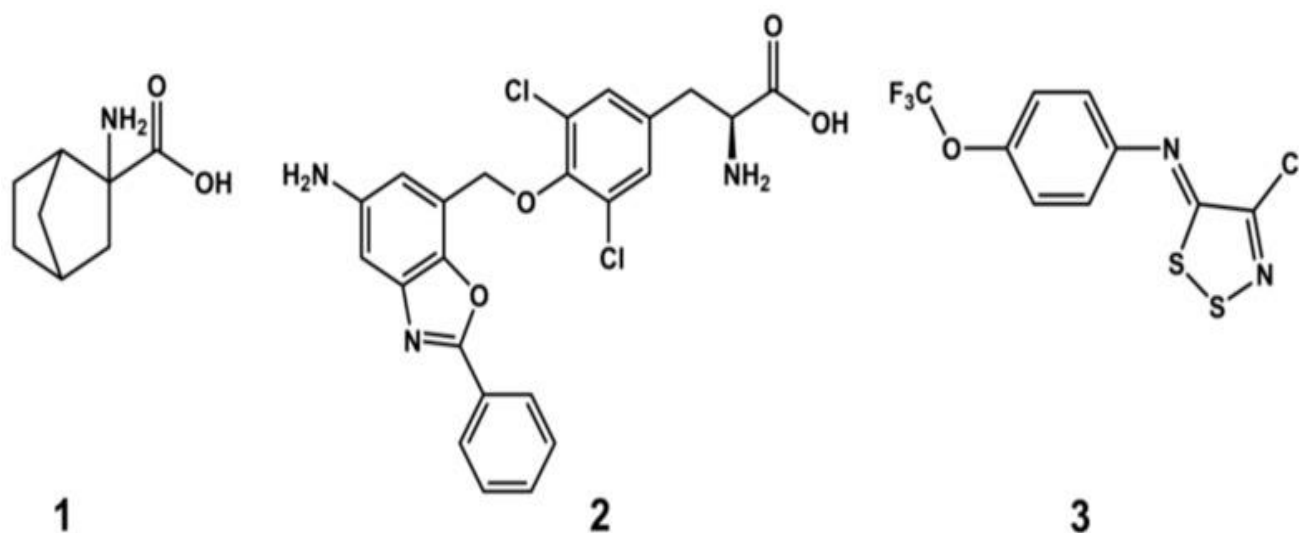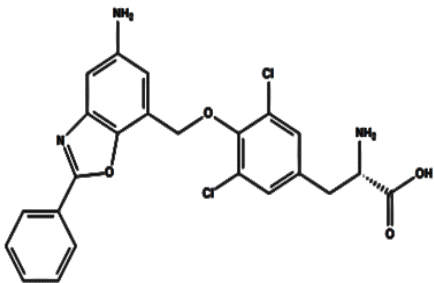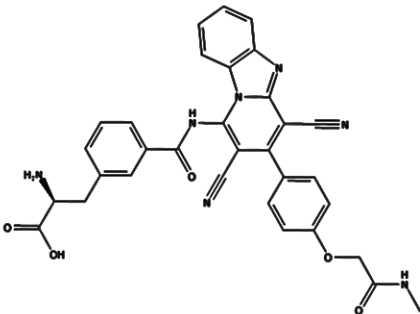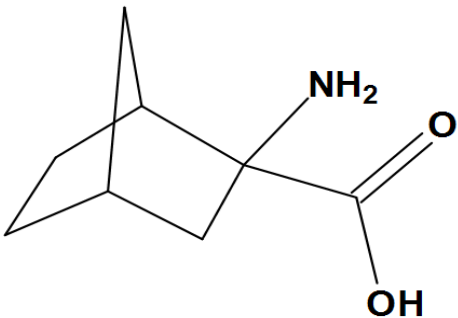

Figure 2.4: Following are the chemical structure of the compounds that are involved in LAT1 inhibition, BCH **(1)**, KYT0353 **(2)**, and Z-4-Chloro-N-4-trifluoromethoxy phenyl-5H-1,2,3-dithiazol-5-imine **(3)**.

The development of novel substances that can imitate LAT1 substrate and can compete for the binding of target has been a key factor in the drug discovery of LAT1 inhibitors. However, the substances discovered using this method need to be present in large quantities in order to have an impact on biology, such as BCH (10 mM). Moreover, many inhibitors of LAT1 were also designed and one of them is JPH203 which is by far the most selective and potential inhibitor of LAT1. It blocks LAT1 substrate binding site with high activity i.e., IC_{50} of 60-790nm, depending

on the type of tissue. On the other hand, BCH is a non-selective inhibitor of LAT1 so it is problematic to use this inhibitor because it can also block LAT2, LAT3 and LAT4.

The virtual screening exertions have facilitated the documentation of novel ligands, signifying that AdiC-based LAT1 models can be valuable for structure–function studies.

Table 2.1: Inducers of LAT1 with specific IC_{50} in clinical trials.

Drug	Chemical Name	IC_{50}	Mol.weight
JPH203/KYT-0353		0.14 µM	545.24
KMH233		0.98 µM	587.60
BCH		112 µM	155.2

Chapter 3

METHODOLOGY

3.1 Methodology Overview:

The overall methodology of this research study is given in **figure 3.1**. The research methodology of this project is a structure-based method for understanding the binding pattern of LAT1 with their respective inhibitors. This will help us identify the significant binding residues of proteins and 3D features of ligands. The structure-based method started by collecting data of Target protein (LAT1) and inhibitor datasets against this protein. Then molecular dynamic simulation was used to stabilize the protein structures. This is followed by the molecular docking protocol, optimization to probe the binding pockets of LAT1. Pose analysis was performed after docking to select the best binding pose. A molecular dynamic simulation was employed to stabilize the docking complexes. After that a structure-based pharmacophore modelling was performed.
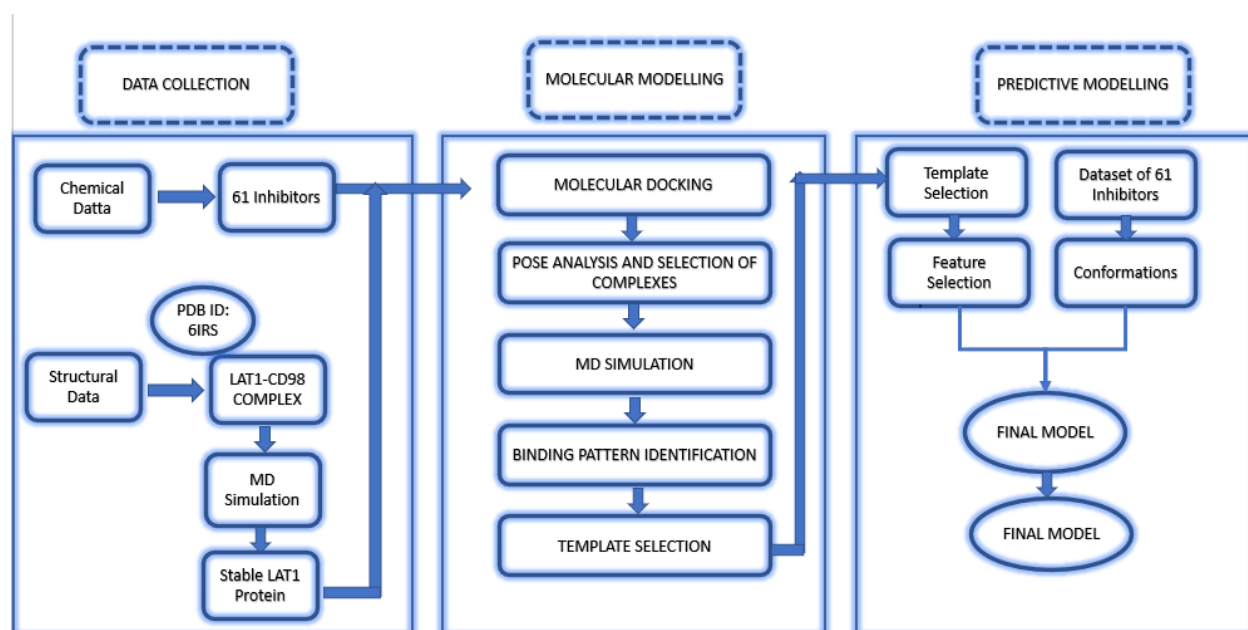
Figure 3.1: The flow diagram of methodology (Molecular Modeling). First, the data collection was done. LAT1 structural and chemical data was collected and preprocessed. The screening set of LAT1 ligands was generated using molecular docking. Molecular modeling steps were performed on LAT1 dataset. Docking results were evaluated using molecular dynamics (MD) simulations. The binding pattern was identified which helped in the selection of template. Further, the predictive modeling was executed using template and rest of dataset to generate conformations. Template was used for the selection of features. The final model was evaluated.

3.2 Structure-Based Methodology:

The structure-based methodology is used in drug discovery research when structural information about protein is present and structural data of ligand is limited. This method aid in the recognition of unique binding features of the protein, which in turn help in the identification of potential drug compounds for a protein. The structure-based methodology is used in this research to identify the interaction pattern of a protein with respective ligands. This will facilitate us to construct a binding hypothesis for LAT1. For this purpose, first co-crystallized structure of LAT1 was downloaded from PDB and then it is stabilized using MD simulation for further analysis.

3.3 Collection of Dataset

A dataset of 72 compounds was selected from ChEMBL database and literature along with their IC_{50} values in nM against L-type amino acid transporter 1. After data preprocessing, which includes removal of duplicates, 58 compounds are left, which are amino acid derivatives and belong to different classes of compounds. These selected compounds are assembled into 3D structures and their energy is minimized through Molecular Operating Environment 2015.

Chembl contains the chemical data of different compounds and their IC_{50} against different protein targets. **Table 3.1** represents the complete inhibitor data against LAT1 that was used in this study.

CODE	LIGAND ID	IC_{50} VALUE (nM)	Molecular Weight
L1	Lig_1	790	472.33
L2	Lig_2	980	313.71
L3	Lig_3	3480	441.75

L4	Lig_4	6600	241.29
L5	Lig_5	7300	255.32
L6	Lig_6	9100	271.32
L7	Lig_7	17000	265.31
L8	Lig_8	18200	587.6
L9	Lig_9	20000	155.16
L10	Lig_10	27700	396.83
L11	Lig_11	29000	253.25
L12	Lig_12	32380	380.83
L13	Lig_13	36000	223.23
L14	Lig_14	46000	165.19
L15	Lig_15	68000	181.19
L16	Lig_16	69000	165.19
L17	Lig_17	76000	237.25
L18	Lig_18	83000	195.22

L19	Lig_19	85000	131.18
L20	Lig_20	92000	207.23
L21	Lig_21	95000	237.25
L22	Lig_22	96000	222.24
L23	Lig_23	100000	197.19
L24	Lig_24	100000	166.18
L25	Lig_25	101000	180.21
L26	Lig_26	110000	222.24
L27	Lig_27	110000	155.16
L28	Lig_28	112000	155.20
L29	Lig_29	120000	149.22
L30	Lig_30	130000	209.20
L31	Lig_31	130000	179.22
L32	Lig_32	130000	181.19
L33	Lig_33	140000	131.18

L34	Lig_34	150000	223.23
L35	Lig_35	160000	166.18
L36	Lig_36	160000	204.23
L37	Lig_37	160000	156.14
L38	Lig_38	170000	245.28
L39	Lig_39	170000	149.22
L40	Lig_40	190000	169.18
L41	Lig_41	200000	171.24
L42	Lig_42	220000	131.18
L43	Lig_43	240000	239.34
L44	Lig_44	260000	223.23
L45	Lig_45	260000	171.24
L46	Lig_46	340000	206.21
L47	Lig_47	380000	181.19
L48	Lig_48	380000	204.23

L49	Lig_49	440000	170.17
L50	Lig_50	460000	155.16
L51	Lig_51	470000	194.23
L52	Lig_52	680000	223.23
L53	Lig_53	810000	179.22
L54	Lig_54	1000000	186.17
L55	Lig_55	1000000	170.17
L56	Lig_56	1000000	232.24
L57	Lig_57	3000000	131.18
L58	Lig_58	50000000	117.15

3.4 Pre-processing of Chemical Data

Specific pre-processing techniques were applied to the chemical data to filter the initial dataset against LAT1 to get the precise, targeted and valuable inhibitors with significant IC_{50} value against the potential target. The chemical dataset is filtered based on following criteria:

- Duplicate compounds having the same ChEMBL ID are deleted because they belong to the same study, causing the noise during the analysis of results.

- Deletion of compounds that are not published in scientific research articles and biological assays.

- Deletion of those compounds that have insignificant structural variation with the identical biological activity values (IC_{50}).

- Deletion of compounds which have same simplified molecular input line entry system (SMILES) codes because this also leads to duplication of compounds.

- Deletion of compounds that have molecular weight less than 100 because these molecules are unable to dock within the binding pocket of protein during docking.

- Deletion of those compounds which have IC_{50} value with the sign "<" or ">" because exact IC_{50} value is unknown which leads to plausible justification of results.

Shortlisted and finalized dataset of inhibitors, comprising of 58 compounds has been selected. Furthermore, after the cleaning of dataset, inhibitors dataset is subjected to energy minimization through force field of MMFF94 and conserved into 3D structures via Molecular Operating Environment (MOE) 2019 software. This energy minimized dataset of ligand is further used in Docking protocol.

3.5 Physiochemical Properties

A drug's activity depends on two main factors, that are its ability to bind to the target's active site and its way to the target protein. The way to the target explains the transport behavior of potential inhibitors to reach the target site by overcoming the difficulties of complex system. Therefore, to observe the transportation properties of LAT1 ligands inhibitor dataset, certain properties such as logP, molecular weight and pIC_{50} has been calculated via MOE software and a correlation graph was plotted between descriptors and pIC_{50} to see how these descriptors influenced biological activity.

3.6 Biological Data

The second requirement for docking protocol is the 3D structure of target protein which should also be energy minimized. Therefore, respective crystal structure of therapeutic target protein that is L-type amino acid protein 1 (LAT1) was downloaded from protein data bank (PDB) under PDB ID of 6IRT with resolution of 3.5Å. furthermore, this protein crystal structure is then subjected to energy minimization using AMBER99 force field via Molecular Operating Environment (MOE) 2019 software. This stable energy minimized structure is then used further stabilized by Molecular Dynamic simulation using SCHRODINGER.

3.7 Target protein preparation

Further, the human LAT1 protein was stabilized by molecular dynamics (MD) simulations using SCHRODINGER because a stable protein structure will lead to better binding interactions. MD simulation uses Newton's law of motion to monitor the movement of atoms and molecules for the specified time interval usually in nanoseconds to check the stability of molecular interactions. MD simulation steps include preparation of structure (optimization and minimization), Periodic boundary conditions (selection of force fields, shape, and size of boundary box), Solvation (Addition of ions), and Energy minimization of the system and MD production (for simulation the specified time). Initially, the protein complex was prepared and refined using a protein preparation wizard. The hydrogens were added, and disulfide bonds were created. The pH of the protein was changed to 7.4. During refinement, the water molecules beyond 3Å were removed, and the protein was minimized. After protein preparation, the system was build using the TIP3P water model in a cubic box using Desmond software. The system was neutralized by adding sodium ions. The molecular dynamics simulation was run at 200ns to stabilize the protein. The stable protein was analyzed using protein RMSD. This stable structure was retrieved for further molecular modeling analysis.

3.8 Molecular Docking

Molecular docking protocol was used to target LAT1, to predict the most preferential and potential binding modes of the ligands of LAT1 within the binding pocket of LAT1. Because favorable binding poses of ligands helps in understanding of the 3D properties of ligands and their native conformation. Docking protocol was performed using the dataset of 58 potential inhibitors of LAT1 that are docked within the binding pocket of stabilized structure of LAT1 under PDB ID 6IRT.

To initiate docking, firstly crystalized structure of LAT1 was energy minimized using Molecular Operating environment (MOE) using AMBER99 force field. Secondly, the dataset of inhibitors is also energy minimized using MMFF94 force field using the same software MOE for the stable ligand-protein interaction during docking protocol. Thirdly, GOLD suite (Genetic Optimization for Ligand Docking) software (version 5.6.1), is used for the execution of docking. The binding pocket was selected using the point selection method, and the x, y, and z coordinates were adjusted to select the specific binding pocket residues reported previously. The binding pocket coordinated for LAT1 are shown in the table.

Table 3.2 X, Y, Z Coordinates selected in GOLD for the binding pocket.

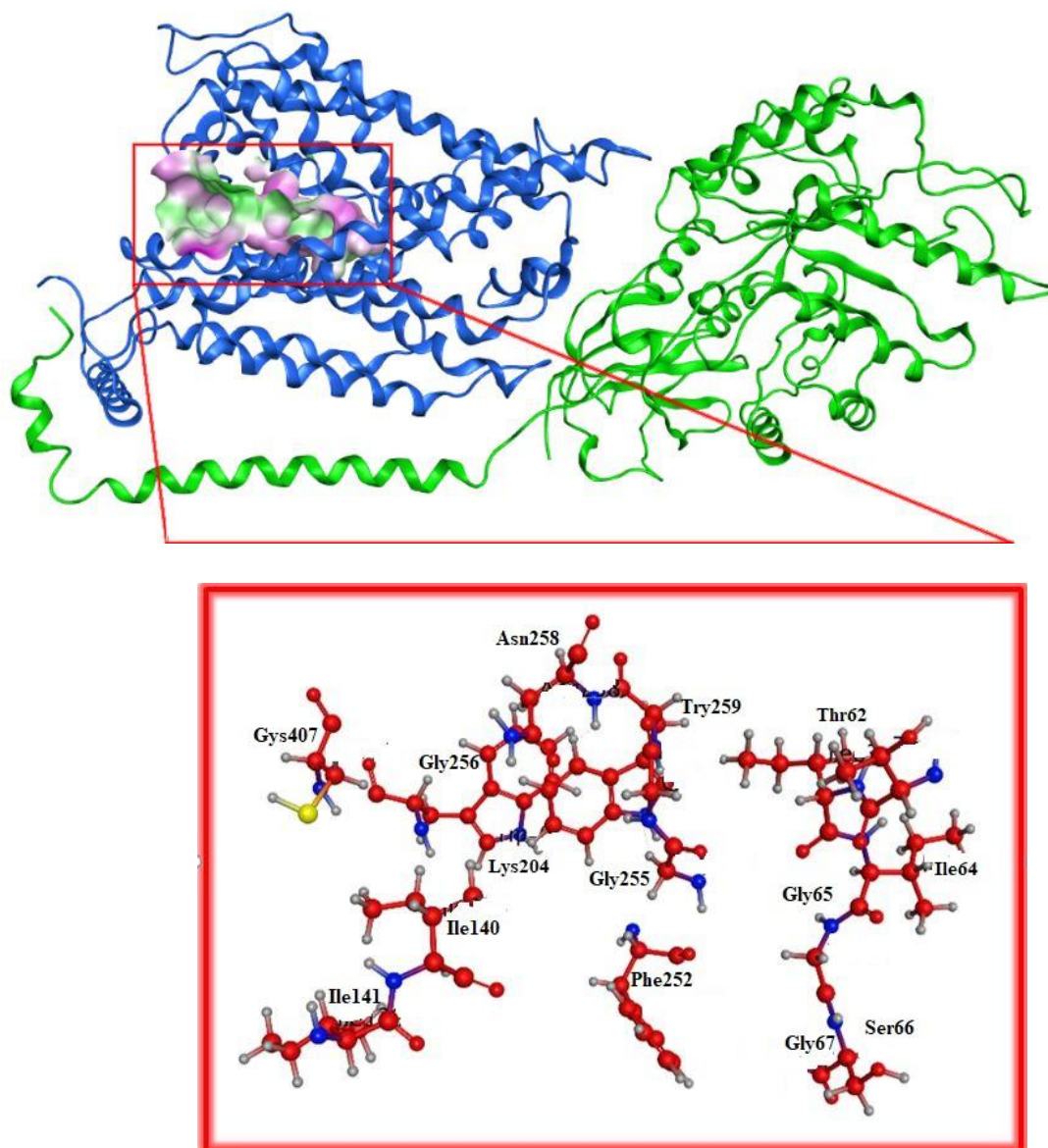| Protein	X	Y	Z
LAT1	3.7800	3.4725	-0.9642

Figure 3.2: Binding pocket of LAT1 along with binding residues which are important in binding the substrate to LAT1 and are proved crucial in Mutagenesis studies.

Moreover, the binding site area for the protein was at 15Å to facilitate all the possible and likely ligand protein interaction and also to include all the crucial amino acid residues confirmed through literature. The important amino acid residues include **I62, I63, I64, G65, G67, S66, I139, I140, A144, V148, F252, A253, G256, G255, W257, N258, F262, C335, S338, S342, F402, W405 and C407**. After this a maximum of 100 genetic runs per ligand against LAT1 are

generated and are ranked based on the GOLD score scoring function. GOLD fitness score is calculated using the following formula:

$$\Delta G_{(BIND)} = \Delta G(hb\_ext) + \Delta G(hb\_int) + \Delta G(vdw\_ext) + \Delta G(vdw\_int)$$

hb_ext = Intermolecular H-bonds

hb_int = Intramolecular H-bonds

vdw_ext = Van der waals interactions

vdw_int = Intramolecular van der waals interactions

No other constrains are applied and all the other features are set to default. However, the slow protocol is used to increase the precision and accuracy of results. The general workflow of the docking protocol has been shown in the following diagram:
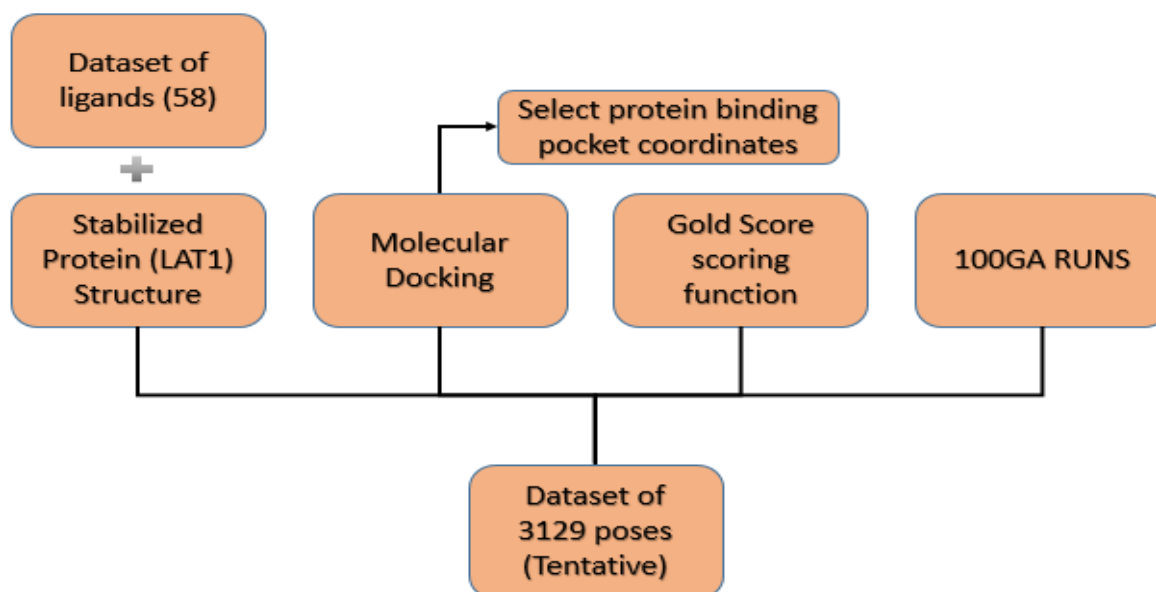

Figure 3.2.1: Workflow of Molecular Docking. The biological data was retrieved from Protein Databank under the PDB id 6IRT. However, the chemical data of 58 ligands were collected from Chembl, and Literature. Then molecular docking was performed by GOLD software where binding pocket was identified. By taking the coordinates 3.7800 (X), 3.4725 (Y), and -0.9642 (Z) docking was performed. After that, the pose analysis and selection were made for correlation analysis and binding hypothesis formation.

3.9 Pose Analysis:

Docking resulted in different docked poses of inhibitors within binding site of LAT1. We adopted the strategy of correlating the docking score with the pIC50 value. The pIC50 represents the activity of the inhibitor against a particular target. pIC50 was calculated from the IC50 given in Table 2 using the following formula.

$$pIC_{50} = 1/LOG10[IC_{50}(M)]$$

OR

$$pIC_{50} = -[LOG10(IC_{50}(M))]$$

pIC50 was plotted against the Gold fitness score/ Gold fitness score represents the binding energy. Secondly, correlation of molecular weight of inhibitors with pIC50 for was also studied as it represents the biological activity due to the transport of ligand towards the target. LogP (o/w) was also studies in correlation with pIC50. LogP (o/w) is the partition coefficient of the between octanal and water also known as Lipophilicity. It is a physicochemical feature describe the solubility of given substance in fat. As to reach the target a drug compound must cross many lipophilic and hydrophobic barrier, but the high lipophilicity can dissolve the drug hence low activity.

3.10 Molecular Dynamic Simulation

Some of the protein-ligand complexes generated after docking the LAT1 data set were stabilized by molecular dynamic simulation. The top poses of the ligands with the highest Gold score were used. A total of SIX complexes were stabilized using SCHRODINGER. So to stabilize the interacting complex, molecular dynamic simulations (MDS) were executed using Maestro-SCHRODINGER software [87]. For this purpose, ligand and protein complex was prepared in MOE [88]. Then, the complex was prepared in Desmond-SCHRODINGER software at pH 7.4 [89]. The workplace structure was preprocessed by adding hydrogen and refined by optimizing the H-bond assessment at pH 7.4. A default force field of OPLS4 was selected for energy minimization to remove any strong van der Waals interactions that may cause structure distortion within the complex. The complex was then solvated in a TIP3P water modeled cubic box of 5A^{o}, where Na+ or Cl- were added to neutralize the system [90]. After equilibrating the protein-ligand complex, MDS production was made at the standard temperature (300K) and pressure (1.01325

bar) for 100 Nano sec. The stability of complexes was analyzed by αC RMSD, αC RMSF, and the hydrogen bond analysis.
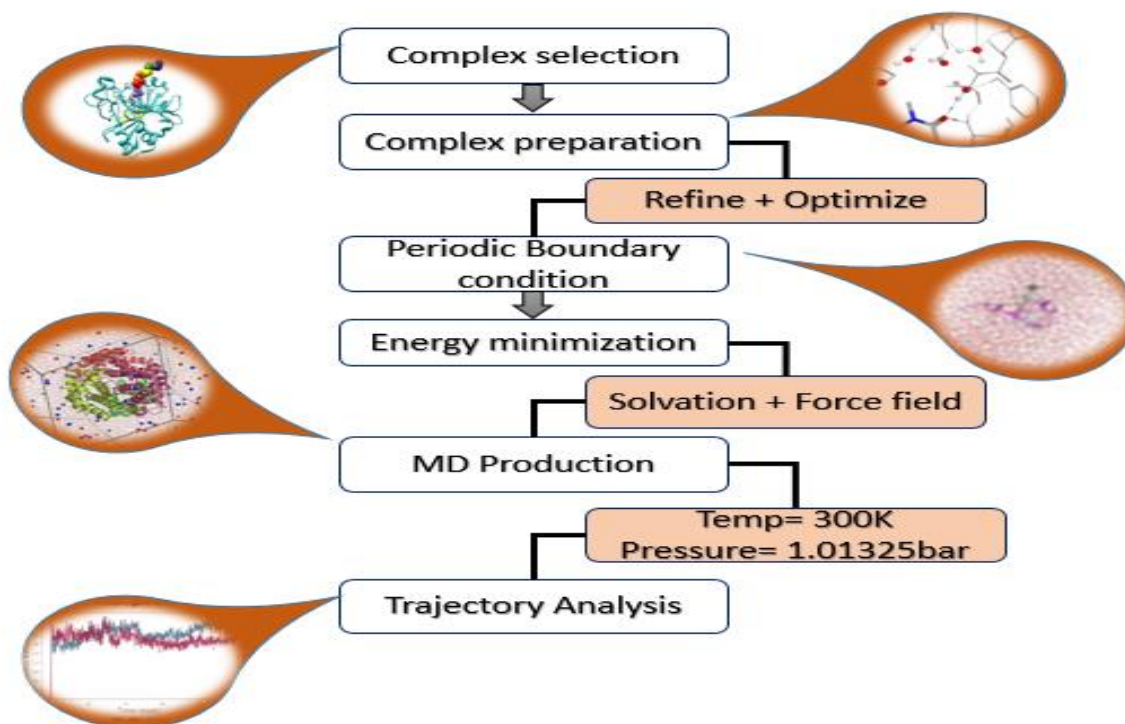

Figure 3.3: Overall workflow of Molecular Dynamics Simulations of selected ligand complex. This process was done by moving LAT1 complexes from the docked complex and processed towards system building. After energy minimization MD production for 100nsec was made and the results were analyzed by means of trajectory analysis.

3.11 Pharmacophore Modelling

Pharmacophore Modelling is a key tool for the identification of hit compounds. A pharmacophore model represents the essential steric and electronic features that are required for the recognition of a ligand by a specific biological target to produce a specific biological response. This model distinguishes between actives and inactive via identifying pharmacophore features named as hydrophobic, hydrogen bond donor/acceptor, and aromatic rings. These features with specific radii and distance assist in forming a pharmacophore query.

METHODOLOGY

3.11.1 Pharmacophore model development

Pharmacophore model was constructed for all the ligands by applying a threshold of >=18200nM biological activity values. LAT1 ligands were classified into active and inactive based on the defined activity threshold. Compounds having $IC_{50}<=18200nM$ were considered as active and those having $IC_{50}>=18200nM$ were marked as inactive. Pharmacophore model was generated by using LIGANDSCOUT 4.1.3 version. The most stable complex with highest activity value was selected as a template. After the formation of features with their specified radius, and selecting minimum number of similar features, hit identifications were made. The conformational database was used as input in the pharmacophore search. The algorithm searched for all possible hits with features similar to the input ones. By evaluating the number of actives and inactive in the internal hits, the respected pharmacophore model validation was made. This step was crucial to predict the reliability of a model.
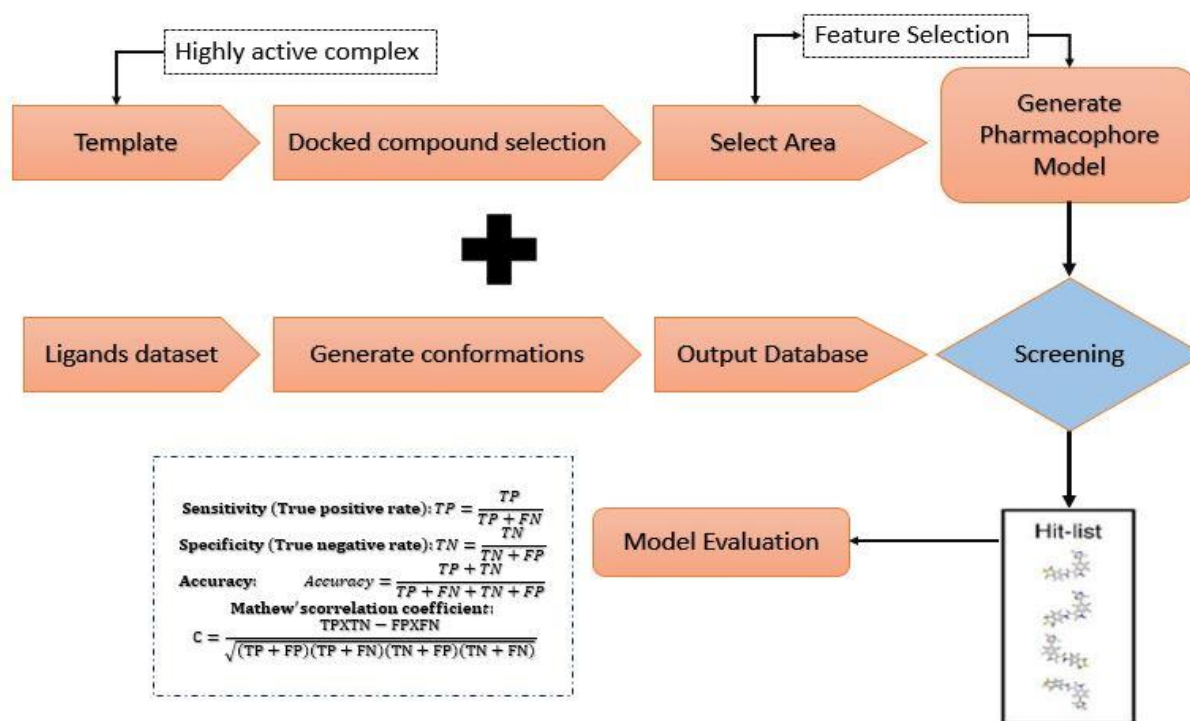

Figure 3.4: Overall workflow of structure-based Pharmacophore Model Generation using stable complex from MD simulation studies. The step was done by extracting the feature from the template and generation of confirmation from rest of the ligand data. Based on features, model was generated and screened against the packed confirmation for internal set validation.

3.11.2 Pharmacophore Model Evaluation

To evaluate the quality of pharmacophore model, certain statistical parameters were calculated that validated the predictive ability of model in differentiating active from inactive compounds. Those ligands which were actives and predicted actives by the model were stated a True positives (TP). Similarly, True negative (TN) were those inactive compounds that were predicted as inactive by model. While those that are actives in nature but do not appear in hits, i.e., predicted as inactive, were False Negatives (FN). Likewise, False Positives (FP) were those ligands that were inactive but recognized as actives by the model. After classification of ligands, evaluations were made on certain statistical parameters such as Specificity (true negative rate), Sensitivity (true positive rate), Accuracy (overall prediction rate), and Precision (positively predicted values). However, the decision was clarified based on Matthews Correlation Coefficient (MCC), which correlated the actual and predicted value by taking all classified variables (TP, TN, FP, and FN). The model was predicted best by its prediction statistics and utilized further for the virtual screening of different libraries.

TP= True positive   TN= True negative

FP= False positive   FN= False negative

Sensitivity (True positive rate): $TP = \frac{TP}{TP+FN}$………………………………….…… Eq 1

Specificity (True negative rate): $TN = \frac{TN}{TN+FP}$……………………………………… Eq 2

Accuracy: $Accuracy = \frac{TP+TN}{TP+FN+TN+FP}$………………….…… Eq 3

Mathew's correlation coefficient: $C = \frac{TPXTN-FPXFN}{\sqrt{(TP+FP)(TP+FN)(TN+FP)(TN+FN)}}$…………...Eq 4

CHAPTER 4

RESULTS

RESULTS

4.1 Target protein preparation

The X-ray crystallographic structure of L-type amino acid transporter1 LAT1-4F2hc complex bound with BCH having the resolution of $3.5A^0$ in active state was used, it has two chains, heavy chain (CD98) and light chain (LAT1). Lat1 has transporter activity while CD98 has chaperone function. Therefore, we remove the heavy chain from the complex structure and only use the Light chain (LAT1). The Lat1 chain is then stabilized using MD simulation at 200 nano second simulation time. The stability of the LAT1 chain was evaluated by the deviation of αC of the backbone of a protein in terms of root mean square deviation (RMSD).

4.2 Molecular Dynamics Simulations (MDS) of LAT1

The modeled protein was further subjected to molecular dynamics simulations (MDS) utilizing Maestro-Schrodinger for further optimization. The stability of structures was measured in terms of the deviation of backbone (α-carbon) structure with reference to its initial confirmation [98]. For this purpose, the root mean square deviation (RMSD) plot was visualized for all structures. RMSD (eq1) measured the average change in dislocation of atoms in a protein with a simulation time frame. It was measured by

$$RMSD = \sqrt{ 1\ N \sum (r\ '(tx\ )) - r'(tref)\ N\ i{=}1\ 2} \ldots\ldots\ldots\ldots\ldots\ldots\ldots\text{Eq1}$$

Where N and r' were selected atoms and position of modeled protein, tref was time reference of the first-time; step, and tx was the total simulation trajectory time frame. The simulation took time due to the presence of loops at the middle and end of the structure. The structure was stabilized at 200 nano seconds due to presence of loops. The **figure 4.1** represents the RMSD values in association with the time frame required for the stabilization of the structure. The peaks are stable at 2.2 RMSD value.
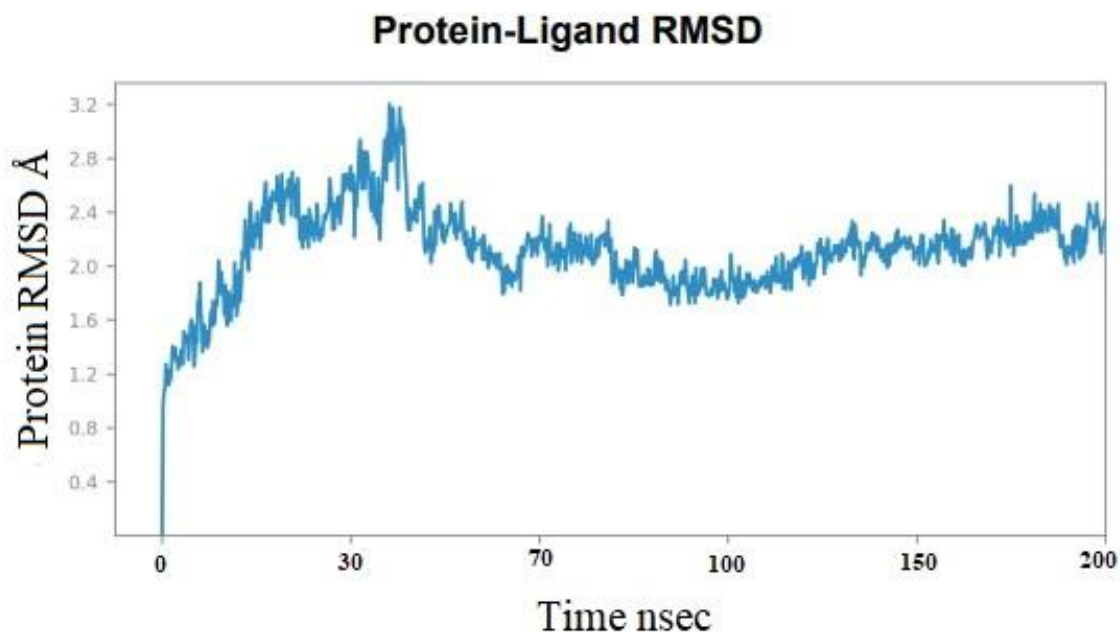
RESULTS

Protein-Ligand RMSD

Figure 4.1: Protein RMSD plot of LAT1 protein after MD. RMSD stabilized after 200ns at 2.0-2.4Å.

However, the RMSF versus residue Index graph showed high peaks at the middle and end of the structure as represented in the **figure 4.2**. These peaks are due to the presence of long loops in the middle and end of the LAT1 chain. The loops are present in the following regions:

- From amino acid 221-243
- From amino acid 421-424

Both the RMSF versus Residue index graph and the highlighted amino acid residues ion LAT1 chain depicts the reason for the extended stabilization of the protein structure in MD simulation.
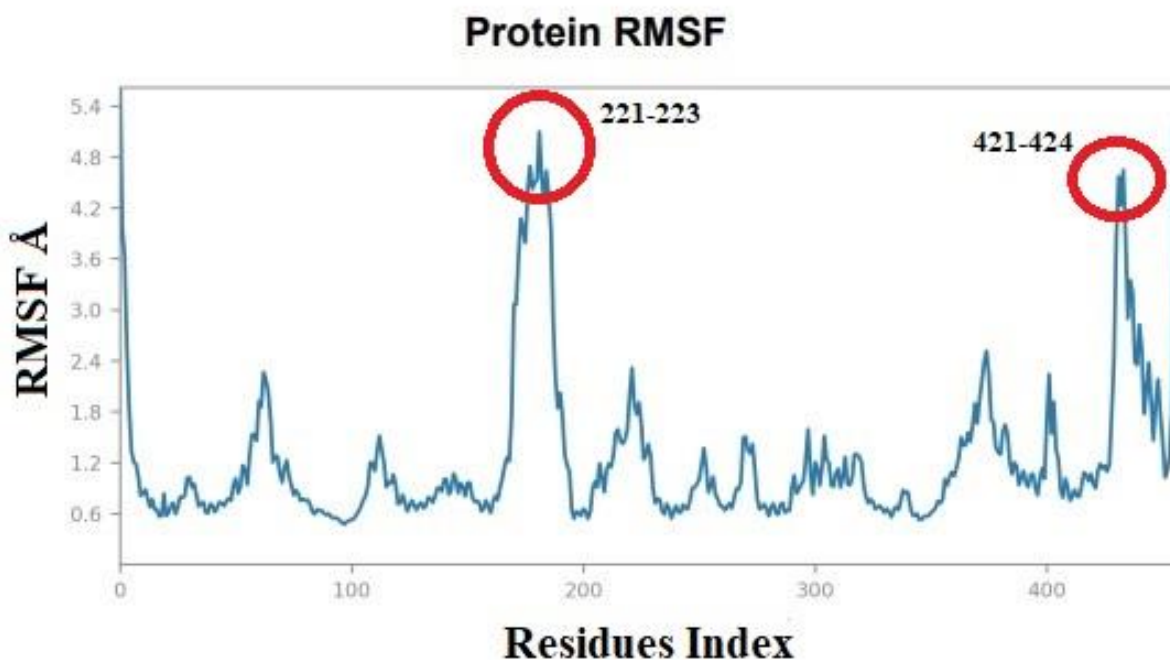
Protein RMSF

Figure 4.2. Protein RMSF plot of stabilized LAT1 complex Two regions (221-243 & 421-424) showed fluctuations due to the presence of loops.

The root mean square fluctuation (RMSF) of the LAT1 complex was also calculated to evaluate the mobility of individual residues. **Figure 4.2** shows the instability in 221-243 and 421-424 regions between RMSF 1-5.1 Å. These residues are the small loops between the α-helices of the LAT1 complex. Below in **figure 4.2.1** are the two images that shows the amino acid residues of loop region.
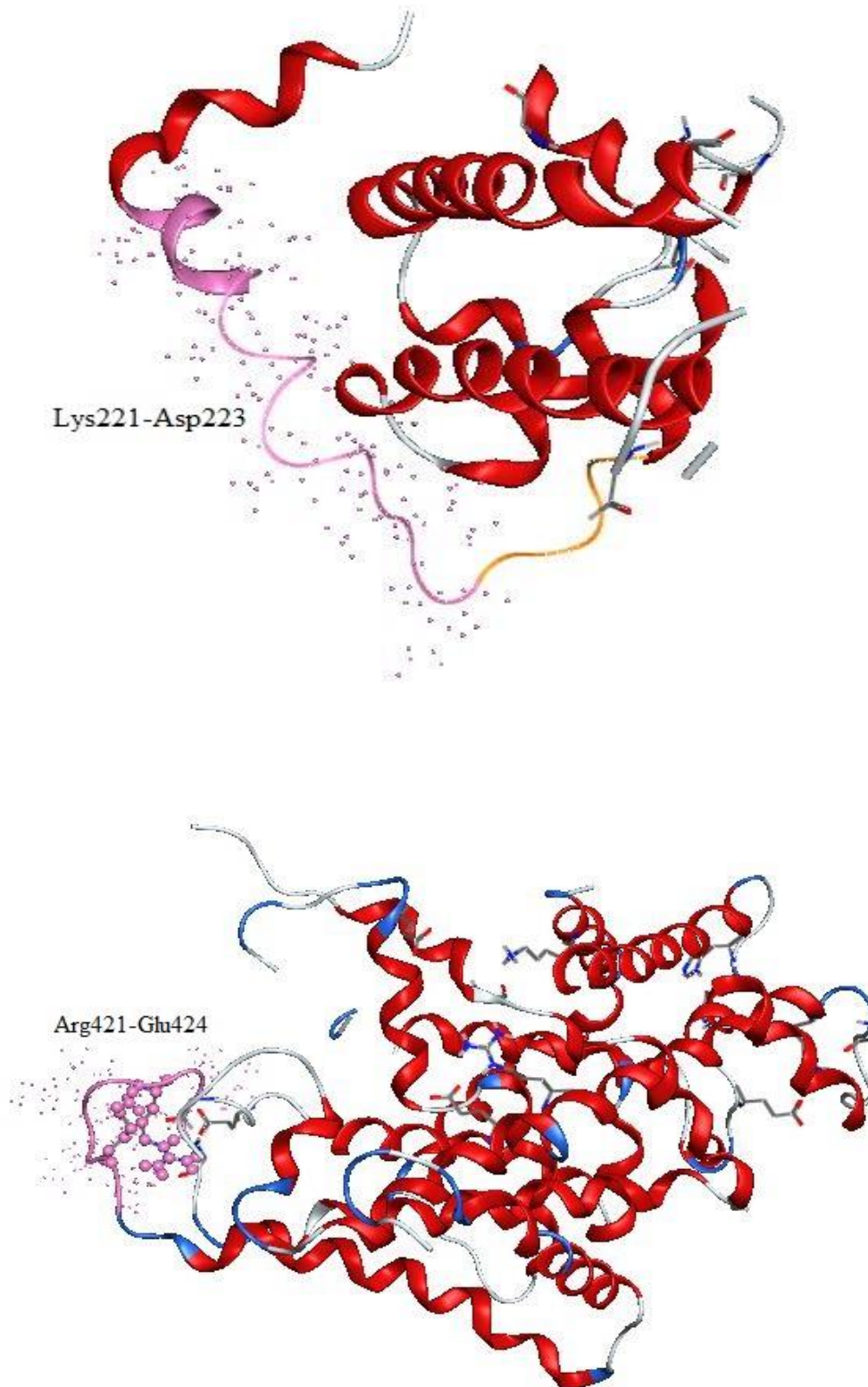
Figure 4.2.1: The 3D structure of LAT1. The pink region shows the loop area in both diagram which corresponds to amino acid residues (Lys221-Asp223) and (Arg421-Glu424) respectively.

RESULTS

4.3 Molecular Docking

Molecular docking is the most effective approach in molecular modelling for modelling atomic-level interactions between protein and ligands. It enables the understanding of fundamental biological processes by analyzing the behavior of chemical compounds in the target protein's binding region. The goal of molecular docking is to acquire the most probable binding conformations of ligands for virtual screening. The dataset of 58 ligands was docked against the LAT1 protein obtained after MD simulation. The GOLD (Genetic Algorithm for Ligand Docking) software was used [18]. The previously reported binding pocket residues were selected using the x, y, and z coordinates from the central point as 3.7800, 3.4725, and -0.9642, with the cavity size of 15Å. The ligands were docked on the same binding pocket as reported previously. For 58 ligands a total of 3149 poses were generated. The ligands bind at the binding pocket of LAT1 validate the accuracy of the docking procedure. For each ligand, 100 poses were generated with the high precision protocol. The resultant GOLD fitness score (eq 2) [100] was calculated by considering all the energy values as follow:

GOLD Fitness = Score(hb_ext) + Score(vdw_ext) + Score(hb_int) + Score (vdw_int) …………. Eq2

The GOLD fitness score is the sum of all external H-bond and Vander Waal energies of interacting ligand and protein and ligand's internal energies such as torsion strain energy, intramolecular H-bond energy, and Vander Waal energy between the ligand's atoms. However, the fitness score for each ligand was in the continuous range.

To analyze the interacting binding pattern of 3149 poses with a specific GOLD fitness score, a correlation plot (R) was made by taking the GOLD fitness score on the x-axis and pIC_{50} on the y-axis **(Figure 4.4).** The resultant graph showed a correlation of (R=0.6495), which suggested a strong positive correlation between the GOLD score and activity values. The positive correlation value represents that Gold Score has a high correlation with the pIC_{50} which means the biological activity value of each inhibitor is defined by the interaction pattern of each inhibitor with the LAT1 protein. Moreover, it was also observed that inhibitors have a high pIC_{50} as well as high Gold score as displayed in the (**Figure 4.5** displayed in red color) but difference in Gold score is not of greater than 5 which indicated that pIC_{50} behavior is also depended by an additional physiochemical property i.e., Molecular weight. These inhibitors biological activity value was further investigated with the

help of Molecular weight. (**Figure 4.3**) shows the correlation of pIC_{50} with Molecular Weight (g/mol). It shows that the correlation between pIC_{50} and Molecular weight is R=0.6466 and R_2 = 0.4181, which also represents a positive correlation. This means that some inhibitor may have activity due to the proximity towards the target. To validate the stability of these complexes MD simulation of the complexes of these inhibitors with the LAT1 protein was performed. This will also validate our docking protocol as biological activity (pIC_{50}) have direct correlation with binding affinity i.e., Gold score. Generally, it is assumed that the highly active compound should have a stable binding pattern, thus a high GOLD fitness score [88]. However, in the plot in Figure 4.5 it can be observed that some of the ligands show the outlier behavior such as ligand 2, 8, 13, and 57.
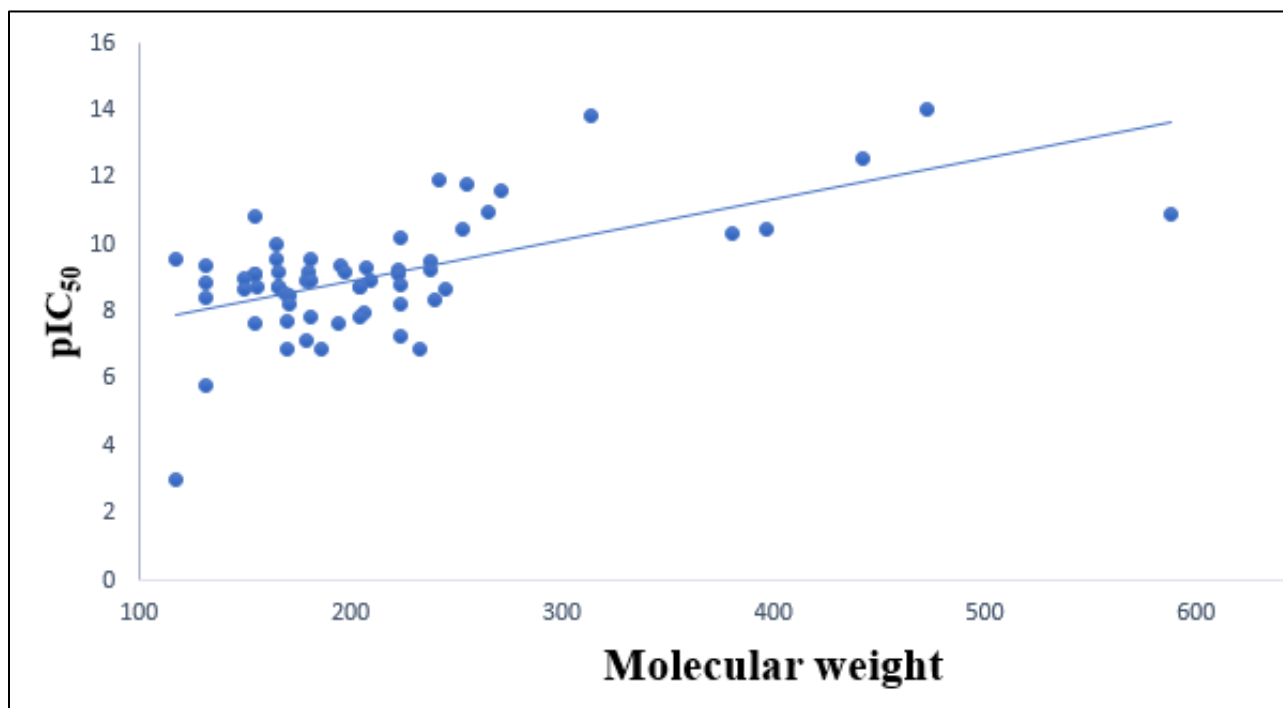

Figure 4.3: Correlation plots between biological activity values (pIC_{50}) and Molecular weight. The R in the plots denotes the correlation coefficient which shows direct positive correlation.
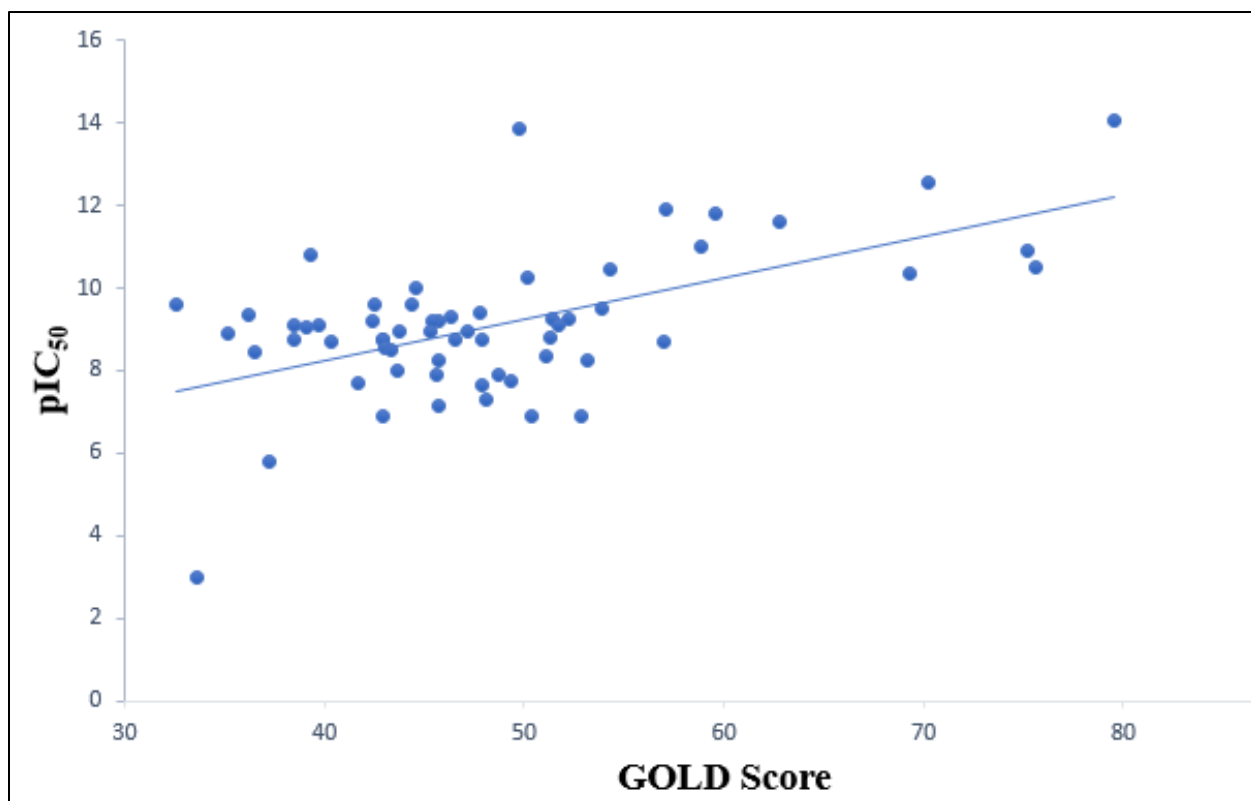
Figure 4.5: The docking results of Top poses of LAT1 Representation of Gold Score on X-axis and biological activity (pIC_{50}) on Y-axis. The red data points are ligand 1,2,8,13,54 and 58.

The analysis of (**Figure 4.5**) shows some anomaly cases, the red datapoints 1 and 8 represent two inhibitors with a greater difference in the pIC_{50} but a small difference in the Gold Score. The red data points 2 represent the data points that have high pIC_{50} but less gold score, 13 and 57 with greater difference in pIC_{50} value but with same GOLD score which indicates these inhibitors pIC_{50} is not sufficiently defined by the docking interaction. Moreover, the correlation of activity value and logP (lipophilicity) was also analyzed to determine ligands' physiochemical behavior and transport properties. There is a positive correlation R= 0.6149 between logP and pIC_{50} values of ligands as shown in the **(Figure 4.6)**. To validate the binding pattern and explore the stability of these inhibitors' complexes with the LAT1, MD simulation was used.
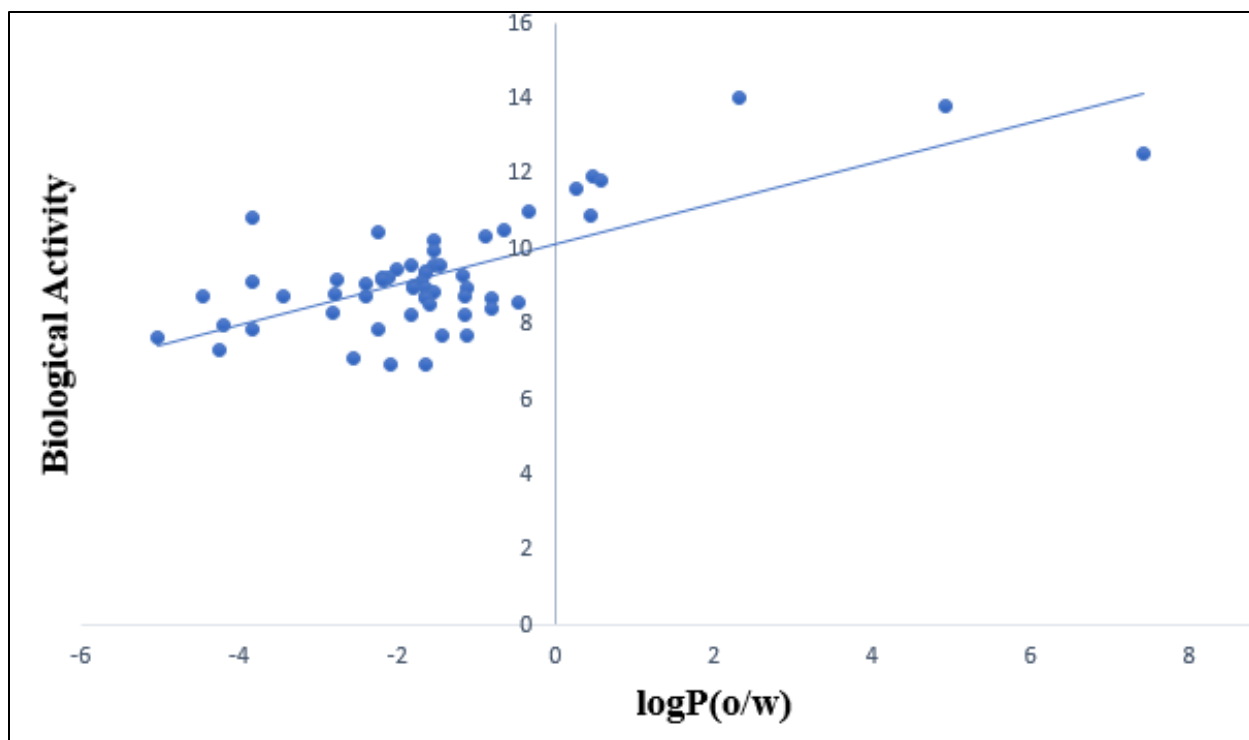
Figure 4.6: Correlation plots between biological activity values and logP(o/w). The R_2 in the plots denotes the correlation coefficient.

The highly active compound- ligand 1 (790nM) showed the highest GOLD score of 79.4881 and pIC_{50} value of 14.0512 while the least active ligand 61 showed the lowest GOLD score of 33.6394 with pIC_{50} Value of 2.9957. From the docking interaction pattern, we formulated a hypothesis, i.e., the larger the R group associated with amino group of ligands-greater will be their activity value because ligands having high molecular weight has high activity values which conclude that Molecular weight may not have bad impact in the lead optimization. Therefore, for the stabilization of binding interaction and confirmation of the hypothesis further processing was necessary. So, for this reason, a highly active ligand, a least active ligand, and the ligands that show outlier behavior are selected for MD simulations. We selected ligand 1, 2, 8, 13, 57 and 58 for further analysis because of their abnormal behavior which is evident is docking results. The analyses of protein-ligand interaction of these ligands showed the prevalence of following protein residues occurring in both actives and in-actives. These include Tyr259, and Arg144. The detailed interaction diagrams of selected ligands are given in **Figure 4.7**. The ligand_2 showed no interactions pattern before MD simulation despite of the fact that it has 2nd highest pIC_{50} value. This may be because as we know a ligand's efficiency depends on two factors:
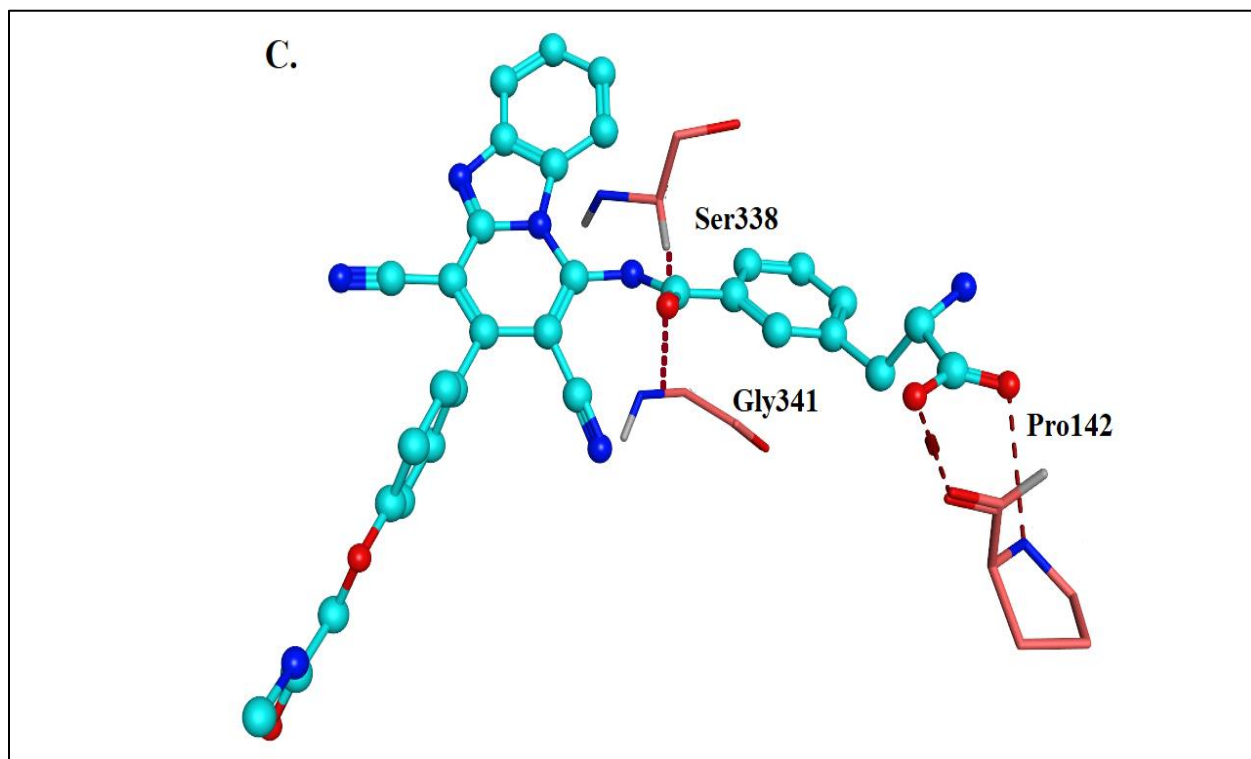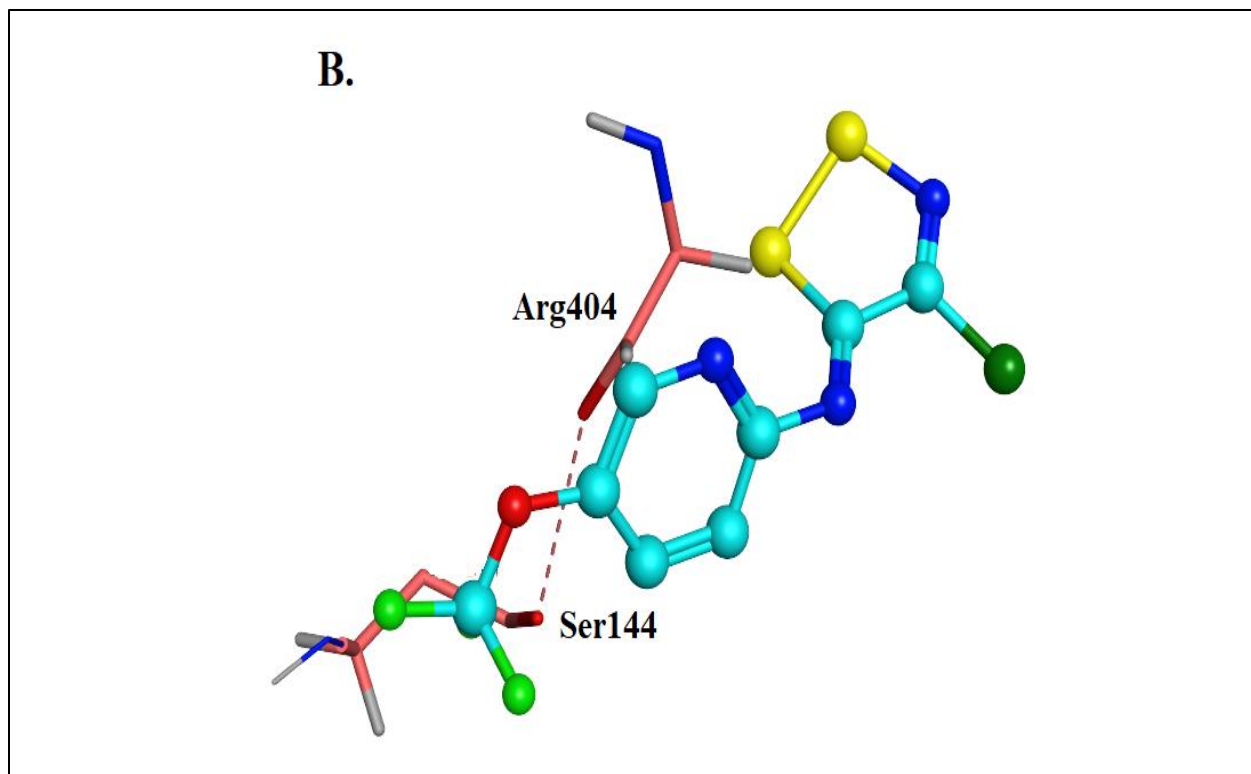
RESULTS

- Number of interactions with the target protein
- Way to the target protein.

So, may be ligand 2 has better solubility and way to the target proteins which explains it's high activity value.

By comparing the interacting pattern before and after molecular dynamics simulations of **LAT1** complex, it is revealed that the ligand translocated its position during MD simulation when an external force field was (OPLS4) applied. The interacting residues during the docking studies were Ile58, Val60, Gly61, Thr62, Ile64, Gly65, Ser66, Gly67, Tyr103 and Asp116, stabilized to the actual binding cavity of LAT1. The resultant stable interacting pattern was observed among residues Ile64, Gly65, Ser66, Gly67, Tyr103, which were the reported residues in the literature. The ligand after MD achieved its stable conformation and persisted for 100nsec time step at the end. Here, the ligands atom remained enact with the binding cavity residues, the final ligand structure was subjected to 3D feature extraction based on its new stable 3D conformation.
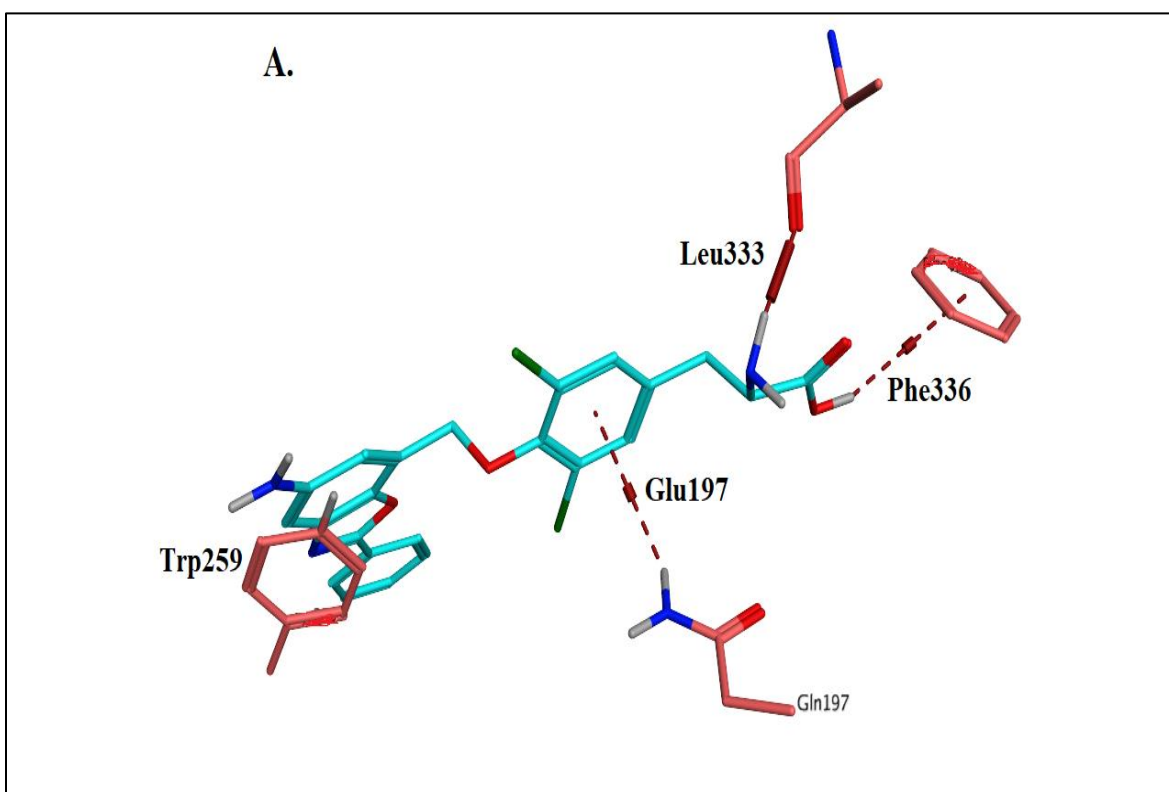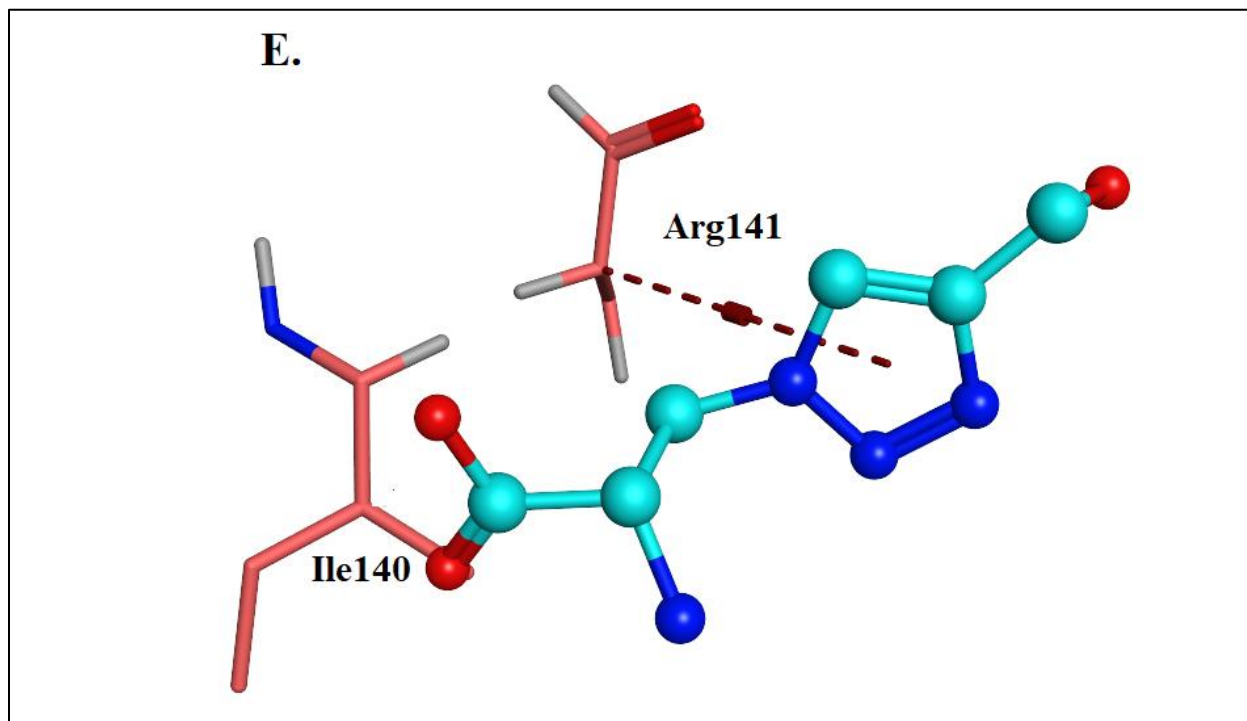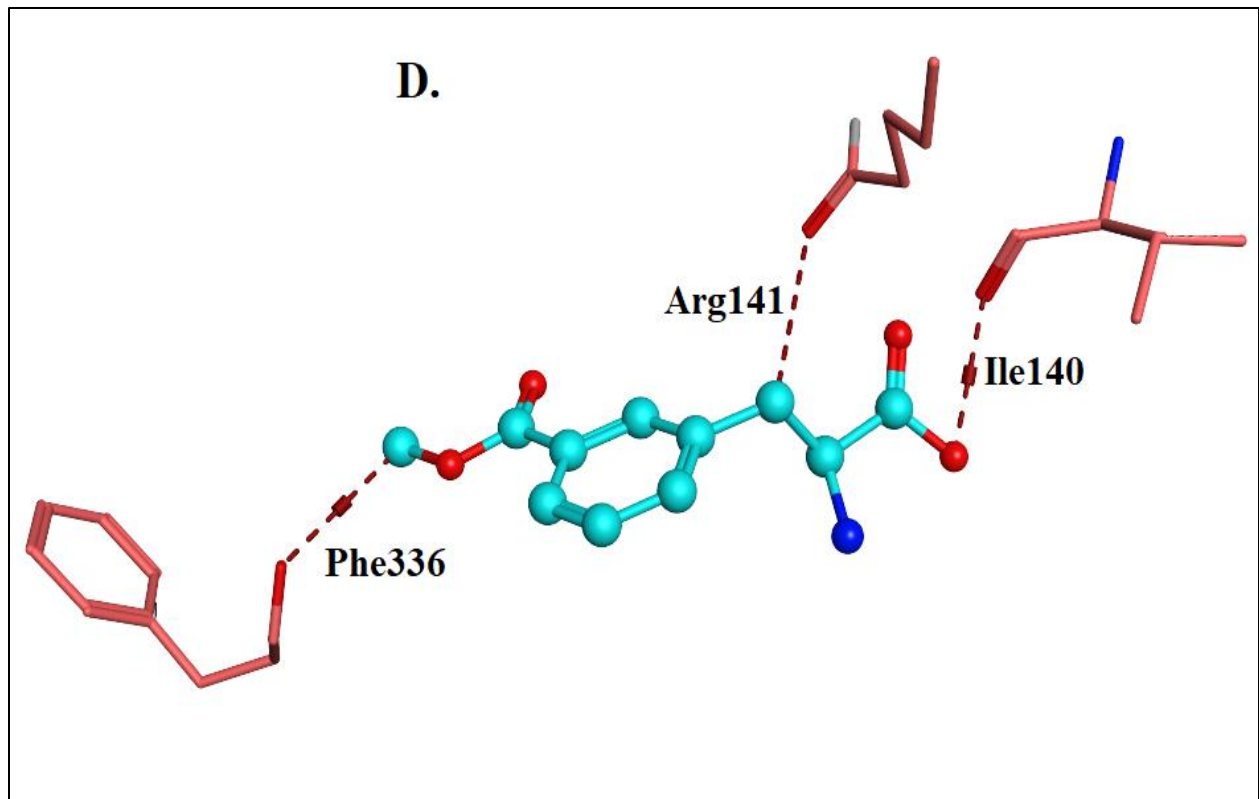
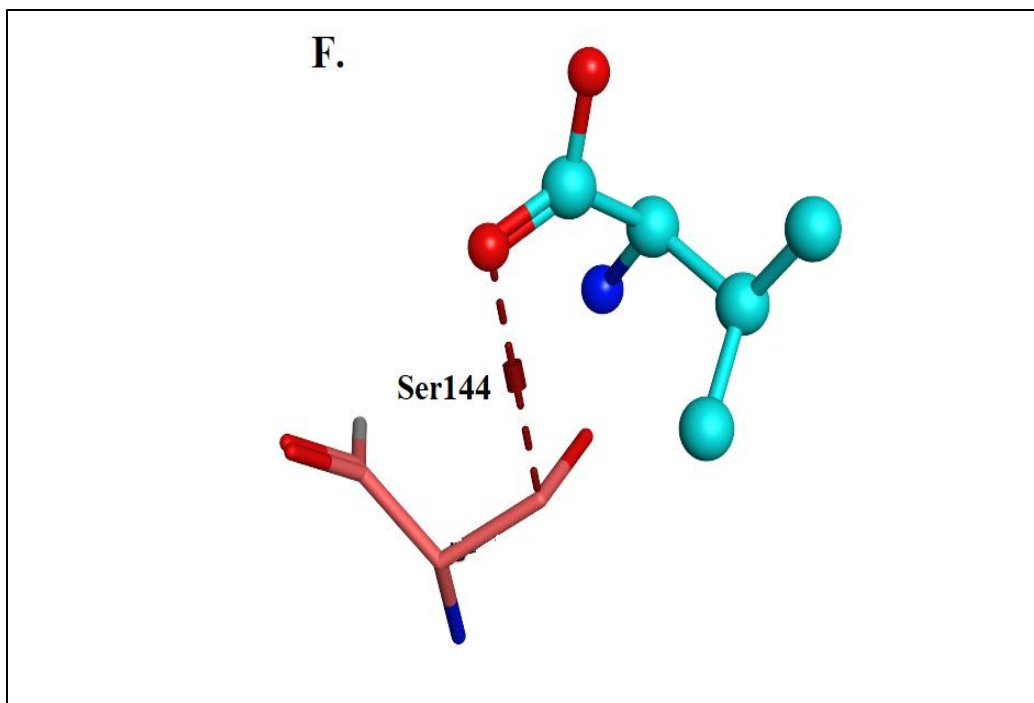**Figure 4.7:** Protein-ligand interactions of selected ligands docked on LAT1 complex. (A.) Ligand_1 showed interactions with P336, G197, T259, L333 (B.) Ligand_2 does not show any interaction before MD simulation (C.) Liagnd_3 showed unique interactions with P142, P338, G341 (D.) Ligand_4 showed interactions with I140, A141, P336 and (E.) Ligand_5 interacted with I140, A141. (F.) Ligand_6 interacted with S144.

4.4 Molecular Dynamic Simulation of Docking Complexes:

The molecular dynamic simulation of the selected inhibitors complexes with LAT1 will help us in achieving stability at the human body temperature and pressure. The stability of protein-ligand interactions was analyzed by giving an artificial body environment to the system. The selected inhibitors i.e., Lig_1, Lig_2, Lig_8, Lig_13, Lig_54 and Lig_58. The most active ligand (Ligand 1) docked with protein was stabilized at 100ns therefore, all other complexes were also observed at a 100ns time frame. The stability of the complexes was evaluated using the root mean square deviation (RMSD) plot. However, the H-bond stability graph was also evaluated to validate the docking interactions. CαRMSD measured the average deviation in atomic disruption of the Carbon-α backbone with simulation time frame. It was measured by

$$C\alpha RMSD = \sqrt{\frac{1}{N}\Sigma(r'(t_x)) - r'(t_{ref})N_{i=1}2}\ldots\ldots\ldots\ldots\ldots\ldots\text{Eq3}$$

RESULTS

The protein-ligand complex of the most active ligand (Lig-1) was stabilized at 100ns, with the protein RSMD between 1.5-2.4 Å and ligand RMSD of 2-2.8 Å **(figure 4.8).**
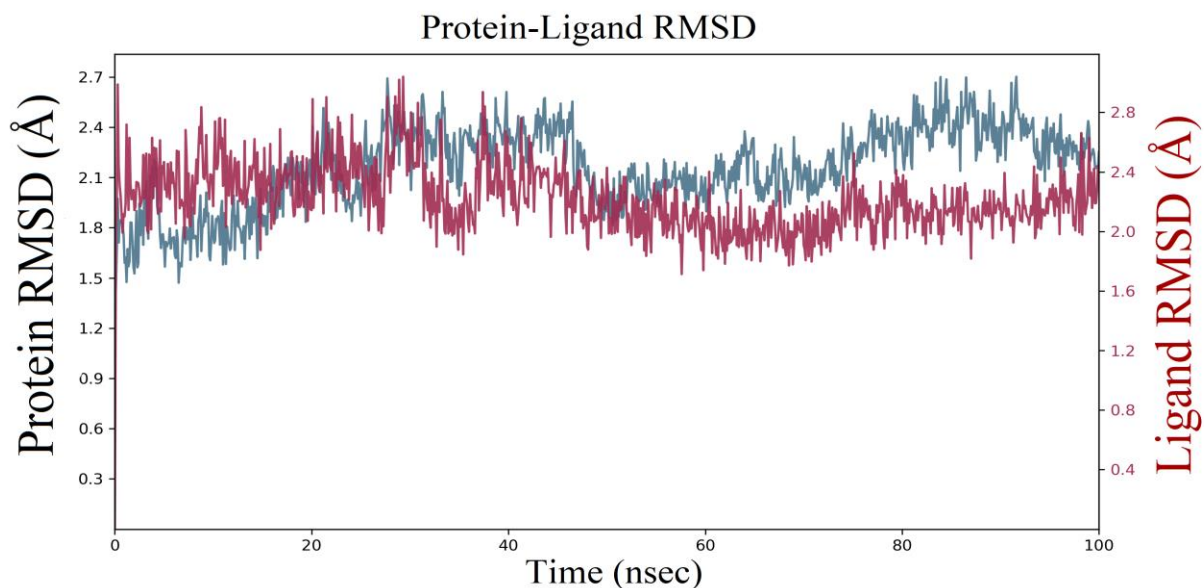
Figure 4.8: RMSD plots of protein-ligand complex_1 of active ligand 1, the complex showed less deviation after 40ns.

The RMSD plot proposed the complex_2 (Lig-2) complex stabilized after 70ns with protein RMSD of 2.8-3.2 Å and ligand RMSD of 7.0-8.0 Å. **Figure 4.9**
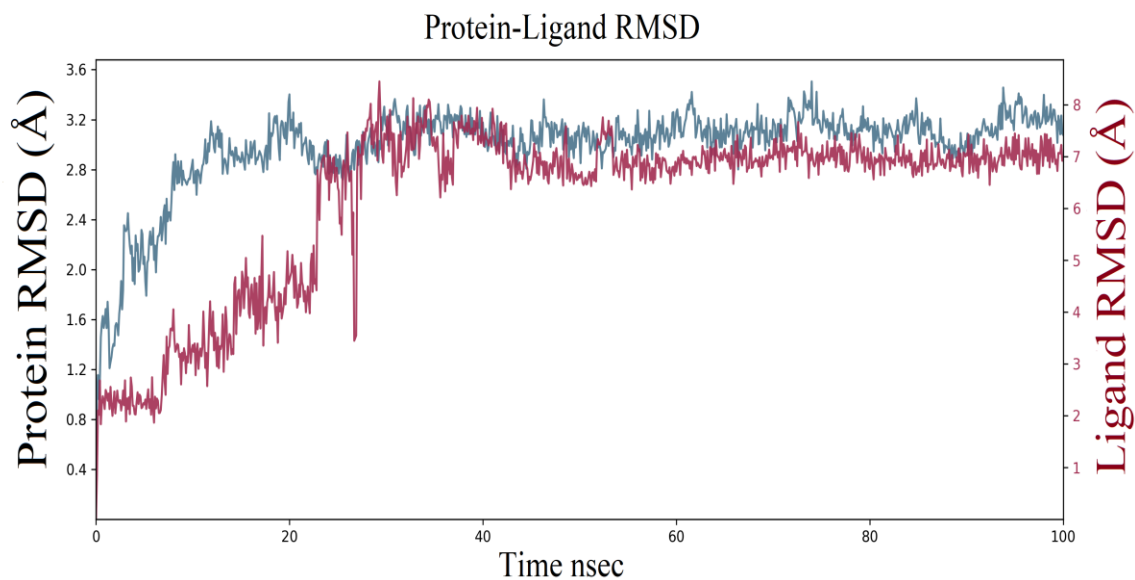
RESULTS

Figure 4.9: RMSD plots of protein-ligand complex_2 with active ligand 2, ligand_2 stabilized after 40ns with less deviations.

The complex_3 (Lig-8) showed vigorous fluctuations at the start and stabilized after a simulation time of 80ns with protein and ligand RMSD between 2-2.4 Å and 2-2.6 Å, respectively (figure 4.10)
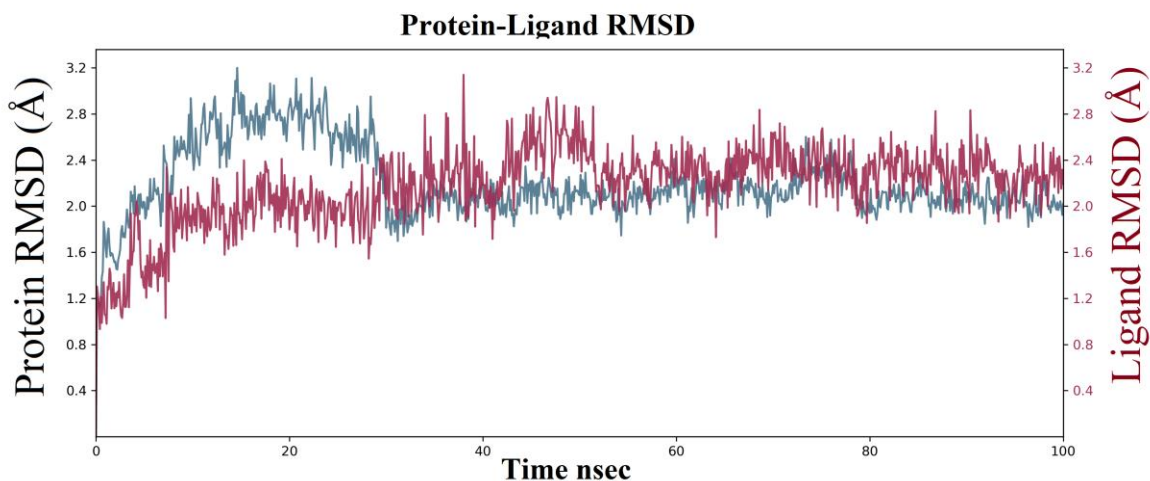
Figure 4.10: RMSD plots of protein-ligand complex_3 of active ligand 8, ligand_8 stabilized after 50ns with less deviations.

Complex_4 (Lig-54) was unstable initially and stabilized with a simulation time of 100ns, and after 60ns, the complex stabilized with protein RMSD around 2-2.4 Å and ligand around 0.8-2.4 Å. **Figure 4.11**

Figure 4.11: RMSD plots of protein-ligand complexes of inactive ligand_54.

Complex_5 (Lig-13) was unstable initially and stabilized with a simulation time of 100ns, and after 60ns, the complex stabilized with protein RMSD around 1.6-2.4 Å and ligand around 3.6-4.2 Å.
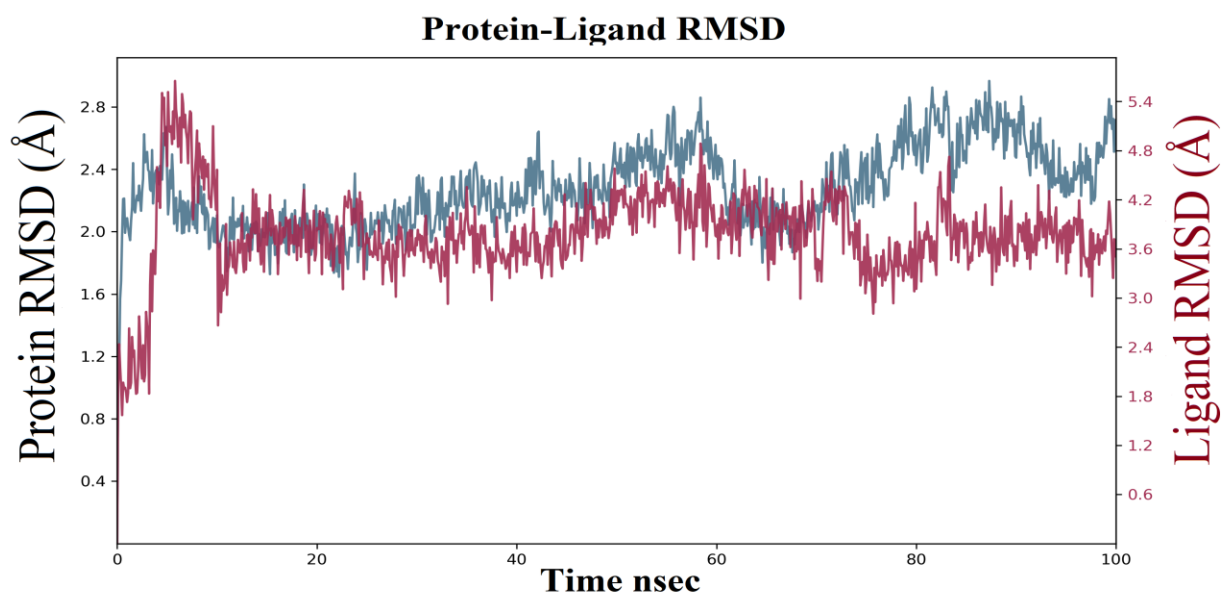
Figure 4.12: RMSD plots of protein-ligand complexes of active ligand_13.

Complex_6 (Lig-58) does not show stability. The protein remained stable with RMSD 2-2.4 Å at the start. However, the ligand remained unstable at the end with a RMSD of 2-4 Å (figure 4.9). At last,

the complex with Lig-61 having the lowest pIC50 was unstable throughout the period of 100ns simulation (**Figure 4.12**). This can also be due to the small molecular weight of Lig-61**. Figure 4.13**
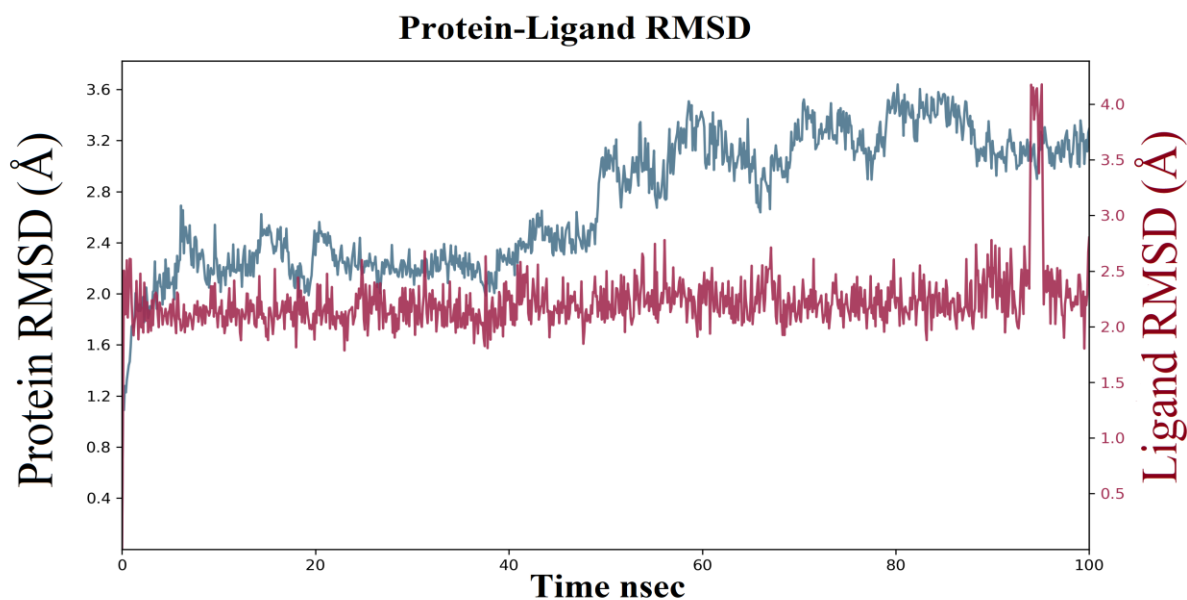
Figure 4.13: RMSD plots of protein-ligand complex_6 of inactive ligand_58 which does not show stability throughout 100ns simulation time.

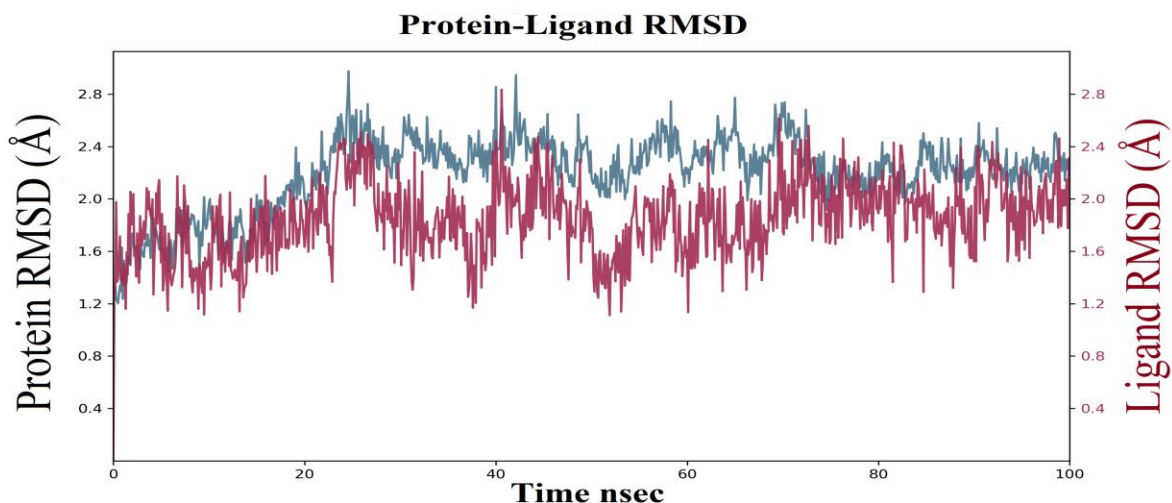The MD simulation of in-active ligand (Ligand 54 and 58) complexes indicated unstable complexes with unstable interactions. The RMSD plot of the ligand_54 complex proposed an unstable complex throughout the simulation time of 100ns with robust fluctuations towards the end. The ligand_58 protein complex had an irregular pattern with an increase in instability after 50ns.

The protein-ligand interactions of MD stabilized complexes were analyzed and validated using the H-bond stability plot. Few new protein-ligand interactions were observed after MD stabilization. The protein residues, Phe252, Lys204, Ser66, made interactions with ligands that were absent before MD simulation. The protein-ligand complexes with active ligands remained stable on the proposed binding pocket. After MD, the ligand_1 complex changed its interaction patterns and made stable interactions with S66, G136, A141, L204, T259, and P252. The stability of interactions can be visualized using H-bond plot. Protein residues like Glu136, Arg141, Ser66, Lys204 made stable interactions which remained stable throughout the MD simulation. Some of these residues were part of the previously reported LAT1 interface. The Ser66, Glu136 and Arg141 was involved in making H-bond with ligand whereas Lys204 and Tyr259 had hydrophobic interactions.
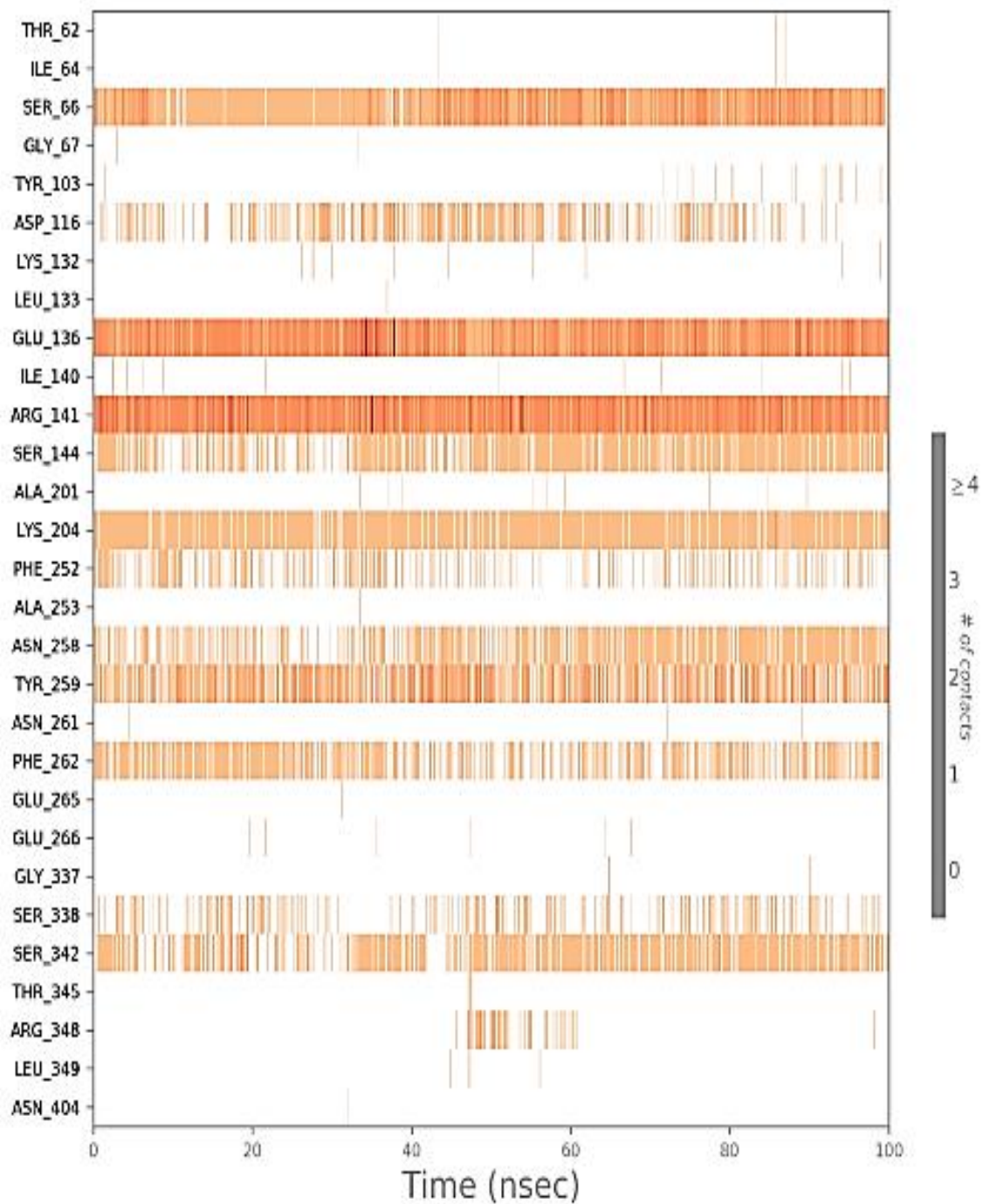
Figure 4.14: H-bond plot analysis of protein complex with ligand_1. The protein residues, S66, L204, T259, A141, G136, P252, Ser338 had a stable interaction with ligand.
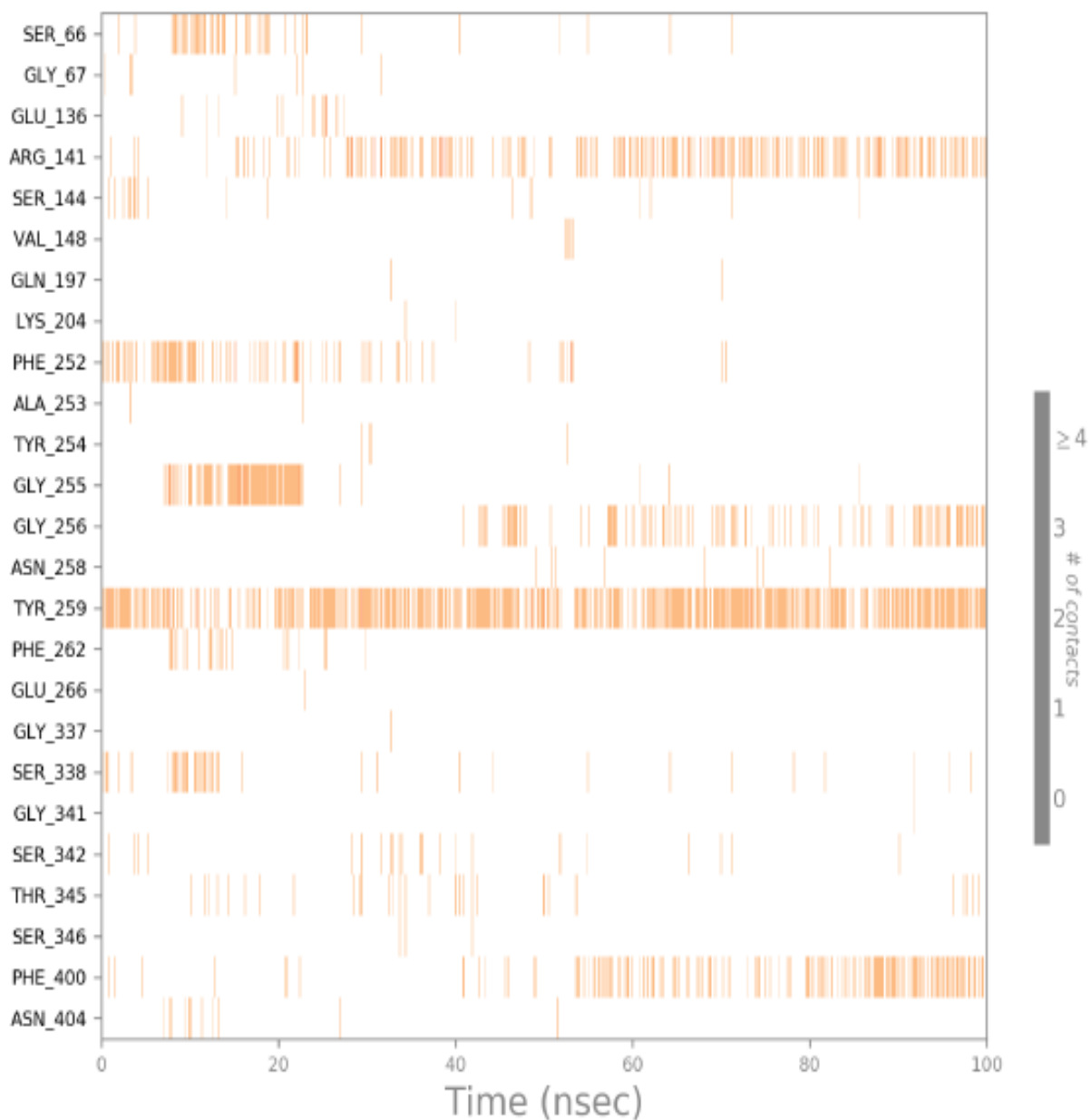
Figure 4.15: H-bond plot of ligand_2 protein complex. T259, Arg141, Gly256, Phe252, Phe400 had interaction in the simulation time of 100ns.

Analyzing the interaction pattern of the protein with ligand_2 indicated the abnormal behavior as no stable interaction was observed. However, slight interactions were indicated with Tyr259, Arg141 and Gly256 (figure 4.15). This may be due to the reason the ligand 2 has less molecular weight which might cause no optimal fit in the binding pocket, but it's increase activity may be due to some other factors like good Pharmacokinetics.

Figure 4.16: Some protein residues Arg141, Lys204, Tyr259, Phe252, Ser338, Gly197, Ser66 showed highly stable interaction pattern throughout simulation time in protein complex with ligand_3.

Figure 4.17: H-bond plot of ligand_4. The residues Arg141, Ser144, Ser342, Tyr259, Ile140, Ser338 showed stable interactions throughout the simulation time.

Figure 4.18: H-bond plot of ligand_5. Asp116, Lys132, Asn258, Gly136, Tyr259, Ser342, Tyr103 had stable interactions throughout the simulation time.

Figure 4.19: H-bond plot of ligand_6 protein complex. Ligand showed a stable interaction with protein residues, Ser144, Phe252, Tyr259.

Analyzing the before MD and after MD interaction patterns indicated the contrasting differences. Only few of the frequent occurring protein residues retained after MD stabilization which are Tyr259, Gly197, Arg141, Ser144. After MD, the three crucial protein residues, Ser66, Lys204 and Phe252 interactions were observed. These are residues present in the reported binding

cavity, made stable interactions after MD. After MD, the protein residues, Ser66, Lys204, Phe252 interacted with 1, 1, 3, 1, 3, 6 and 4 ligands, respectively, out of 6 ligands. The Lys204, Tyr259 and Arg141 interacted with three of the active ligands (1, 2, 8). Moreover, the protein residues, Phe336, Ser338, and Ile140 indicated multiple interactions before MD were deficient after MD. Therefore, the Lys204, Ser66, Phe252, Ser338 and Tyr259 were the crucial residues for inhibiting LAT1 interaction identified after MD. Furthermore, the pharmacophore modeling was done using ligand_1 complex as a template to discover more compounds inhibiting LAT1.

Comparison of protein-ligand interaction patterns of LAT1 with its inhibitors before and after MD is shown in the **Table 4.1.** The protein residues in bold were retained before and after MD.

No	Molecule ID	Before MD			After MD		
		Protein Residue		**Interaction Type**	**Protein Residue**		**Interaction Type**
1.	**CHEMBL4538666** Lig_1	Phe336 Gln197 **Tyr259** Leu333		H-bond H-bond Hydrophobic H-bond	Ser66 Gly136 Arg141 Lys204 **Tyr259** Ser338 Phe252		H-bond H-bond H-bond Hydrophobic Hydrophobic H-bond H-bond
2.	**CHEMBL4526588** Lig_2				Tyr259 Arg141 Gly256 Phe400 Phe252		Hydrophobic H-bond H-bond Hydrophobic Hydrophobic
3.	**CHEMBL4522605** Lig_8	Pro142 **Ser338** Gly341		H-bond Hydrophobic H-bond	Arg141 Lys204 Tyr259 Phe252 **Ser338** Gly197 Ser66		H-bond H-bond Hydrophobic Hydrophobic Hydrophobic H-bond H-bond
4.	**CHEMBL4241703** Lig_13	**Ile140** **Arg141** **Phe336**		Hydrophobic H-bond H-bond	**Arg141** Ser144 Ser342		H-bond H-bond H-bond

					Tyr259		Hydrophobic
					Ile140		Hydrophobic
5.	**CHEMBL4569744** Lig_54	Ile140 Arg141		Hydrophobic H-bond	Asp116 Lys132 Asn258 Gly136 Tyr103 Ser342 Tyr259		H-bond H-bond Hydrophobic H-bond H-bond H-bond Hydrophobic
6.	**CHEMBL1232398** Lig_58	**Ser144**		H-bond	**Ser144** Phe252 Tyr259		H-bond Hydrophobic Hydrophobic
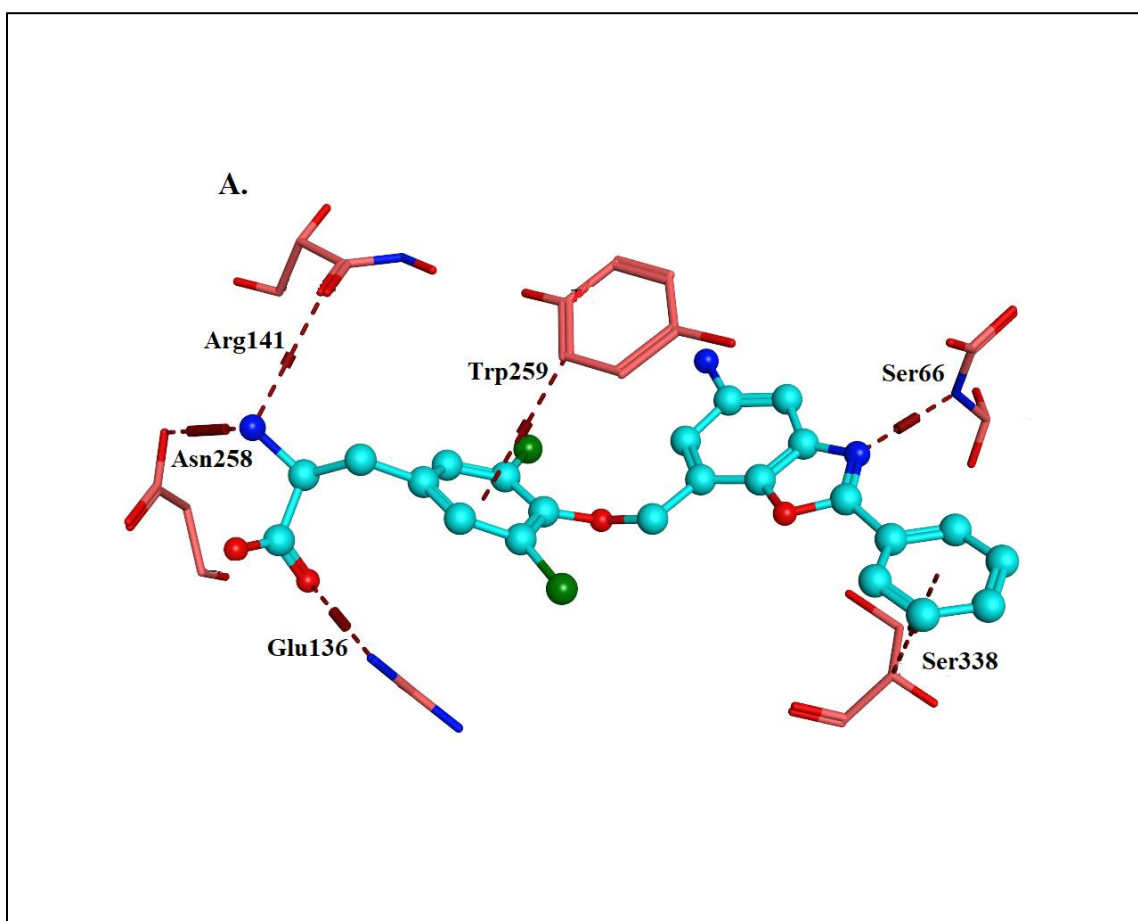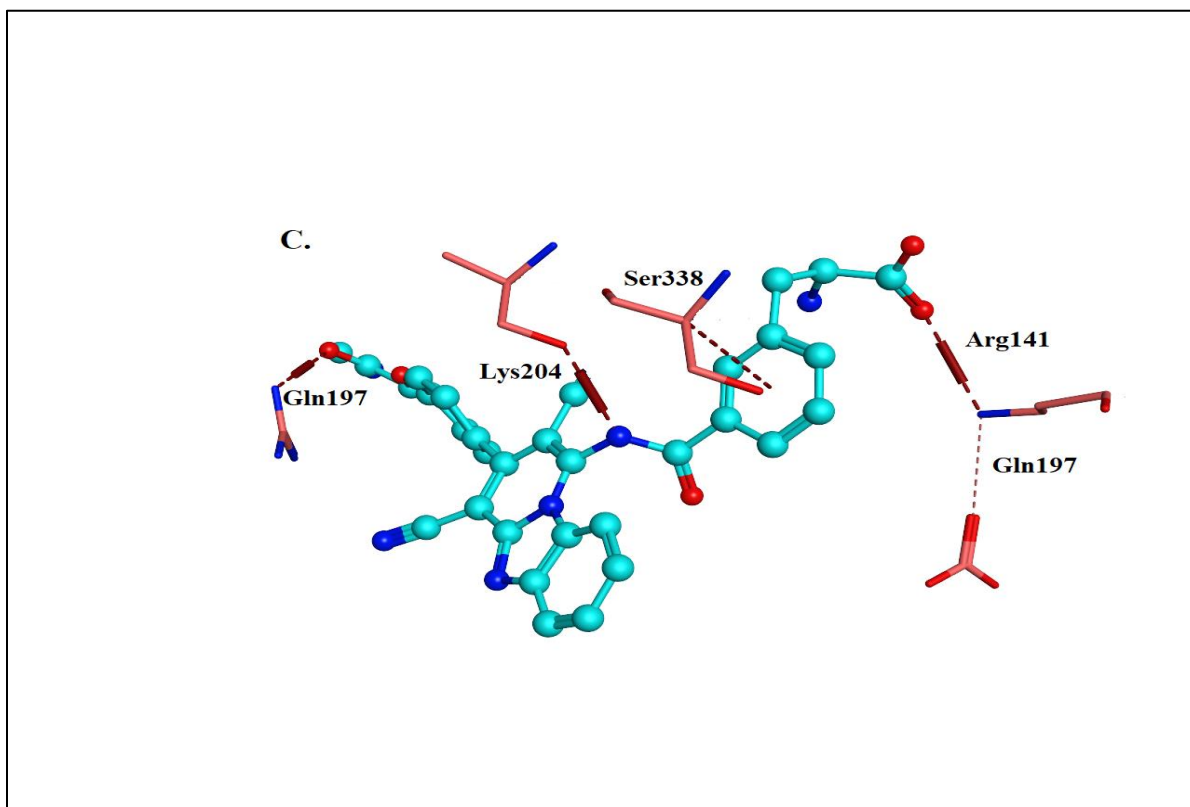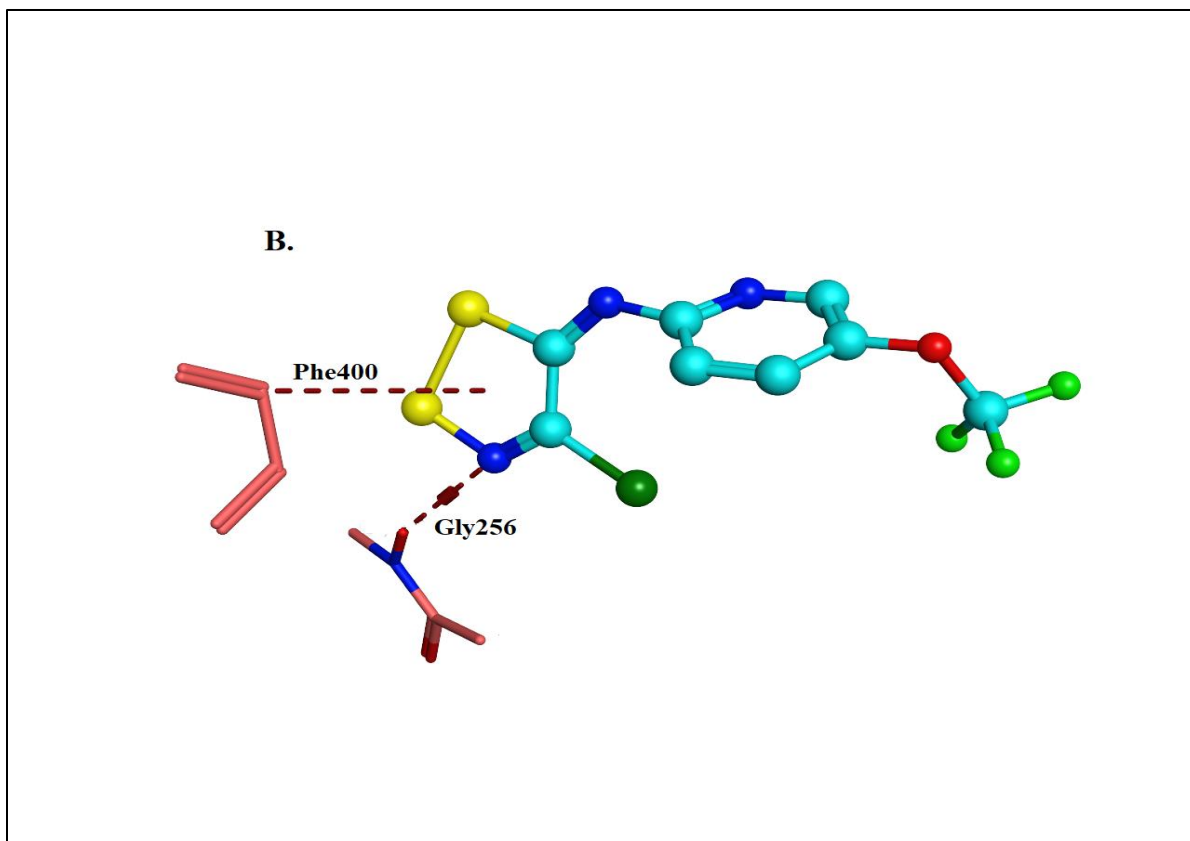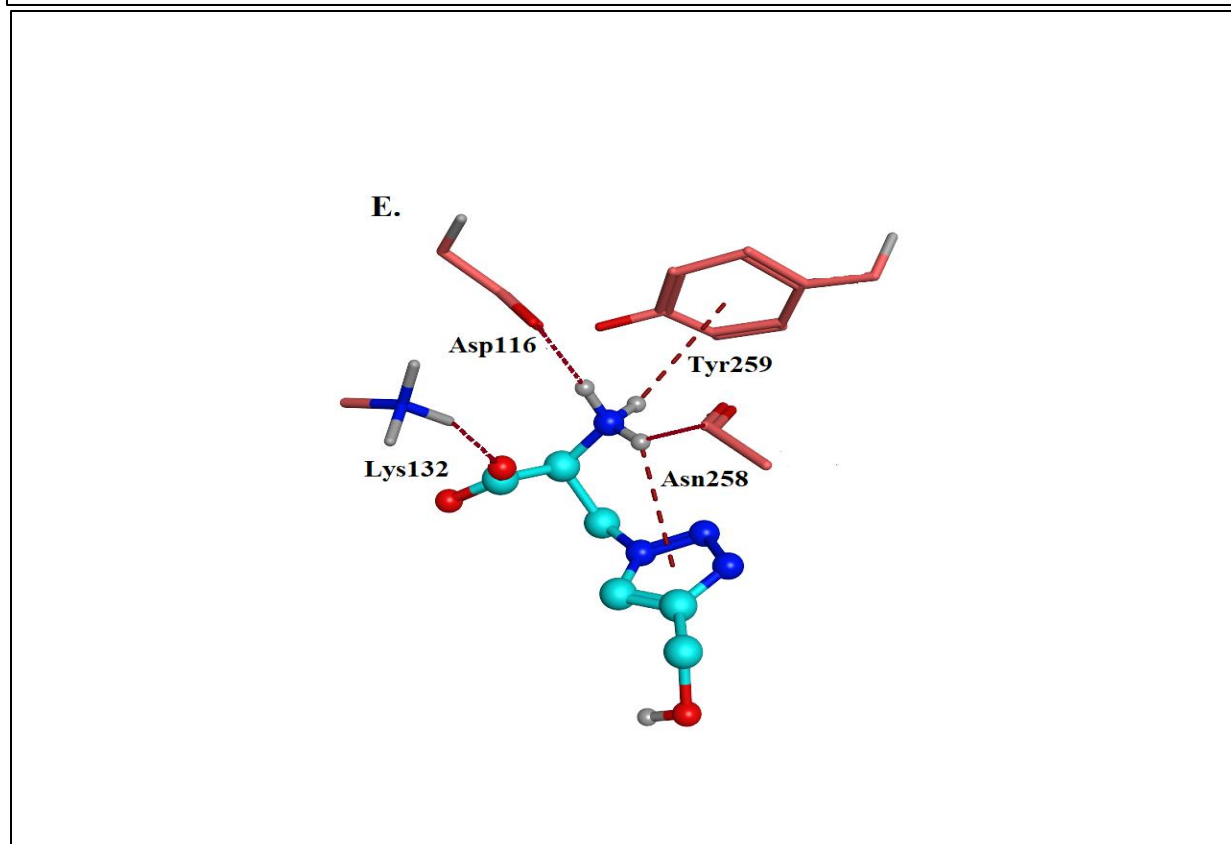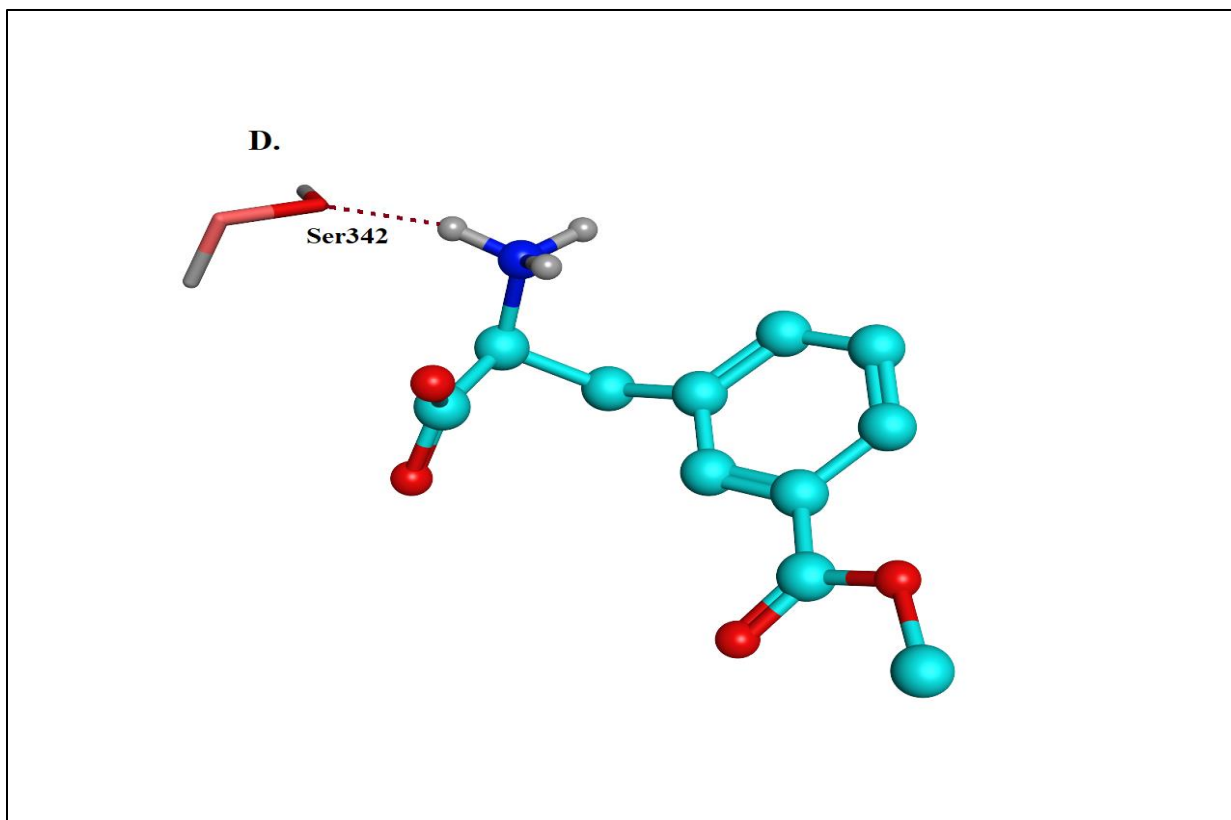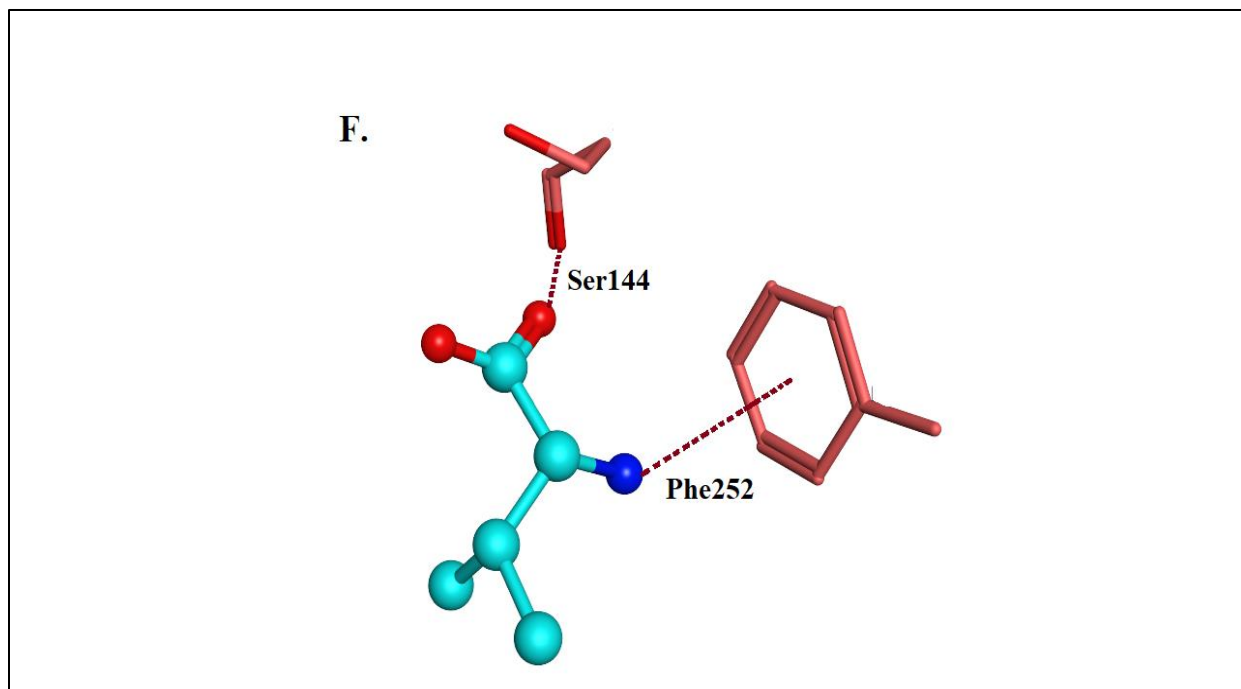
A.

Arg141

Trp259

Ser66

Asn258

Glu136

Ser338

77

Figure 4.20: Interaction pattern of active ligand-protein complexes after MD. (A.) ligand_1 (B.) ligand_2 (C.) ligand_3 (D.) ligand_4 (E.) ligand_5 and (F.) Ligand_6

1. Overall, after the Structural methodology analysis, it can be concluded that the identified binding site of LAT1 is highly significant for its inhibition as it remains stable during MD simulation

2. The analysis of binding residues and interaction suggest that the Ser66 forming the hydrogen bond is highly significant as it was found common in the highly active inhibitors and Lys204, Tyr259, Phe252 are also important residues because they are involved in the Hydrophobic interactions after the MD simulation.

3. Moreover, binding site before and after the MD simulation is hydrogen doner Hydrophobic residues so the inhibitor of the LAT1 should be hydrogen bond acceptor.

4. The LAT1 binding site identified by the docking protocol remains somehow stable during MD simulation.

4.5 Pharmacophore Modeling

The Complex-1 (ligand_1) after MD was chosen as a template for structure-based Pharmacophore modeling due to its stability during MD simulation and highest inhibitory activity value (IC$_{50}$ 790 nM). The activity threshold was defined to divide the dataset into active and in-actives. The activity threshold of 20,000nM was used and the IC$_{50}$ < 20,000nM were selected as actives, and the IC$_{50}$ > 20,000nM were selected as in-actives. Therefore, the first 9 ligands (ligand_1-ligand_9) lay in the active category, and the remaining ligands (ligand_10-ligand_58) came in the in-active category.

After the selection of the template, the Pharmacophore quires of ligand_1 were generated using LIGANDSCOUT 4.4.3. The features such as hydrogen bond donor (D), hydrogen bond acceptor (A), aromatic ring (R), hydrophobic (H), positive ionic charges (P), and negative ionic charges (N) were explored. A minimum of four features was used to build the model.

The final model generated using ligand_1 as a template had four features. Those include three hydrophobic features and 1 hydrogen bond donor (D).
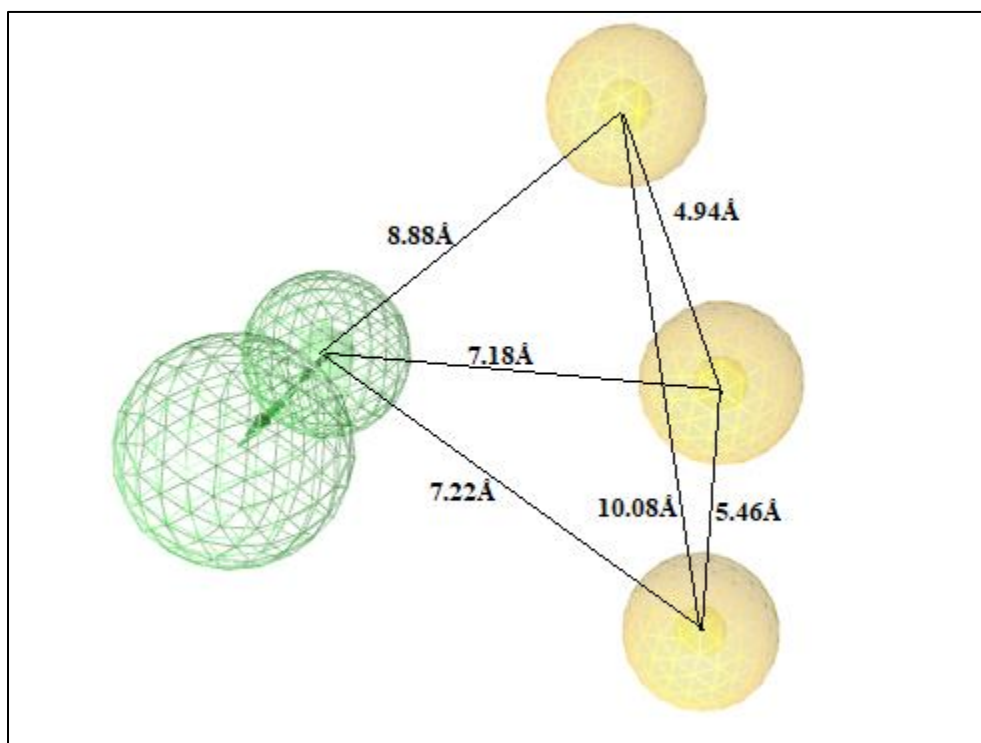
RESULTS

Figure 4.22: Pharmacophore model using ligand_1 complex as a template. Four features were used to build a model. The feature in green represents hydrogen bond donor, and yellow is hydrophobic feature. The lines represent the distance between features.

Table 4.2 Distance between the Four Pharmacophore features (F1_Don, F2_Don, F3_Don and F4_Hyd) and their radius in A°.

	F1_Don	**F2_Don**	**F3_Don**	**F4_Hyd**	**Radius for Model**
F1_Don	---------	4.94	10.08	8.88	0.9A°
F2_Don	4.94	----------	5.46	7.18	0.9A°
F3_Don	10.08	5.46	------------	7.22	0.9A°
F4_Don	8.88	7.18	7.22	---------	0.9A°

The accuracy of the model was evaluated. The model had an accuracy of 95% for the overall dataset. Due to the availability of diverse dataset, it was difficult to develop a perfect Pharmacophore model to predict inhibitors from an external dataset. The selected features were like the interacting residues after MD (Lys204, Ser66, Phe252, Ser338 and Tyr259). The model developed had seven true positives and fifty true negatives with two false positives and one false negative. The Pharmacophore model was then screened from the rest of the docked dataset for internal test validation. The model was able to classify the ligands as TP = 7, TN = 50, FP = 2 and FN =1. The statistics of the classification were then evaluated via a confusion matrix. The resultant of the matrix showed an accuracy of 95%, asserting that the Pharmacophore model was able to predict and classify the ligands as precisely (actives as actives, inactive as inactive). However, the value of precision and specificity or True Negative Rate (TNR), i.e., 0.96, declared that the model is specified. Similarly, the model's sensitivity or True Positive Rate (TPR) (0.87) indicated that the model is sensitive for all features associated with actives compounds (TP). The specificity (TNR) of 0.96 declared the given feature predicted inactive more precisely than actives (table 4.2).

RESULTS

Table 4.3 Statistical evaluation of the Pharmacophore model w.r.t internal Data

	Accuracy	TP Rate (Sensitivity)	TN Rate (Specificity)	FP Rate	Precision	MCC
Value	0.95	0.875	0.96	0.038	0.78	0.7964

Another statistical parameter was used to measure the predictive ability of the model. The Matthews Correlation Coefficient (MCC) measures the quality of agreement between predicted and actual values. Furthermore, the model was evaluated using the Matthews correlation coefficient (MCC). The model had an MCC of 0.79, indicating the presence of all features for inhibition of LAT1. Therefore, the model was considered as the potential model for virtual screening. The model evaluation statistics are given in table 4.2.

It is a correlation coefficient that takes all variables (TP, TN, FP, and FN) and gives scores based on model classification. The value near to or closer to 1 indicates the best agreement between predicted and actual responses. The MCC value (calculated via eq 4) [102] for the Pharmacophore model was 0.79, which indicated that the selected template and all true positive compounds with respective features have the ability to induce LAT1 Inhibition.

$$MCC = TP.TN - FP.FN \sqrt{(TP+FP).(TP+FN).(TN+FP).(TN+FN)} \ldots\ldots\ldots\ldots\ldots\ldots\ldots Eq4$$

CHAPTER 5

DISCUSSIONS

Discussion:

LAT1 is the most predominant L-type amino acid transporter in the human malignancies, wherever it supplies essential amino acids for growth and proliferation. As the biological significance of this transporter has become evident, our understanding of its structure and function has evolved significantly in recent decades. LAT1 is the most often overexpressed system L transporter in variety of tumor growths which makes it a promising therapeutic target. The increased localization and overexpression of LAT1 in cancers has made it a valuable target in cancer treatments because of its ability to decrease cancer cell proliferation and growth by reducing the supply of essential amino acids to the tumor cell. As a result, inhibiting LAT1 activity is considered as a promising target for cancer treatment. Some inhibitors inhibit LAT1 and ASCT2 in a powerful and irreversible manner. Because ASCT2 and LAT1 work together to control leucine transport and activate the mTOR pathway, these covalent inhibitors may be effective in inhibiting tumor development by acting on both pathways. Acivicin is an excellent example of a drug that inhibits cancer growth by inhibiting both LAT1 and ASCT2 and binding to metabolic enzymes (e.g., the aldehyde dehydrogenase enzyme family). Many LAT1 selective inhibitors have been identified because of SAR-guided experimental research, with KYT-0353 emerging as a promising and robust molecule now undergoing clinical trials. Thanks to the growing availability of X-ray crystallographic structures of many trans membrane transporters, including LAT1, MD simulation in conjunction with molecular docking has been successfully utilized in the creation of novel ligands for various protein targets of the SLC family.

Furthermore, these computational models have demonstrated their use in elucidating the molecular basis of drug transporter interaction for therapeutic targets. We provide a successful structure-based design method that resulted in the discovery of potent novel LAT1 inhibitors with an exceptional hit rate. The aim of this study was the investigation of the inhibitors and binding interaction and identification of the important residues for the inhibition of LAT1. The study of the interaction pattern is not possible without the 3D molecular structure of the protein. In this case, the PDB had the 3D X-ray crystallographic structure of LAT1 available. An approach to further increase stability of the binding of complexes, MD simulation was employed. MD simulation before docking protein will lead to better binding poses as well as a more stable protein-ligand complex during the docking. The LAT1 protein was stable at 250 ns with RMSD between 2.0-2.4 Å. This step not only reduces the number of loops in the structure but also increases the stability of LAT1. For the

DISCUSSIONS

inhibitors data against LAT1, it was collected from literature and ChEMBL database. A total of fifty-eight inhibitors were retrieved from the CHEMBL Database.

After the structure is stabilized by the MD simulation, the docking of proteins was next the step. As the exhaustive literature review and Chembl Database led to discovery of 58 inhibitors against LAT1. Docking of LAT1 was performed by selecting the binding cavity near the residues reported in the previous docking studies. For each inhibitor 100 poses were generated within the binding cavity. The correlation between the Gold Score of the best binding poses and affinity of the compound expressed as pIC_{50} for LAT1 was found to be $R_2 = 0.64$ which demonstrates the strong direct correlation. This correlation validates the docking protocol and explains the activity of most of the inhibitors due to the binding energy of compounds. Few exceptions were also observed; these inhibitors may have the activity due to the transport of compound towards the target rather than the interaction of inhibitor with the target. To get a deeper look, a correlation between the molecular weight and pIC_{50} was also studied which relived that a positive correlation of 0.64 exists between these variables. This correlation value also shows direct positive correlation; it shows that the selected inhibitor had a high difference in the molecular weight which cause the change in the pIC_{50} value. From this we can say that High molecular weight may not have a bad impact on the lead optimization.

MD simulation of selected complexes of LAT1 was performed and it was found that almost all the active ligand complexes achieved a stable RMSD between 2.0 to 7.0 Å for the simulation of 100 ns duration. The MD simulation is the process that helps in the identification of the actively meaningful interaction for a specific period under the human body temperature and pressure [53]. The continuous force exerted on the molecules of complex only sustains the most stable interaction while breaking the less stable bonds. This resulted in the change of the binding site from the docking results. This change in binding site is more stable than docking results, as docking only provides a single snapshot of many interactions and docking score is also restricted by the binding cavity definition based on before docking studies.

Although LAT1 lack a common interaction between all the selected inhibitor, it was found that try259, Ser66, Lys204 and Phe252 were present in more than one highly active inhibitor interaction and hence are significant for inhibition. Moreover, the hydrogen bond interactions were common in all the selected inhibitors of LAT1 which represents that ligand with complimentary properties can be used for inhibition.

DISCUSSIONS

LAT1's X ray crystallographic structure revealed significant details about the substrate binding region. LAT1's binding site is well-organized and centrally positioned, having hydrophilic and hydrophobic areas that mediate the binding of the amino acid moiety and side chain. Docking results revealed that the hydrogen bond contacts of the amino acid moiety are sustained between LAT1 and AdiC, and the residues on TM1 and TM6 are important for ligand binding. The positively charged amino group is bound by Ile63, Phe252, and Gly255 of the GSG motif, whereas the negatively charged carboxyl group is bound by Ser66 and Gly67 of the GSG motif via backbone hydrogen bond interactions. Moreover, the side chains of residues Ser66 and Ser338 engage with the carboxyl group electrostatically. Hydrophobic interactions with aromatic Phe252, Phe402, Trp405, and aliphatic Ile139 and Ile140 are involved in the ligand's side chain binding. Phe252A mutation completely abolishes LAT1 transport activity, indicating that Phe252 serves as a proximal gate that prevents the substrate from entering the periplasm, according to Napolitano and colleagues [29]. Moreover, it was identified that lig_1, lig_2 and lig_8 made the most stable complexes with the protein after MD. These ligands had interactions with protein residues Ser66, Lys204, Tyr259 and Phe252. Furthermore, lig_1 complex with the highest inhibitory activity value (IC$_{50}$ 790nM) obtained after MD was used as a template to develop a pharmacophore model to predict potential hits for inhibiting LAT1. We uncovered critical pharmacophoric properties of active ligands that are involved in binding by adding dynamics into structure-based pharmacophores. Four pharmacophoric features were identified during the structure-based Pharmacophore Modeling; those four features include three-hydrophobic features (H1, H2, and H3) and one Hydrogen bond donor feature. Furthermore, this study will expand the area of future SAR analyses, which might aid in the rational drug design and production of novel LAT1 inhibitors. In conclusion, our endorsed structure-based technique might be applied in drug-discovery operations aimed at additional transporters which are important biologically.

CHAPTER 6

CONCLUSION

CONCLUSION

In conclusion, the present study was designed with the therapeutic intervention of Inhibiting the L-Type amino acid transporter 1 for anti-cancer treatment. It was accomplished by stabilizing the target protein through MD simulation and then performing molecular docking to elucidate the binding hypothesis between LAT1 and its inhibitors. Based on docking results, a highly active ligand, a least active ligand along with some ligands that show outlier behavior were selected and subjected to MD simulation to accomplished stable interaction and validate our binding hypothesis. The stable residues in the actual binding cavity demonstrating the energy contours in the virtual receptor site were Ser66, Lys204, Tyr259 and Phe252. After MD simulation, the highly active ligand complex (lig_1) was then used as a template for the feature extraction and predictive model formation. The structure-based Pharmacophore model was generated to predict LAT1 inhibitors. The bioactive pharmacophore model exhibits one H-bond donor and three hydrophobic features. With respective features, the statistical evaluation was made against the rest of the ligand dataset. The accuracy of 95% declared the significance of the model. Overall, the presented project gives a new in-silico dimension in the therapeutics of anti-cancer treatments and will provide insightful measures in rational drug designing in the future.

CHAPTER 7

REFERENCES

References

1. Hanahan, D.; Weinberg, R.A. Hallmarks of cancer: The next generation. Cell 2011, 144, 646–674.

2. Eagle, H. Nutrition needs of mammalian cells in tissue culture. Science 1955, 122, 501–514.

3. Qi, W.; Guan, Q.; Sun, T.; Cao, Y.; Zhang, L.; Guo, Y. Improving detection sensitivity of amino acids in thyroid tissues by using phthalic acid as a mobile phase additive in hydrophilic interaction chromatography-electrospray ionization-tandem mass spectrometry. Anal. Chim. Acta 2015, 870, 75–82.

4. Kirikae, M.; Diksic, M.; Yamamoto, Y.L. Quantitative measurements of regional glucose utilization and rate of valine incorporation into proteins by double-tracer autoradiography in the rat brain tumor model. J. Cereb. Blood Flow Metab. 1989, 9, 87–95.

5. Wang, L.-B.; Shen, J.-G.; Zhang, S.-Z.; Ding, K.-F.; Zheng, S. Amino acid uptake in arterio-venous serum of normal and cancerous colon tissues. World J. Gastroenterol. 2004, 10, 1297–1300.

6. Hosios, A.M.; Hecht, V.C.; Danai, L.V.; Johnson, M.O.; Rathmell, J.C.; Steinhauser, M.L.; Manalis, S.R.; Vander Heiden, M.G. Amino Acids Rather than Glucose Account for the Majority of Cell Mass in Proliferating Mammalian Cells. Dev. Cell 2016, 36, 540–549.

7. Wang, Q.; Holst, J. L-type amino acid transport and cancer: Targeting the mTORC1 pathway to inhibit neoplasia. Am. J. Cancer Res. 2015, 5, 1281–1294.

8. Nakamura, E.; Sato, M.; Yang, H.; Miyagawa, F.; Harasaki, M.; Tomita, K.; Matsuoka, S.; Noma, A.; Iwai, K.; Minato, N. 4F2 (CD98) heavy chain is associated covalently with an amino acid transporter and controls intracellular trafficking and membrane topology of 4F2 heterodimer. J. Biol. Chem. 1999, 274, 3009–3016.

9. Kanai, Y.; Segawa, H.; Miyamoto, K.; Uchino, H.; Takeda, E.; Endou, H. Expression cloning and characterization of a transporter for large neutral amino acids activated by the heavy chain of 4F2 antigen (CD98). J. Biol. Chem. 1998, 273, 23629–23632.

REFERENCES

10. Mastroberardino, L.; Spindler, B.; Pfeiffer, R.; Skelly, P.J.; Loffing, J.; Shoemaker, C.B.; Verrey, F. Amino-acid transport by heterodimers of 4F2hc/CD98 and members of a permease family. Nature 1998, 395, 288–291.

11. Meier, C.; Ristic, Z.; Klauser, S.; Verrey, F. Activation of system L heterodimeric amino acid exchangers by intracellular substrates. EMBO J. 2002, 21, 580–589.

12. Yanagida, O.; Kanai, Y.; Chairoungdua, A.; Kim, D.K.; Segawa, H.; Nii, T.; Cha, S.H.; Matsuo, H.; Fukushima, J.; Fukasawa, Y.; et al. Human L-type amino acid transporter 1 (LAT1): Characterization of function and expression in tumor cell lines. Biochim. Biophys. Acta 2001, 1514, 291–302.

13. Furuya, M.; Horiguchi, J.; Nakajima, H.; Kanai, Y.; Oyama, T. Correlation of L-type amino acid transporter 1 and CD98 expression with triple negative breast cancer prognosis. Cancer Sci. 2012, 103, 382–389.

14. Liang, Z.; Cho, H.T.; Williams, L.; Zhu, A.; Liang, K.; Huang, K.; Wu, H.; Jiang, C.; Hong, S.; Crowe, R.; et al. Potential Biomarker of L-type Amino Acid Transporter 1 in Breast Cancer Progression. Nucl. Med. Mol. Imaging 2011, 45, 93–102.

15. Segawa, A.; Nagamori, S.; Kanai, Y.; Masawa, N.; Oyama, T. L-type amino acid transporter 1 expression is highly correlated with Gleason score in prostate cancer. Mol. Clin. Oncol. 2013, 1, 274–280.

16. Sakata, T.; Ferdous, G.; Tsuruta, T.; Satoh, T.; Baba, S.; Muto, T.; Ueno, A.; Kanai, Y.; Endou, H.; Okayasu, I. L-type amino-acid transporter 1 as a novel biomarker for high-grade malignancy in prostate cancer. Pathol. Int. 2009, 59, 7–18.

17. Xu, M.; Sakamoto, S.; Matsushima, J.; Kimura, T.; Ueda, T.; Mizokami, A.; Kanai, Y.; Ichikawa, T. Up-Regulation of LAT1 during Antiandrogen Therapy Contributes to Progression in Prostate Cancer Cells. J. Urol. 2016, 195, 1588–1597.

18. Takeuchi, K.; Ogata, S.; Nakanishi, K.; Ozeki, Y.; Hiroi, S.; Tominaga, S.; Aida, S.; Matsuo, H.; Sakata, T.; Kawai, T. LAT1 expression in non-small-cell lung carcinomas: Analyses by semiquantitative reverse transcription-PCR (237 cases) and immunohistochemistry (295 cases). Lung Cancer 2010, 68, 58–65.

REFERENCES

19. Kaira, K.; Oriuchi, N.; Imai, H.; Shimizu, K.; Yanagitani, N.; Sunaga, N.; Hisada, T.; Ishizuka, T.; Kanai, Y.; Endou, H.; et al. Prognostic significance of L-type amino acid transporter 1 (LAT1) and 4F2 heavy chain (CD98) expression in early stage squamous cell carcinoma of the lung. Cancer Sci. 2009, 100, 249–254.

20. Kaira, K.; Oriuchi, N.; Imai, H.; Shimizu, K.; Yanagitani, N.; Sunaga, N.; Hisada, T.; Ishizuka, T.; Kanai, Y.; Nakajima, T.; et al. Prognostic significance of L-type amino acid transporter 1 (LAT1) and 4F2 heavy chain (CD98) expression in stage I pulmonary adenocarcinoma. Lung Cancer 2009, 66, 120–126.

21. Kaira, K.; Oriuchi, N.; Imai, H.; Shimizu, K.; Yanagitani, N.; Sunaga, N.; Hisada, T.; Tanaka, S.; Ishizuka, T.; Kanai, Y.; et al. Prognostic significance of L-type amino acid transporter 1 expression in resectable stage I-III nonsmall cell lung cancer. Br. J. Cancer 2008, 98, 742–748.

22. Yazawa, T.; Shimizu, K.; Kaira, K.; Nagashima, T.; Ohtaki, Y.; Atsumi, J.; Obayashi, K.; Nagamori, S.; Kanai, Y.; Oyama, T.; et al. Clinical significance of coexpression of L-type amino acid transporter 1 (LAT1) and ASC amino acid transporter 2 (ASCT2) in lung adenocarcinoma. Am. J. Transl. Res. 2015, 7, 1126–1139.

23. Kaira, K.; Oriuchi, N.; Imai, H.; Shimizu, K.; Yanagitani, N.; Sunaga, N.; Hisada, T.; Kawashima, O.; Iijima, H.; Ishizuka, T.; et al. Expression of L-type amino acid transporter 1 (LAT1) in neuroendocrine tumors of the lung. Pathol. Res. Pract. 2008, 204, 553–561.

24. Nakanishi, K.; Matsuo, H.; Kanai, Y.; Endou, H.; Hiroi, S.; Tominaga, S.; Mukai, M.; Ikeda, E.; Ozeki, Y.; Aida, S.; et al. LAT1 expression in normal lung and in atypical adenomatous hyperplasia and adenocarcinoma of the lung. Virchows Arch. 2006, 448, 142–150.

25. Kaira, K.; Oriuchi, N.; Imai, H.; Shimizu, K.; Yanagitani, N.; Sunaga, N.; Hisada, T.; Kawashima, O.; Kamide, Y.; Ishizuka, T.; et al. Prognostic significance of L-type amino acid transporter 1 (LAT1) and 4F2 heavy chain (CD98) expression in surgically resectable stage III non-small cell lung cancer. Exp. Ther. Med. 2010, 1, 799–808.

26. Kaira, K.; Oriuchi, N.; Imai, H.; Shimizu, K.; Yanagitani, N.; Sunaga, N.; Hisada, T.; Kawashima, O.; Kamide, Y.; Ishizuka, T.; et al. CD98 expression is associated with poor

REFERENCES

prognosis in resected non-small-cell lung cancer with lymph node metastases. Ann. Surg. Oncol. 2009, 16, 3473–3481.

27. Kaira, K.; Oriuchi, N.; Shimizu, K.; Imai, H.; Tominaga, H.; Yanagitani, N.; Sunaga, N.; Hisada, T.; Ishizuka, T.; Kanai, Y.; et al. Comparison of l-type amino acid transporter 1 expression and l-[3-18F]-α-methyl tyrosine uptake in outcome of non-small cell lung cancer. Nucl. Med. Biol. 2010, 37, 911–916.

28. Kaira, K.; Kawashima, O.; Endoh, H.; Imaizumi, K.; Goto, Y.; Kamiyoshihara, M.; Sugano, M.; Yamamoto, R.; Osaki, T.; Tanaka, S.; et al. Expression of amino acid transporter (LAT1 and 4F2hc) in pulmonary pleomorphic carcinoma. Hum. Pathol. 2018, 84, 142–149.

29. Imai, H.; Kaira, K.; Oriuchi, N.; Yanagitani, N.; Sunaga, N.; Ishizuka, T.; Kanai, Y.; Endou, H.; Nakajima, T.; Mori, M. L-type amino acid transporter 1 expression is a prognostic marker in patients with surgically resected stage I non-small cell lung cancer. Histopathology 2009, 54, 804–813.

30. Imai, H.; Kaira, K.; Oriuchi, N.; Shimizu, K.; Tominaga, H.; Yanagitani, N.; Sunaga, N.; Ishizuka, T.; Nagamori, S.; Promchan, K.; et al. Inhibition of L-type amino acid transporter 1 has antitumor activity in non-small cell lung cancer. Anticancer Res. 2010, 30, 4819–4828.

31. Xie, X.-L.; Kakehashi, A.; Wei, M.; Yamano, S.; Takeshita, M.; Yunoki, T.; Wanibuchi, H. L-Leucine and L-isoleucine enhance growth of BBN-induced urothelial tumors in the rat bladder by modulating expression of amino acid transporters and tumorigenesis-associated genes. Food Chem. Toxicol. 2013, 59, 137–144.

32. Koshi, H.; Sano, T.; Handa, T.; Yanagawa, T.; Saitou, K.; Nagamori, S.; Kanai, Y.; Takagishi, K.; Oyama, T. L-type amino acid transporter-1 and CD98 expression in bone and soft tissue tumors. Pathol. Int. 2015, 65, 460–467.

33. Haining, Z.; Kawai, N.; Miyake, K.; Okada, M.; Okubo, S.; Zhang, X.; Fei, Z.; Tamiya, T. Relation of LAT1/4F2hc expression with pathological grade, proliferation and angiogenesis in human gliomas. BMC Clin. Pathol. 2012, 12, 4.

REFERENCES

34. Nawashiro, H.; Otani, N.; Shinomiya, N.; Fukui, S.; Ooigawa, H.; Shima, K.; Matsuo, H.; Kanai, Y.; Endou, H. L-type amino acid transporter 1 as a potential molecular target in human astrocytic tumors. Int. J. Cancer 2006, 119, 484–492.

35. Uno, K.; Kuwabara, H.; Terado, Y.; Kojima, K.; Kawakami, T.; Kamma, H.; Sakurai, H.; Sakamoto, A.; Kurata, A. Divergent expression of L-type amino acid transporter 1 during uterine cervical carcinogenesis. Hum. Pathol. 2011, 42, 1660–1666.

36. Marshall, A.D.; van Geldermalsen, M.; Otte, N.J.; Anderson, L.A.; Lum, T.; Vellozzi, M.A.; Zhang, B.K.; Thoeng, A.; Wang, Q.; Rasko, J.E.J.; et al. LAT1 is a putative therapeutic target in endometrioid endometrial carcinoma. Int. J. Cancer 2016, 139, 2529–2539.

37. Kobayashi, H.; Ishii, Y.; Takayama, T. Expression of L-type amino acid transporter 1 (LAT1) in esophageal carcinoma. J. Surg. Oncol. 2005, 90, 233–238.

38. Honjo, H.; Kaira, K.; Miyazaki, T.; Yokobori, T.; Kanai, Y.; Nagamori, S.; Oyama, T.; Asao, T.; Kuwano, H. Clinicopathological significance of LAT1 and ASCT2 in patients with surgically resected esophageal squamous cell carcinoma. J. Surg. Oncol. 2016, 113, 381–389.

39. Hashimoto, H.; Kurata, A.; Kikuchi, H.; Masuda, Y.; Fujita, K.; Okuyama, R.; Inoue, S.; Horiuchi, H.; Kuroda, M. L-type amino acid transporter 1 expression in esophageal carcinogenesis according to WHO and Japanese classifications of intraepithelial neoplasia. Pathol. Int. 2017, 67, 247–255.

40. Ichinoe, M.; Yanagisawa, N.; Mikami, T.; Hana, K.; Nakada, N.; Endou, H.; Okayasu, I.; Murakumo, Y. L-Type amino acid transporter 1 (LAT1) expression in lymph node metastasis of gastric carcinoma: Its correlation with size of metastatic lesion and Ki-67 labeling. Pathol. Res. Pract. 2015, 211, 533–538.

41. Ichinoe, M.; Mikami, T.; Yoshida, T.; Igawa, I.; Tsuruta, T.; Nakada, N.; Anzai, N.; Suzuki, Y.; Endou, H.; Okayasu, I. High expression of L-type amino-acid transporter 1 (LAT1) in gastric carcinomas: Comparison with non-cancerous lesions. Pathol. Int. 2011, 61, 281–289.

42. Ohkame, H.; Masuda, H.; Ishii, Y.; Kanai, Y. Expression of L-type amino acid transporter 1 (LAT1) and 4F2 heavy chain (4F2hc) in liver tumor lesions of rat models. J. Surg. Oncol. 2001, 78, 265–271; discussion 271–272.

REFERENCES

43. Li, J.; Qiang, J.; Chen, S.-F.; Wang, X.; Fu, J.; Chen, Y. The impact of L-type amino acid transporter 1 (LAT1) in human hepatocellular carcinoma. Tumour Biol. 2013, 34, 2977–2981.

44. Ogihara, K.; Naya, Y.; Sato, R.; Onda, K.; Ochiai, H. Analysis of L-type amino acid transporter in canine hepatocellular carcinoma. J. Vet. Med. Sci. 2015, 77, e1-2.

45. Namikawa, M.; Kakizaki, S.; Kaira, K.; Tojima, H.; Yamazaki, Y.; Horiguchi, N.; Sato, K.; Oriuchi, N.; Tominaga, H.; Sunose, Y.; et al. Expression of amino acid transporters (LAT1, ASCT2 and xCT) as clinical significance in hepatocellular carcinoma. Hepatol. Res. 2015, 45, 1014–1022.

46. Kaira, K.; Sunose, Y.; Arakawa, K.; Ogawa, T.; Sunaga, N.; Shimizu, K.; Tominaga, H.; Oriuchi, N.; Itoh, H.; Nagamori, S.; et al. Prognostic significance of L-type amino-acid transporter 1 expression in surgically resected pancreatic cancer. Br. J. Cancer 2012, 107, 632–638.

47. Yanagisawa, N.; Ichinoe, M.; Mikami, T.; Nakada, N.; Hana, K.; Koizumi, W.; Endou, H.; Okayasu, I. High expression of L-type amino acid transporter 1 (LAT1) predicts poor prognosis in pancreatic ductal adenocarcinomas. J. Clin. Pathol. 2012, 65, 1019–1023.

48. Toyoda, M.; Kaira, K.; Ohshima, Y.; Ishioka, N.S.; Shino, M.; Sakakura, K.; Takayasu, Y.; Takahashi, K.; Tominaga, H.; Oriuchi, N.; et al. Prognostic significance of amino-acid transporter expression (LAT1, ASCT2, and xCT) in surgically resected tongue cancer. Br. J. Cancer 2014, 110, 2506–2513.

49. Betsunoh, H.; Fukuda, T.; Anzai, N.; Nishihara, D.; Mizuno, T.; Yuki, H.; Masuda, A.; Yamaguchi, Y.; Abe, H.; Yashi, M.; et al. Increased expression of system large amino acid transporter (LAT)-1 mRNA is associated with invasive potential and unfavorable prognosis of human clear cell renal cell carcinoma. BMC Cancer 2013, 13, 509.

50. Rosilio, C.; Nebout, M.; Imbert, V.; Griessinger, E.; Neffati, Z.; Benadiba, J.; Hagenbeek, T.; Spits, H.; Reverso, J.; Ambrosetti, D.; et al. L-type amino-acid transporter 1 (LAT1): A therapeutic target supporting growth and survival of T-cell lymphoblastic lymphoma/T-cell acute lymphoblastic leukemia. Leukemia 2015, 29, 1253–1266.

REFERENCES

51. Shimizu, A.; Kaira, K.; Kato, M.; Yasuda, M.; Takahashi, A.; Tominaga, H.; Oriuchi, N.; Nagamori, S.; Kanai, Y.; Oyama, T.; et al. Prognostic significance of L-type amino acid transporter 1 (LAT1) expression in cutaneous melanoma. Melanoma Res. 2015, 25, 399–405.

52. Fukumoto, S.; Hanazono, K.; Fu, D.-R.; Endo, Y.; Kadosawa, T.; Iwano, H.; Uchide, T. A new treatment for human malignant melanoma targeting L-type amino acid transporter 1 (LAT1): A pilot study in a canine model. Biochem. Biophys. Res. Commun. 2013, 439, 103–108.

53. Wang, Q.; Beaumont, K.A.; Otte, N.J.; Font, J.; Bailey, C.G.; van Geldermalsen, M.; Sharp, D.M.; Tiffen, J.C.; Ryan, R.M.; Jormakka, M.; et al. Targeting glutamine transport to suppress melanoma cell growth. Int. J. Cancer 2014, 135, 1060–1071.

54. Hirano, K.; Uno, K.; Kuwabara, H.; Kojima, K.; Ohno, S.-I.; Sakurai, H.; Kamma, H.; Kurata, A. Expression of L-type amino acid transporter 1 in various skin lesions. Pathol. Res. Pract. 2014, 210, 634–639.

55. Bolzoni, M.; Chiu, M.; Accardi, F.; Vescovini, R.; Airoldi, I.; Storti, P.; Todoerti, K.; Agnelli, L.; Missale, G.; Andreoli, R.; et al. Dependence on glutamine uptake and glutamine addiction characterize myeloma cells: A new attractive target. Blood 2016, 128, 667–679.

56. Isoda, A.; Kaira, K.; Iwashina, M.; Oriuchi, N.; Tominaga, H.; Nagamori, S.; Kanai, Y.; Oyama, T.; Asao, T.; Matsumoto, M.; et al. Expression of L-type amino acid transporter 1 (LAT1) as a prognostic and therapeutic indicator in multiple myeloma. Cancer Sci. 2014, 105, 1496–1502.

57. Kaira, K.; Oriuchi, N.; Imai, H.; Shimizu, K.; Yanagitani, N.; Sunaga, N.; Hisada, T.; Ishizuka, T.; Kanai, Y.; Endou, H.; et al. L-type amino acid transporter 1 (LAT1) is frequently expressed in thymic carcinomas but is absent in thymomas. J. Surg. Oncol. 2009, 99, 433–438.

58. Barollo, S.; Bertazza, L.; Watutantrige-Fernando, S.; Censi, S.; Cavedon, E.; Galuppini, F.; Pennelli, G.; Fassina, A.; Citton, M.; Rubin, B.; et al. Overexpression of L-Type Amino Acid Transporter 1 (LAT1) and 2 (LAT2): Novel Markers of Neuroendocrine Tumors. PLoS ONE 2016, 11, e0156044.

REFERENCES

59. Häfliger, P.; Graff, J.; Rubin, M.; Stooss, A.; Dettmer, M.S.; Altmann, K.-H.; Gertsch, J.; Charles, R.-P. The LAT1 inhibitor JPH203 reduces growth of thyroid carcinoma in a fully immunocompetent mouse model. J. Exp. Clin. Cancer Res. 2018, 37, 234.

60. Yanagisawa, N.; Hana, K.; Nakada, N.; Ichinoe, M.; Koizumi, W.; Endou, H.; Okayasu, I.; Murakumo, Y. High expression of L-type amino acid transporter 1 as a prognostic marker in bile duct adenocarcinomas. Cancer Med. 2014, 3, 1246–1255.

61. Kaira, K.; Sunose, Y.; Ohshima, Y.; Ishioka, N.S.; Arakawa, K.; Ogawa, T.; Sunaga, N.; Shimizu, K.; Tominaga, H.; Oriuchi, N.; et al. Clinical significance of L-type amino acid transporter 1 expression as a prognostic marker and potential of new targeting therapy in biliary tract cancer. BMC Cancer 2013, 13, 482.

62. Kaira, K.; Nakamura, K.; Hirakawa, T.; Imai, H.; Tominaga, H.; Oriuchi, N.; Nagamori, S.; Kanai, Y.; Tsukamoto, N.; Oyama, T.; et al. Prognostic significance of L-type amino acid transporter 1 (LAT1) expression in patients with ovarian tumors. Am. J. Transl. Res. 2015, 7, 1161–1171.

63. Kaira, K.; Oriuchi, N.; Takahashi, T.; Nakagawa, K.; Ohde, Y.; Okumura, T.; Murakami, H.; Shukuya, T.; Kenmotsu, H.; Naito, T.; et al. LAT1 expression is closely associated with hypoxic markers and mTOR in resected non-small cell lung cancer. Am. J. Transl. Res. 2011, 3, 468–478.

64. Kaira, K.; Oriuchi, N.; Takahashi, T.; Nakagawa, K.; Ohde, Y.; Okumura, T.; Murakami, H.; Shukuya, T.; Kenmotsu, H.; Naito, T.; et al. L-type amino acid transporter 1 (LAT1) expression in malignant pleural mesothelioma. Anticancer Res. 2011, 31, 4075–4082.

65. Yothaisong, S.; Namwat, N.; Yongvanit, P.; Khuntikeo, N.; Puapairoj, A.; Jutabha, P.; Anzai, N.; Tassaneeyakul, W.; Tangsucharit, P.; Loilome, W. Increase in L-type amino acid transporter 1 expression during cholangiocarcinogenesis caused by liver fluke infection and its prognostic significance. Parasitol. Int. 2017, 66, 471–478.

66. Baniasadi, S.; Chairoungdua, A.; Iribe, Y.; Kanai, Y.; Endou, H.; Aisaki, K.; Igarashi, K.; Kanno, J. Gene expression profiles in T24 human bladder carcinoma cells by inhibiting an L-type amino acid transporter, LAT1. Arch. Pharm. Res. 2007, 30, 444–452.

REFERENCES

67. Kim, C.S.; Cho, S.-H.; Chun, H.S.; Lee, S.-Y.; Endou, H.; Kanai, Y.; Kim, D.K. BCH, an inhibitor of system L amino acid transporters, induces apoptosis in cancer cells. Biol. Pharm. Bull. 2008, 31, 1096–1100.

68. Kobayashi, K.; Ohnishi, A.; Promsuk, J.; Shimizu, S.; Kanai, Y.; Shiokawa, Y.; Nagane, M. Enhanced tumor growth elicited by L-type amino acid transporter 1 in human malignant glioma cells. Neurosurgery 2008, 62, 493–503; discussion 503–504.

69. Li, L.; Di, X.; Zhang, S.; Kan, Q.; Liu, H.; Lu, T.; Wang, Y.; Fu, Q.; Sun, J.; He, Z. Large amino acid transporter 1 mediated glutamate modified docetaxel-loaded liposomes for glioma targeting. Colloids Surf. B. Biointerfaces 2016, 141, 260–267.

70. Bhunia, S.; Vangala, V.; Bhattacharya, D.; Ravuri, H.G.; Kuncha, M.; Chakravarty, S.; Sistla, R.; Chaudhuri, A. Large Amino Acid Transporter 1 Selective Liposomes of l -DOPA Functionalized Amphiphile for Combating Glioblastoma. Mol. Pharm. 2017, 14, 3834–3847.

71. Cormerais, Y.; Pagnuzzi-Boncompagni, M.; Schrötter, S.; Giuliano, S.; Tambutté, E.; Endou, H.; Wempe, M.F.; Pagès, G.; Pouysségur, J.; Picco, V. Inhibition of the amino-acid transporter LAT1 demonstrates anti-neoplastic activity in medulloblastoma. J. Cell. Mol. Med. 2019, 23, 2711–2718.

72. Halldorsson, S.; Rohatgi, N.; Magnusdottir, M.; Choudhary, K.S.; Gudjonsson, T.; Knutsen, E.; Barkovskaya, A.; Hilmarsdottir, B.; Perander, M.; Mælandsmo, G.M.; et al. Metabolic re-wiring of isogenic breast epithelial cell lines following epithelial to mesenchymal transition. Cancer Lett. 2017, 396, 117–129.

73. Shennan, D.B.; Thomson, J. Inhibition of system L (LAT1/CD98hc) reduces the growth of cultured human breast cancer cells. Oncol. Rep. 2008, 20, 885–889.

74. Li, L.; Di, X.; Wu, M.; Sun, Z.; Zhong, L.; Wang, Y.; Fu, Q.; Kan, Q.; Sun, J.; He, Z. Targeting tumor highly-expressed LAT1 transporter with amino acid-modified nanoparticles: Toward a novel active targeting strategy in breast cancer therapy. Nanomedicine 2017, 13, 987–998.

75. Ong, Z.Y.; Chen, S.; Nabavi, E.; Regoutz, A.; Payne, D.J.; Elson, D.S.; Dexter, D.T.; Dunlop, I.E.; Porter, A.E. Multibranched Gold Nanoparticles with Intrinsic LAT-1 Targeting

REFERENCES

Capabilities for Selective Photothermal Therapy of Breast Cancer. ACS Appl. Mater. Interfaces 2017, 9, 39259–39270.

76. Napolitano, L.; Scalise, M.; Koyioni, M.; Koutentis, P.; Catto, M.; Eberini, I.; Parravicini, C.; Palazzolo, L.; Pisani, L.; Galluccio, M.; et al. Potent inhibitors of human LAT1 (SLC7A5) transporter based on dithiazole and dithiazine compounds for development of anticancer drugs. Biochem. Pharmacol. 2017, 143, 39–52.

77. Ebara, T.; Kaira, K.; Saito, J.-I.; Shioya, M.; Asao, T.; Takahashi, T.; Sakurai, H.; Kanai, Y.; Kuwano, H.; Nakano, T. L-type amino-acid transporter 1 expression predicts the response to preoperative hyperthermo-chemoradiotherapy for advanced rectal cancer. Anticancer Res. 2010, 30, 4223–4227.

78. Cormerais, Y.; Giuliano, S.; LeFloch, R.; Front, B.; Durivault, J.; Tambutté, E.; Massard, P.-A.; de la Ballina, L.R.; Endou, H.; Wempe, M.F.; et al. Genetic Disruption of the Multifunctional CD98/LAT1 Complex Demonstrates the Key Role of Essential Amino Acid Transport in the Control of mTORC1 and Tumor Growth. Cancer Res. 2016, 76, 4481–4492.

79. Oda, K.; Hosoda, N.; Endo, H.; Saito, K.; Tsujihara, K.; Yamamura, M.; Sakata, T.; Anzai, N.; Wempe, M.F.; Kanai, Y.; et al. L-Type amino acid transporter 1 inhibitors inhibit tumor cell growth. Cancer Sci. 2010, 101, 173–179.

80. Muto, Y.; Furihata, T.; Kaneko, M.; Higuchi, K.; Okunushi, K.; Morio, H.; Reien, Y.; Uesato, M.; Matsubara, H.; Anzai, N. Different Response Profiles of Gastrointestinal Cancer Cells to an L-Type Amino Acid Transporter Inhibitor, JPH203. Anticancer Res. 2019, 39, 159–165.

81. Ueda, S.; Hayashi, H.; Miyamoto, T.; Abe, S.; Hirai, K.; Matsukura, K.; Yagi, H.; Hara, Y.; Yoshida, K.; Okazaki, S.; et al. Anti-tumor effects of mAb against l-type amino acid transporter 1 (LAT1) bound to human and monkey LAT1 with dual avidity modes. Cancer Sci. 2019, 110, 674–685.

82. Ohshima, Y.; Kaira, K.; Yamaguchi, A.; Oriuchi, N.; Tominaga, H.; Nagamori, S.; Kanai, Y.; Yokobori, T.; Miyazaki, T.; Asao, T.; et al. Efficacy of system l amino acid transporter 1

inhibition as a therapeutic target in esophageal squamous cell carcinoma. Cancer Sci. 2016, 107, 1499–1505.

83. Shi, L.; Luo, W.; Huang, W.; Huang, S.; Huang, G. Downregulation of L-type amino acid transporter 1 expression inhibits the growth, migration and invasion of gastric cancer cells. Oncol. Lett. 2013, 6, 106–112.

84. Kim, C.; Park, K.J.; Park, J.R.; Kanai, Y.; Endou, H.; Park, J.; Kim, D.K. The RNA Interference of Amino Acid Transporter LAT1 Inhibits the Growth of KB Human Oral Cancer Cells. Anticancer Res. 2006, 26, 2943–2948.

85. Yamauchi, K.; Sakurai, H.; Kimura, T.; Wiriyasermkul, P.; Nagamori, S.; Kanai, Y.; Kohno, N. System L amino acid transporter inhibitor enhances anti-tumor activity of cisplatin in a head and neck squamous cell carcinoma cell line. Cancer Lett. 2009, 276, 95–101.

86. Ueno, S.; Kimura, T.; Yamaga, T.; Kawada, A.; Ochiai, T.; Endou, H.; Sakurai, H. Metformin enhances anti-tumor effect of L-type amino acid transporter 1 (LAT1) inhibitor. J. Pharmacol. Sci. 2016, 131, 110–117.

87. Kaira, K.; Takahashi, T.; Murakami, H.; Shukuya, T.; Kenmotsu, H.; Naito, T.; Oriuchi, N.; Kanai, Y.; Endo, M.; Kondo, H.; et al. Relationship between LAT1 expression and response to platinum-based chemotherapy in non-small cell lung cancer patients with postoperative recurrence. Anticancer Res. 2011, 31, 3775–3782.

88. Kongpracha, P.; Nagamori, S.; Wiriyasermkul, P.; Tanaka, Y.; Kaneda, K.; Okuda, S.; Ohgaki, R.; Kanai, Y. Structure-activity relationship of a novel series of inhibitors for cancer type transporter L-type amino acid transporter 1 (LAT1). J. Pharmacol. Sci. 2017, 133, 96–102.

89. Sato, K.; Miyamoto, M.; Takano, M.; Furuya, K.; Tsuda, H. Significant relationship between the LAT1 expression pattern and chemoresistance in ovarian clear cell carcinoma. Virchows Arch. 2019.

90. Fan, X.; Ross, D.D.; Arakawa, H.; Ganapathy, V.; Tamai, I.; Nakanishi, T. Impact of system L amino acid transporter 1 (LAT1) on proliferation of human ovarian cancer cells: A possible target for combination therapy with anti-proliferative aminopeptidase inhibitors. Biochem. Pharmacol. 2010, 80, 811–818.

REFERENCES

91. Kaji, M.; Kabir-Salmani, M.; Anzai, N.; Jin, C.J.; Akimoto, Y.; Horita, A.; Sakamoto, A.; Kanai, Y.; Sakurai, H.; Iwashita, M. Properties of L-type amino acid transporter 1 in epidermal ovarian cancer. Int. J. Gynecol. Cancer 2010, 20, 329–336.

92. Altan, B.; Kaira, K.; Watanabe, A.; Kubo, N.; Bao, P.; Dolgormaa, G.; Bilguun, E.O.; Araki, K.; Kanai, Y.; Yokobori, T.; et al. Relationship between LAT1 expression and resistance to chemotherapy in pancreatic ductal adenocarcinoma. Cancer Chemother. Pharmacol. 2018, 81, 141–153.

93. Wang, Q.; Bailey, C.G.; Ng, C.; Tiffen, J.; Thoeng, A.; Minhas, V.; Lehman, M.L.; Hendy, S.C.; Buchanan, G.; Nelson, C.C.; et al. Androgen receptor and nutrient signaling pathways coordinate the demand for increased amino acid transport during prostate cancer progression. Cancer Res. 2011, 71, 7525–7536.

94. Wang, Q.; Tiffen, J.; Bailey, C.G.; Lehman, M.L.; Ritchie, W.; Fazli, L.; Metierre, C.; Feng, Y.J.; Li, E.; Gleave, M.; et al. Targeting amino acid transport in metastatic castration-resistant prostate cancer: Effects on cell cycle, cell growth, and tumor development. J. Natl. Cancer Inst. 2013, 105, 1463–1473.

95. Otsuki, H.; Kimura, T.; Yamaga, T.; Kosaka, T.; Suehiro, J.-I.; Sakurai, H. Prostate Cancer Cells in Different Androgen Receptor Status Employ Different Leucine Transporters. Prostate 2017, 77, 222–233.

96. Hayashi, K.; Jutabha, P.; Maeda, S.; Supak, Y.; Ouchi, M.; Endou, H.; Fujita, T.; Chida, M.; Anzai, N. LAT1 acts as a crucial transporter of amino acids in human thymic carcinoma cells. J. Pharmacol. Sci. 2016, 132, 201–204.

97. Nakanishi, K.; Ogata, S.; Matsuo, H.; Kanai, Y.; Endou, H.; Hiroi, S.; Tominaga, S.; Aida, S.; Kasamatsu, H.; Kawai, T. Expression of LAT1 predicts risk of progression of transitional cell carcinoma of the upper urinary tract. Virchows Arch. 2007, 451, 681–690.

98. Elorza, A.; Soro-Arnáiz, I.; Meléndez-Rodríguez, F.; Rodríguez-Vaello, V.; Marsboom, G.; de Cárcer, G.; Acosta-Iborra, B.; Albacete-Albacete, L.; Ordóñez, A.; Serrano-Oviedo, L.; et al. HIF2α acts as an mTORC1 activator through the amino acid carrier SLC7A5. Mol. Cell 2012, 48, 681–691.

REFERENCES

99. Levy, A.P.; Levy, N.S.; Wegner, S.; Goldberg, M.A. Transcriptional regulation of the rat vascular endothelial growth factor gene by hypoxia. J. Biol. Chem. 1995, 270, 13333–13340.

100. Forsythe, J.A.; Jiang, B.H.; Iyer, N.V.; Agani, F.; Leung, S.W.; Koos, R.D.; Semenza, G.L. Activation of vascular endothelial growth factor gene transcription by hypoxia-inducible factor 1. Mol. Cell. Biol. 1996, 16, 4604–4613.

101. Chen, R.; Zou, Y.; Mao, D.; Sun, D.; Gao, G.; Shi, J.; Liu, X.; Zhu, C.; Yang, M.; Ye, W.; et al. The general amino acid control pathway regulates mTOR and autophagy during serum/glutamine starvation. J. Cell Biol. 2014, 206, 173–182.

102. Hayashi, K.; Jutabha, P.; Endou, H.; Anzai, N. c-Myc is crucial for the expression of LAT1 in MIA Paca-2 human pancreatic cancer cells. Oncol. Rep. 2012, 28, 862–866.

103. Shimizu, A.; Kaira, K.; Okubo, Y.; Utsumi, D.; Yasuda, M.; Tominaga, H.; Oriuchi, N.; Kanai, Y.; Takahashi, K.; Ishikawa, O. Prognostic impact of LAT1 and CD98 expression in cutaneous angiosarcoma. Neoplasma 2017, 64, 283–288.

104. Kaira, K.; Oriuchi, N.; Imai, H.; Shimizu, K.; Yanagitani, N.; Sunaga, N.; Hisada, T.; Tanaka, S.; Ishizuka, T.; Kanai, Y.; et al. L-type amino acid transporter 1 and CD98 expression in primary and metastatic sites of human neoplasms. Cancer Sci. 2008, 99, 2380–2386.

105. Bodoy, S.; Martín, L.; Zorzano, A.; Palacín, M.; Estévez, R.; Bertran, J. Identification of LAT4, a novel amino acid transporter with system L activity. J. Biol. Chem. 2005, 280, 12002–12011.

106. Babu, E.; Kanai, Y.; Chairoungdua, A.; Kim, D.K.; Iribe, Y.; Tangtrongsup, S.; Jutabha, P.; Li, Y.; Ahmed, N.; Sakamoto, S.; et al. Identification of a Novel System L Amino Acid Transporter Structurally Distinct from Heterodimeric Amino Acid Transporters. J. Biol. Chem. 2003, 278, 43838–43845.

107. Segawa, H.; Fukasawa, Y.; Miyamoto, K.; Takeda, E.; Endou, H.; Kanai, Y. Identification and functional characterization of a Na+-independent neutral amino acid transporter with broad substrate selectivity. J. Biol. Chem. 1999, 274, 19745–19751.

108. Uchino, H.; Kanai, Y.; Kim, D.K.; Wempe, M.F.; Chairoungdua, A.; Morimoto, E.; Anders, M.W.; Endou, H. Transport of amino acid-related compounds mediated by L-type amino acid

transporter 1 (LAT1): Insights into the mechanisms of substrate recognition. Mol. Pharmacol. 2002, 61, 729–737.

109. Morimoto, E.; Kanai, Y.; Kim, D.K.; Chairoungdua, A.; Choi, H.W.; Wempe, M.F.; Anzai, N.; Endou, H. Establishment and characterization of mammalian cell lines stably expressing human L-type amino acid transporters. J. Pharmacol. Sci. 2008, 108, 505–516.

110. Shingyoji, M.; Iizasa, T.; Higashiyama, M.; Imamura, F.; Saruki, N.; Imaizumi, A.; Yamamoto, H.; Daimon, T.; Tochikubo, O.; Mitsushima, T.; et al. The significance and robustness of a plasma free amino acid (PFAA) profile-based multiplex function for detecting lung cancer. BMC Cancer 2013, 13, 77.

111. Maeda, J.; Higashiyama, M.; Imaizumi, A.; Nakayama, T.; Yamamoto, H.; Daimon, T.; Yamakado, M.; Imamura, F.; Kodama, K. Possibility of multivariate function composed of plasma amino acid profiles as a novel screening index for non-small cell lung cancer: A case control study. BMC Cancer 2010, 10, 690.

112. Giskeødegård, G.F.; Hansen, A.F.; Bertilsson, H.; Gonzalez, S.V.; Kristiansen, K.A.; Bruheim, P.; Mjøs, S.A.; Angelsen, A.; Bathen, T.F.; Tessem, M.-B. Metabolic markers in blood can separate prostate cancer from benign prostatic hyperplasia. Br. J. Cancer 2015, 113, 1712–1719.

113. Poschke, I.; Mao, Y.; Kiessling, R.; de Boniface, J. Tumor-dependent increase of serum amino acid levels in breast cancer patients has diagnostic potential and correlates with molecular tumor subtypes. J. Transl. Med. 2013, 11, 290.

114. Kubota, A.; Meguid, M.M.; Hitch, D.C. Amino acid profiles correlate diagnostically with organ site in three kinds of malignant tumors. Cancer 1992, 69, 2343–2348.

115. Leichtle, A.B.; Nuoffer, J.-M.; Ceglarek, U.; Kase, J.; Conrad, T.; Witzigmann, H.; Thiery, J.; Fiedler, G.M. Serum amino acid profiles and their alterations in colorectal cancer. Metabolomics 2012, 8, 643–653.

116. Miyagi, Y.; Higashiyama, M.; Gochi, A.; Akaike, M.; Ishikawa, T.; Miura, T.; Saruki, N.; Bando, E.; Kimura, H.; Imamura, F.; et al. Plasma free amino acid profiling of five types of cancer patients and its application for early detection. PLoS ONE 2011, 6, e24143.

REFERENCES

117. Steiner, N.; Müller, U.; Hajek, R.; Sevcikova, S.; Borjan, B.; Jöhrer, K.; Göbel, G.; Pircher, A.; Gunsilius, E. The metabolomic plasma profile of myeloma patients is considerably different from healthy subjects and reveals potential new therapeutic targets. PLoS ONE 2018, 13, e0202045.

118. Vissers, Y.L.J.; Dejong, C.H.C.; Luiking, Y.C.; Fearon, K.C.H.; von Meyenfeldt, M.F.; Deutz, N.E.P. Plasma arginine concentrations are reduced in cancer patients: Evidence for arginine deficiency? Am. J. Clin. Nutr. 2005, 81, 1142–1146.

119. Deja, S.; Porebska, I.; Kowal, A.; Zabek, A.; Barg, W.; Pawelczyk, K.; Stanimirova, I.; Daszykowski, M.; Korzeniewska, A.; Jankowska, R.; et al. Metabolomics provide new insights on lung cancer staging and discrimination from chronic obstructive pulmonary disease. J. Pharm. Biomed. Anal. 2014, 100, 369–380.

120. Lai, H.-S.; Lee, J.-C.; Lee, P.-H.; Wang, S.-T.; Chen, W.-J. Plasma free amino acid profile in cancer patients. Semin. Cancer Biol. 2005, 15, 267–276.

121. Singh, N.; Scalise, M.; Galluccio, M.; Wieder, M.; Seidel, T.; Langer, T.; Indiveri, C.; Ecker, G.F. Discovery of Potent Inhibitors for the Large Neutral Amino Acid Transporter 1 (LAT1) by Structure-Based Methods. Int. J. Mol. Sci. 2018, 20, 27.

122. Okano, N.; Kawai, K.; Yamauchi, Y.; Kobayashi, T.; Naruge, D.; Nagashima, F.; Endou, H.; Furuse, J. First-in-human phase I study of JPH203 in patients with advanced solid tumors. J. Clin. Oncol. 2018, 36, 419.

123. Napolitano, L.; Galluccio, M.; Scalise, M.; Parravicini, C.; Palazzolo, L.; Eberini, I.; Indiveri, C. Novel insights into the transport mechanism of the human amino acid transporter LAT1 (SLC7A5). Probing critical residues for substrate translocation. Biochim. Biophys. Acta Gen. Subj. 2017, 1861, 727–736.

REFERENCES